

INFORMATION TO USERS

This manuscript has been reproduced from the microfilm master. UMI films the text directly from the original or copy submitted. Thus, some thesis and dissertation copies are in typewriter face, while others may be from any type of computer printer.

The quality of this reproduction is dependent upon the quality of the copy submitted. Broken or indistinct print, colored or poor quality illustrations and photographs, print bleedthrough, substandard margins, and improper alignment can adversely affect reproduction.

In the unlikely event that the author did not send UMI a complete manuscript and there are missing pages, these will be noted. Also, if unauthorized copyright material had to be removed, a note will indicate the deletion.

Oversize materials (e.g., maps, drawings, charts) are reproduced by sectioning the original, beginning at the upper left-hand corner and continuing from left to right in equal sections with small overlaps. Each original is also photographed in one exposure and is included in reduced form at the back of the book.

Photographs included in the original manuscript have been reproduced xerographically in this copy. Higher quality 6" x 9" black and white photographic prints are available for any photographs or illustrations appearing in this copy for an additional charge. Contact UMI directly to order.

UMI

**A Bell & Howell Information Company
300 North Zeeb Road, Ann Arbor MI 48106-1346 USA
313/761-4700 800/521-0600**



University of Alberta

**Models of Assembly and Disassembly of Individual
Microtubules and their Ensembles**

By
David S. Sept ©

A dissertation
presented to the Faculty of Graduate Studies and Research
in partial fulfilment of the requirements for the degree
of

Doctor of Philosophy

in

Theoretical Physics
Department of Physics

Edmonton, Alberta

Fall 1997



**National Library
of Canada**

**Acquisitions and
Bibliographic Services**

**395 Wellington Street
Ottawa ON K1A 0N4
Canada**

**Bibliothèque nationale
du Canada**

**Acquisitions et
services bibliographiques**

**395, rue Wellington
Ottawa ON K1A 0N4
Canada**

Your file Votre référence

Our file Notre référence

The author has granted a non-exclusive licence allowing the National Library of Canada to reproduce, loan, distribute or sell copies of this thesis in microform, paper or electronic formats.

The author retains ownership of the copyright in this thesis. Neither the thesis nor substantial extracts from it may be printed or otherwise reproduced without the author's permission.

L'auteur a accordé une licence non exclusive permettant à la Bibliothèque nationale du Canada de reproduire, prêter, distribuer ou vendre des copies de cette thèse sous la forme de microfiche/film, de reproduction sur papier ou sur format électronique.

L'auteur conserve la propriété du droit d'auteur qui protège cette thèse. Ni la thèse ni des extraits substantiels de celle-ci ne doivent être imprimés ou autrement reproduits sans son autorisation.

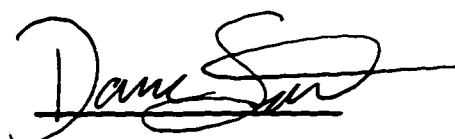
0-612-23068-6

UNIVERSITY OF ALBERTA
LIBRARY RELEASE FORM

NAME OF AUTHOR: David S. Sept
TITLE OF THESIS: Models of Assembly and Disassembly
of Individual Microtubules and their
Ensembles
DEGREE: Doctor of Philosophy
YEAR THE DEGREE GRANTED: 1997

Permission is hereby granted to the University of Alberta Library to reproduce single copies of this thesis and to lend such copies for private, scholarly or scientific research purposes only.

The author reserves all other publication and other rights in association with the copyright in the thesis, and except as hereinbefore provided, neither the thesis nor any substantial portion thereof may be printed or otherwise reproduced in any material form whatever without the author's prior written permission.



David S. Sept

Department of Physics

University of Alberta

Edmonton, Alberta

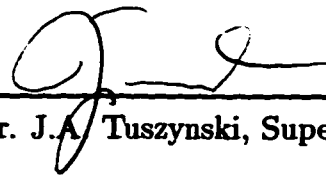
T6G 2J1

Date: SEPT 24, 1997

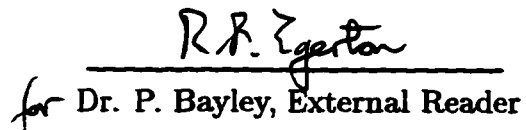
UNIVERSITY OF ALBERTA

FACULTY OF GRADUATE STUDIES AND RESEARCH

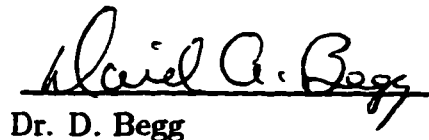
The undersigned certify that they have read, and recommend to the Faculty of Graduate Studies and Research for acceptance, a thesis entitled "Models of Assembly and Disassembly of Individual Microtubules and their Ensembles" submitted by David S. Sept in partial fulfilment of the requirements for the degree of Doctor of Philosophy in Theoretical Physics



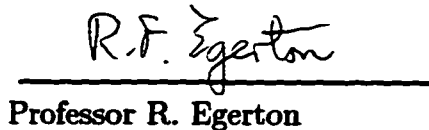
Dr. J.A. Tuszynski, Supervisor



for Dr. P. Bayley, External Reader



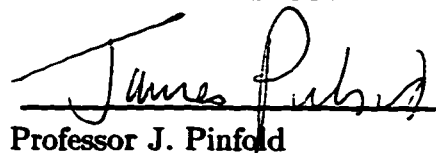
Dr. D. Begg



Professor R. Egerton



Professor F.C. Khanna



Professor J. Pinfold

Date: SEPTEMBER 16, 1997

To my parents

Abstract

Microtubules are tubular polymers that, along with actin filaments and intermediate filaments, comprise the eukaryotic cytoskeleton. They are constructed of tubulin dimers which attach end-to-end to form protofilaments, with 13 protofilaments binding together to form the tubular structure. Microtubules are not only involved, but instrumental in many cell functions such as mitosis and transportation of materials within the cell. Despite being relatively rigid polymers, microtubules are very dynamic and are constantly rearranging themselves. Perhaps the most interesting experimental observation is what has been termed *dynamic instability* where growing and shrinking microtubules may co-exist. The transition from the growing to the shrinking phase is not a smooth or even predictable process. *In vitro* experiments conducted by Horio and Hotani were some of the first to show the seemingly erratic behavior of a single microtubule. In stark contrast, the Mandelkow group in Hamburg then demonstrated how an ensemble of microtubules loses this irregularity and the ensemble as a whole undergoes smooth oscillations.

My modelling begins with that of a single microtubule. The stochastic equations governing the behavior depend on the available free tubulin, the amount of assembled tubulin as well as the interactions between neighboring microtubules. This modelling is very successful, but cannot explain the transition to coherent oscillations. The next step is treating the problem as a first-order phase transition. The Landau-Ginzburg

free energy expansion gives rise to two phases: free tubulin and microtubules. This treatment can reproduce the oscillations that are seen experimentally. A natural extension of this model is to treat the free tubulin and assembled microtubules as interacting entities. The result is a set of reaction equations, and with a further extension to include spatial distribution, reaction-diffusion equations. This system can not only reproduce the temporal dynamics, but the spatial patterns that are observed in experiments.

Acknowledgements

There are many people that need to be acknowledged for their contribution to my education and experience at the University of Alberta. First, my supervisor Jack Tuszynski for providing me with an exciting, multi-faceted research program that involved everything from superconductivity to ferroelectrics, from self-organized criticality to biophysics. As well, I need to thank many members of the Biophysics group past and present: Andrew Brown, Michael Jørgensen and Alex Nip along with all my friends within the department. I owe a debt of gratitude to Faqir Khanna. The summers I spent doing research under Faqir during my undergraduate years made me appreciate scientific research and inspired me to enter graduate school. Finally, I would like to thank my wife Melodie and my parents for their support. They never seemed to think that 'just one more year' of university was too much.

Contents

1	Introduction	1
2	The Cell, the Cytoskeleton and Microtubules	3
2.1	Eukaryotes	3
2.2	The Cytoskeleton	4
2.2.1	Organization and function	4
2.2.2	Constituent filaments	5
2.3	Microtubules	8
2.3.1	Tubulin	8
2.3.2	Assembly of microtubules	9
3	Experimental Results and Previous Modelling	17
3.1	Experimental Results	17
3.1.1	Dynamic instability	18
3.1.2	Microtubule Oscillations	20
3.2	Previous modelling	23
3.2.1	Dynamic instability	23
3.2.2	Microtubule oscillations	24
4	Modelling Single Microtubule Growth	26
4.1	Statistical Analysis	27

4.2	Recursive Maps	31
4.3	Coupled Recursive Maps	38
5	Modelling using a Landau-Ginzburg Approach	43
5.1	Landau-Ginzburg Free energy expansion	44
5.2	Mean Field Dynamics	47
5.2.1	Adding surface energy	47
5.2.2	Solving the equation of motion	49
5.3	Other predictions from the model	51
6	Reaction Kinetics Model	54
6.1	Chemical Kinetics	54
6.2	Oscillations in (Bio)chemical Systems	55
6.3	Models for Microtubule Oscillations	57
6.4	Determining the Rate Constants	60
6.5	Phase Diagram of Microtubule Assembly	63
6.6	Solving the Reaction Equations	65
6.7	Comparison with Experimental Results	67
6.8	Additional Results	78
7	Reaction-Diffusion Modelling	83
7.1	Connection with the Landau-Ginzburg Formulation	83
7.2	The Reaction-Diffusion Model	88
7.3	Results of the model	90
8	Conclusions	100

List of Figures

2.1	The 2-stranded helix of an actin filament. The different shading is only for viewing purposes.	5
2.2	The three basic types of microfilament arrangement: (a) parallel bundles, (b) contractile bundles and (c) gel or lattice-like arrangement.	6
2.3	Illustration of the structure of a microtubule (B lattice) with its relative dimensions.	10
2.4	The A and B lattice types for a microtubule with 13 protofilaments.	12
2.5	Illustration of different cell types with their microtubule arrangement: (a) interphase cell, (b) nerve cell, (c) ciliated cell and (d) a dividing cell.	15
3.1	Experimental data of the growth of a single microtubule. Data courtesy of E. Mandelkow.	19
3.2	Experimental data showing the oscillations of an ensemble of microtubules. The amount of oscillation varies with the tubulin concentration (given in the inset). Data courtesy of E. Mandelkow.	25
4.1	Three sets of experimental data for single microtubule growth and their Fourier transforms. Top two set of data courtesy of E. Mandelkow and the bottom data courtesy of S. Pedigo.	28
4.2	Recursive maps and Hurst analysis for the three sets of experimental data given in Figure 4.1.	30

4.3	Growth profiles, recursive maps and Hurst analysis for two simulations with: (a) $P = 0.10$ and (b) $P = 0.05$. The resulting Hurst exponents are given in the inset.	33
4.4	Growth profiles, recursive maps and Hurst analysis for two simulations with: (a) $P_1 = 0.5$ and (b) $P_1 = 0.9$. The resulting Hurst exponents are given in the inset.	35
4.5	(a) Schematic representation of the growth of a microtubule (adapted from Alberts et al. [2]) and (b) the derivative of this plot showing rate of growth.	36
4.6	Growth profiles, recursive maps and Hurst analysis for a simulation with $P_0 = 0.05$, $P_1 = 0.7$ and $P_3 = 0.2$. The resulting Hurst exponent is given in the inset.	37
4.7	Plot of total assembled tubulin for 5 coupled microtubules (top curve) and a single microtubule.	39
4.8	Plot of total assembled tubulin for 30 coupled microtubules (bottom curve) and 50 coupled microtubules.	40
4.9	Plots of the fraction of assembled tubulin for 300 microtubules. The rate of GDP to GTP conversion at each time step is: 0.3% (top curve), 0.1% (middle curve) and 0.05% (bottom curve).	41
4.10	Plots of the fraction of assembled tubulin for 200 (bottom), 300 and 500 (top) microtubules. The rate of GTP to GDP conversion at each time step is: 0.3%.	42
5.1	A phase diagram for microtubules. Data points taken from Fygenson et al, 1994.	44
5.2	Plots of the free energy potential showing the three phase regions in our theory.	46
5.3	Plots of eqs. (5.8) and (5.10) along with the experimental data points.	48

5.4	The amount of assembled tubulin versus time for (a) 3 μM and (b) 6 μM tubulin concentration. Both solutions performed at 37°C.	50
5.5	The amount of assembled tubulin versus time for (a) 15 μM and (b) 25 μM tubulin concentration. Both solutions performed at 37°C. .	50
5.6	Specific heat predicted by our model as a function of temperature and tubulin concentration.	52
6.1	Arrhenius plot of $\log(k_+)$ vs. $(1/T)$ to determine the values of A and ΔE	62
6.2	Theoretical predictions and experimental data points for the two transition lines from no assembly to assembly and from assembly to oscillations.	66
6.3	Solutions for T_a , T_t , T_d and N as functions of time. Simulations were performed for $T = 37^\circ\text{C}$ and $C = 40 \mu\text{M}$	67
6.4	Solutions for T_a as a function of time for two sets of initial conditions. The solid line is for $T_t = 40 \mu\text{M}$ with all other variables initially set to zero and the dashed line is for $T_d = 40 \mu\text{M}$ and all others set to zero.	68
6.5	Plots of (a) experimental (previous page) and (b) theoretical results for microtubule oscillations at various tubulin concentrations. The results are both for 37°C. Experimental data courtesy of E. Mandelkow. . . .	70
6.6	Plots of (a) experimental [37] (previous page) and (b) theoretical results for microtubule assembly at different temperatures. Simulations are for a tubulin concentration of 40 μM	72
6.7	Experimental [37] (top) and theoretical (bottom) results showing the effect of slowly raising the temperature on oscillations and nucleation. For the theoretical results, in each case the temperature was raised from 0 – 37°C with a half time of 10 (solid curve) and 80 (dashed curve). The time units are the same as the units of the x-axis.	73

6.8	(a) Experimental findings [74] (previous page) and (b) theoretical plots for GTP-rich tubulin (top curves in each case) and the amount of assembled tubulin (bottom curves). Note how in each case the oscillations are in antiphase.	76
6.9	Plots of experimental [37] (bottom curve in top plot) and theoretical results (bottom plot) for adding GTP to a microtubule ensemble after reaching a steady-state.	77
6.10	Plots of the total amount of assembled tubulin for various values of k_r . The values are $k_r = 2 s^{-1}$ (solid curve), $5 s^{-1}$ (dashed curve) and $8 s^{-1}$ (dotted curve). All simulations are for a temperature of 37°C and a tubulin concentration of $40 \mu\text{M}$	78
6.11	The period of microtubule oscillations as a function of the rate of GTP regeneration from experimental work [31] (top) and as predicted from the theoretical model (bottom).	79
6.12	Experimental [32] (top) and theoretical (bottom) results for shearing of the microtubule ensemble. See text for explanation.	80
6.13	Phase diagram showing the different regions of microtubule assembly for different values of k_r and C. The temperature is fixed at 37°C . . .	81
6.14	Plots showing the effect of lowering the temperature after the system has reached a steady-state. The halftimes listed are in the same units as the time on the x-axis.	82
7.1	Plot showing the effect of diffusion on the solutions. The dashed line is for $40 \mu\text{M}$ without diffusion and the solid line with diffusion. See text for details.	91
7.2	Simulation for an initial gradient of Tu-GTP as shown in the top plot. All other variables are initially set to zero.	92

7.3	Simulation for a temperature gradient across the cell as shown in the top plot. Initially, $T_t = 40 \mu\text{M}$ and all other variables are set to zero.	94
7.4	Simulation for an inhomogeneous nucleation rate. The spatial dependence of k_n is shown above the resulting simulation. Waves of assembled tubulin are nucleated at the boundary and propagate towards the middle of the cell. The tubulin concentration is $40 \mu\text{M}$.	95
7.5	Simulation for an inhomogeneous nucleation rate for $100 \mu\text{M}$ tubulin. The spatial dependence of k_n is the same as in Figure 7.4 but $k_r = 2 s^{-1}$ (top) and $k_r = 0.3 s^{-1}$ bottom.	96
7.6	Spatial variation of the nucleation rate constant simulating the effect of a MTOC.	97
7.7	Simulation results for an inhomogeneous nucleation rate constant as shown in Figure 7.5 to simulate a MTOC. The profiles are the last time step for both N and T_a are steady-state profiles and indicated the the microtubules are longer on the edges of the MTOC.	98

Preface

The work presented in this dissertation was carried out at the Department of Physics at the University of Alberta and at the Institut für Theoretische Physik I at the University of Düsseldorf between September 1992 and August 1997. The work was done under the supervision of Jack Tuszyński and in conjunction with Andrew Brown. Many of the results from Chapters 3 and 4 have been published in conference proceedings and the following articles:

J.A. Tuszyński, B. Trpisová and D. Sept, *From Erratic to Coherent Behaviour in the Assembly of Microtubules* (invited), *Neural Network World* 5/95, 675–688

J.A. Tuszyński, D. Sept and B. Trpisová, *The Cell's Microtubules: Growth Dynamics, Ordering of Dipoles and Modes of Energy Propagation*, *Mathematics and Computers in Simulation* 40, 425 – 442 (1996)

J.A. Tuszyński, B. Trpisová, D. Sept and M.V. Satarčić, *The Enigma of Microtubules and their Self-Organizing Behavior in the Cytoskeleton* (invited), *BioSystems*, 42, 153–175 (1997)

J.A. Tuszyński, B. Trpišová, D. Sept and J.A. Brown, *Selected Physical Issues in the Structure and Function of Microtubules* (invited), *Journal of Structural Biology*, 118, 94–106 (1997)

The work from Chapters 5, 6 and 7 has yet to be submitted for publication.

Glossary of Terms

catastrophe A switch from growth to shrinkage in the assembly of a microtubule.

eukaryote An organism composed of cells that contain a nucleus and a cytoplasm.

GDP Guanosine 5'-diphosphate - an important nucleotide in the microtubule assembly cycle.

GTP Guanosine 5'-triphosphate - an important nucleotide in the microtubule assembly cycle.

MAP Microtubule Associated Protein - a protein which can bind to a microtubule and thus affect its properties.

MTOC Microtubule Organizing Centre - a region where microtubules tend to nucleate and grow (eg. centrosome).

rescue A switch from shrinkage to growth in the assembly of a microtubule.

Chapter 1

Introduction

Microtubules are key components of the eukaryotic cytoskeleton. They possess a number of remarkable properties which have made them one of the most active research fields of recent decades. A vast amount of work has been done and is still being done, to try and elucidate information about the structure of microtubules and their constituent dimers. The interactions between microtubules and other proteins within the cell have also been intensely studied. What is most interesting, however, is the dynamic properties of the assembly and disassembly of these polymers.

Microtubules exhibit two distinct types of behaviour in their assembly. The first has been termed 'dynamic instability' and refers to the erratic growth of a single microtubule. This growth is not a smooth process, but the microtubule constantly switches, seemingly at random, between growth and rapid shrinkage. The reason (or reasons) behind this phenomenon is not known and this remains one of the key open questions. What is perhaps more interesting is the second type of behaviour. When microtubules are grouped together, this stochastic growth pattern gives way to smooth oscillations. These oscillations exist in many forms just as there are many manifestations of dynamic instability.

From a physics standpoint, microtubule assembly is simply an example of a sys-

tem undergoing a phase transition. Pattern formation and instabilities are common in systems, including many examples in biology. Monographs such as Haken's *Synergetics* [1] are replete with examples from all areas of science showing how interactions in many-body systems give rise to phenomena such as chaos, oscillations, turbulence and the formation of patterns. In this thesis, we will employ many of the methods put forward by Haken.

After a brief introduction to the molecular biology of the cell and of microtubules, we will model dynamic instability using recursive maps. In order to model a microtubule ensemble, we will couple many of these maps together in an attempt to see the transition to oscillatory growth. Since microtubule assembly is an example of a phase transition, we will next use a Landau free energy expansion to examine the phase dynamics during such a phase change. This formulation will prove to provide us with oscillations in terms of our chosen order parameter, but the interpretation of these results is limited. To alleviate this problem, we will move to a model based on chemical reaction kinetics. Here we have a more complicated but more successful model which will produce many results observed by experimentalists. The last chapter will be an extension of the chemical kinetics approach to a set of coupled reaction-diffusion equations. Here we attempt to produce the spatial patterns that are observed in addition to the temporal dynamics. Aside from trying to answer a number of open questions associated with microtubule dynamics, the hope is to present new questions and ideas which may lead to more research in this field.

Chapter 2

The Cell, the Cytoskeleton and Microtubules

Cells are the basic units of life. They comprise all living organisms from the simplest amoeba to multicellular plants to complicated beings such as ourselves. Obviously, cells are very diverse in their type and the roles and functions that they play. There exist several different methods for classifying cell types [2]. One such classification is based on whether or not the cell contains a nucleus. *Prokaryotes* (literally ‘before nucleus’) are cells that lack a definite membrane bound nucleus. On the other had, *eukaryotes* (meaning ‘true nucleus’) are cells that have a nucleus with chromosomes. It is this second class of cells that we will be interested in since they contain microtubules.

2.1 Eukaryotes

Even with our differentiation between these two classes of cells, we have not really restricted the vast number of cells types by selecting cells that have a nucleus. Some examples or eukaryotes are yeast cells, amoeba, plant and of course animal cells.

Within the human body, there also exists a plethora of eukaryotic cell types: neural, epithelial and muscle cells to name but a few. Eukaryotic cells are also quite variant in size. There are many cells that are on the order of μm while the ostrich egg yolk may be as large as 3 cm in diameter [3]. Despite all these differences, eukaryotic cells have many things in common. The components of these cells are largely the same from one cell to the next. Specific components that we will be interested in are the cytoplasm, the cytoskeleton and the nucleus. The functions that cells perform are also very similar. The three basic functions are self maintenance, cell motility and cell growth and reproduction [4]. Eukaryotic cells contain thousands of different protein types which constitute about 60% of their dry mass [2]. Many of these proteins polymerize to form organized structures within the cell, the most important of which is the cytoskeleton.

2.2 The Cytoskeleton

2.2.1 Organization and function

The cytoskeleton is a complex mixture of proteins that form one of the largest structures in the cell. It is the most rigid formation within the cell, but is also very dynamic and is thus sometimes referred to as the cytomusculature.

Many functions within the cell are served by the cytoskeleton. Most importantly it provides structure, strength and shape to the cell. It is also instrumental in positioning organelles and the transport of materials. Cilia and flagella are two examples of how the cytoskeleton can provide cell motility. Along with these very important but somewhat mundane functions, the cytoskeleton is speculated to be involved with signalling within the cell and possibly information processing, which would make it the 'nervous system' of the cell [5, 6, 7]. One thing we shall see is that microtubules play an important role in all the above processes.

The interaction of cytoskeletal components with one another and with other organelles and vesicles is via molecular interactions [8]. This is often through nucleotide hydrolysis (such as ATP or GTP), calcium signalling or some other process such as phosphorylation. What is clear is that we have a great deal of information about the cytoskeleton, but only a small amount of understanding. We must first attempt to understand the basic components before we examine the entire complex structure. With this in mind, let us examine the individual components of the cytoskeleton.

2.2.2 Constituent filaments

Actin filaments

Actin filaments (also called microfilaments) are a 2-stranded helix comprised of actin monomers (see Figure 2.1). Actin has a molecular weight of 43 kDa and is one of

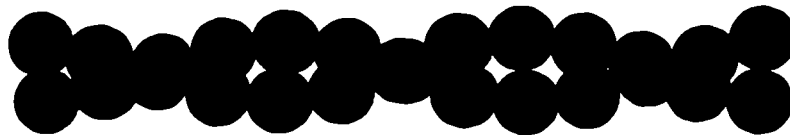


Figure 2.1: The 2-stranded helix of an actin filament. The different shading is only for viewing purposes.

the most abundant proteins within the cell, making up about 5% of the total protein mass [2]. Actin filaments are more prolific than microtubules, tend to be shorter and, due to their structure, they are thinner and more flexible [2]. As we will see with microtubules, the polymerization of actin into filaments requires two things: the presence of ATP as well as potassium and magnesium ions. If the concentration of actin monomers is below a critical level, the monomers will remain in solution. Above a critical concentration, actin polymerization is possible. ATP binds to the monomers which enables them to attach themselves to the growing filament. Shortly after attachment, the ATP hydrolyzes leaving a small 'ATP cap' on the growing end

of a microfilament. If this cap shrinks away, the binding rate of new monomers is reduced and the filament becomes unstable. A similar idea of a 'GTP cap' has been proposed for microtubules, but to date there is no evidence supporting or disproving such a claim.

Filamentous actin is a polar object and the assembly rate constant at the plus end is 5-10 times that of the minus end. This gives rise to an effect called 'treadmilling' where the plus end extends forward while the minus end disassembles. Such a process is common in the leading edge of motile cells. New actin filaments are nucleated, they extend with the leading edge of the cell and are dissolved as new filaments are formed in their place [8]. Rarely do microfilaments exist by themselves, but often in a network where the individual filaments are linked together by actin-associated proteins. These formations provide more strength and stability and may be in the form of sheets of loose bundles, such as lamellipodia, or thin protrusions such as microspikes [2]. There are three basic types of filament arrangements (see Figure

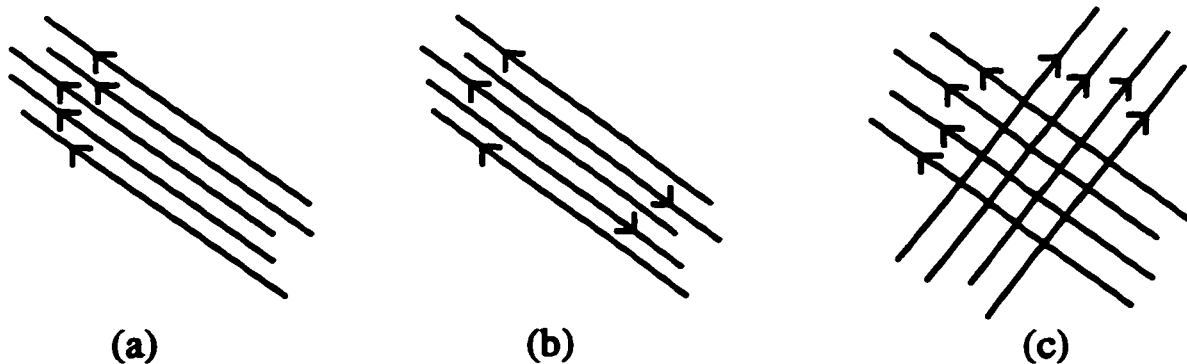


Figure 2.2: The three basic types of microfilament arrangement: (a) parallel bundles, (b) contractile bundles and (c) gel or lattice-like arrangement.

2.2): parallel bundles where the polar filaments are oriented in the same direction, contractile bundles where neighboring filaments are oriented opposite to one another and a gel or lattice-like arrangement where the filaments are orthogonal to one another [2]. Parallel bundles are seen in microspikes while the contractile bundles are what

allows muscle to extend and contract. The gel or lattice arrangement largely performs a structural role, usually at the leading edge of a cell [2].

The role played by actin filaments is a multi-faceted one. They first play a structural role as part of the cytoskeleton. In epithelial cells, the microfilaments give structure to the microvilli. In other cells, they act as 'railroad tracks' for cytoplasmic streaming [8]. The second role is the contractile role. Actin filaments are an intrinsic part of how muscle works, both striated and smooth muscle. In association with myosin, contractile bundles of actin are able to produce muscle movement [8]. They also form the contractile ring in dividing cells [2]. Lastly, actin filaments play an important role in cell motility. There are three basic steps in animal cell movement where microfilaments are involved [2]. These are: protrusion, the formation of lamellipodia and microspikes on the leading edge of a cell; attachment, where the actin cytoskeleton actually attaches itself to the underlying substrate; and traction, where the cell moves forward with the actin filaments pushing the leading edge and pulling the cell body [8].

Intermediate filaments

Intermediate filaments are a general class of filaments associated with the cytoskeleton. They are found in most multicellular animals, but not all [2]. In terms of structure, they are about 10 nm in diameter and have a rod-like structure that is common to all types of intermediate filaments. They represent a large and diverse family of proteins, but there are 3 basic classes within this group. Keratins are a type of intermediate filament typically found in epithelial cells and related cells such as hair, nails, etc. [2]. Vimentin and vimentin-like proteins are the major structural protein found in muscle and glial cells as well as neurons [8]. The last type are neurofilaments which are a unique type of filament found in nerve cells.

Despite the many different varieties of intermediate filaments, their role is largely

the same in providing structure and stability to the cell. Due to their structure and the way in which they bind with one another, they are able to withstand much larger stretching forces than either actin filaments or microtubules.

Microtubules are the third filament type associated with the cytoskeleton and the central theme of this thesis. They are the most complicated of the three types in terms of their structure and behaviour as will be discussed in the next section.

2.3 Microtubules

2.3.1 Tubulin

The basic building block of microtubules is the tubulin dimer. Tubulin is a protein that occurs within the cell in two homologous forms - the α and β -monomer. A third form γ -tubulin will be discussed later in this chapter. Undenatured tubulin is usually found in the form of a heterodimer of $\alpha - \beta$ tubulin. Within mammals, there exist numerous α and β types [2] but very little is known about their exact structure. The primary structure is fairly well known for many different monomer forms, each with around 450 amino acids. The secondary structure is environmentally dependent and contains both α -helices and β -sheets. The tertiary structure is currently being investigated by a large number of experimental groups, but no detailed results are available. It is thought that the folding and assembly of tubulin is largely governed by entropy and the hydrophobic part of the protein. It is also conjectured that the tertiary structure may change because of the hydrolysis of GTP into GDP. In terms of physical parameters, each tubulin monomer has a mass of about 50 kDa, giving the tubulin dimer a mass of 100 kDa. Electron microscopy studies reveal that each monomer subunit divides into two main globular domains and a smaller rod-like extension [8]. It also appears that the connection between the two monomers is hinge-like in nature which would allow for movement due to hydrophobic interactions

or conformational changes due to GTP hydrolysis [8]. Hopefully with more in-depth study, these details can be determined.

There is between 40% and 55% homology rate between α and β tubulin for various species, and a higher degree of homology between the same subunits for different species (comparing α to α , etc.) [8]. This similarity is enough that co-assembly of different tubulin types is possible, even types as different as those found in yeast and humans. For assembly to occur, GTP must be bound to the tubulin dimer. There exist two binding sites for guanine nucleotides within each dimer, a nonexchangeable site (N-site) within the α -monomer and an exchangeable site (E-site) within the β -monomer. The names of these sites refer to the fact that free tubulin dimers can exchange GDP for GTP from the E-site, but not from the N-site. There has been debate over which site is required to have GTP in order for the tubulin to assemble. There are also questions as to whether or not it is possible for transphosphorylation to take place, where a bound GTP molecule can exchange a P_i with a GDP molecule [9, 10]. To this point, this ideas are only speculation.

2.3.2 Assembly of microtubules

The self-assembly of tubulin into microtubules requires several factors: the presence of GTP and Mg^{2+} and a suitable temperature (ideally $37^\circ C$ but certainly above $7^\circ C$). The magnesium ions bind to the tubulin dimers at the E-site and promote assembly [8]. The binding of GTP changes the conformation of the dimer making it suitable for attachment onto a microtubule. This conformational change has several possible effects. First, it allows for the hydrophobic regions of the protein to be driven together (entropy promoting assembly) and second, it may alter the very acidic C-terminus of tubulin making the dimer able to attach itself to a microtubule. If this C-terminus is removed via proteolysis, the tubulin assembles without any problems [8]. All forms of assembled tubulin involve dimers bonded longitudinally into long protofilaments.

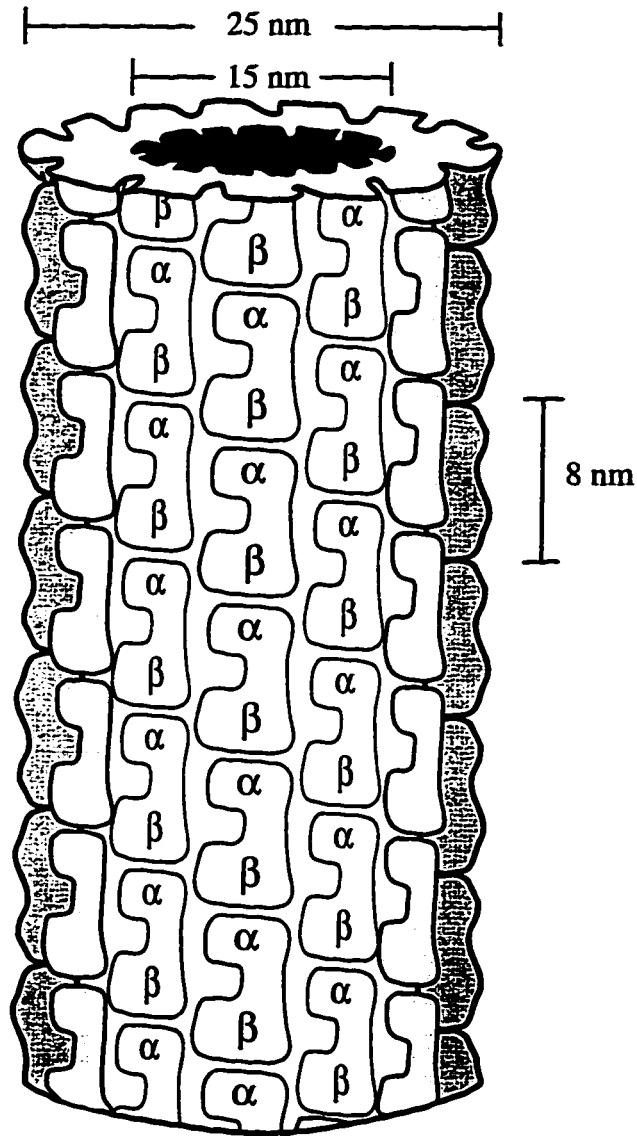


Figure 2.3: Illustration of the structure of a microtubule (B lattice) with its relative dimensions.

These protofilaments are polar and feature alternating tubulin monomers $\alpha - \beta - \alpha - \beta$, and so on. The lateral bonds between these protofilaments give rise to several different configurations. The first and most prolific form is that of microtubules. Their structure basically consists of protofilaments which are oriented in the same direction and bonded together to form a cylinder (see Figure 2.3). *In vivo*, the number of protofilaments is usually 13 or 14, but *in vitro* experiments can produce microtubules with 12 to 17 protofilaments. The dimers around the microtubule are not arranged in rings but rather along a helix. When one follows the $\bar{3}$ -helix around the microtubule, two distinct lattice types are seen. The first is the *A* lattice where the monomers on the helix alternate $\alpha - \beta - \alpha - \beta$. The $\bar{3}$ -helix on the *B* lattice has only one monomer type $\alpha - \alpha - \alpha$ or $\beta - \beta - \beta$. What is different with the *B* lattice is that there is a discontinuity or 'seam' in the microtubule (see Figure 2.4).

Apart from microtubules, with the addition of zinc ions, large Zn sheets may be formed where the protofilaments are bonded together, but the polarization alternates such that neighboring protofilaments point in opposite directions. The last commonly seen form of assembled tubulin is that of tubulin rings and oligomers. These are protofilaments of GDP rich tubulin which are coiled up. This is again evidence of the conformational change induced by GTP hydrolysis.

The first step in the formation of a microtubule *in vivo* is nucleation on a microtubule organizing centre (MTOC). The main site of nucleation within a cell is the centrosome which utilizes another isoform of tubulin called γ -tubulin in order to initiate a microtubule assembly process[2]. Nucleation is a very slow process since it requires several tubulin dimers to interact with one another at the same time. If there are other proteins present, this process can be sped up considerably. After nucleation, the microtubule begins to grow. There is an outstanding question as to the exact form of the nucleus and how a stable microtubule is formed. Two different experimental pictures have emerged. One is where the tube is formed and elongation

Microtubule Lattices

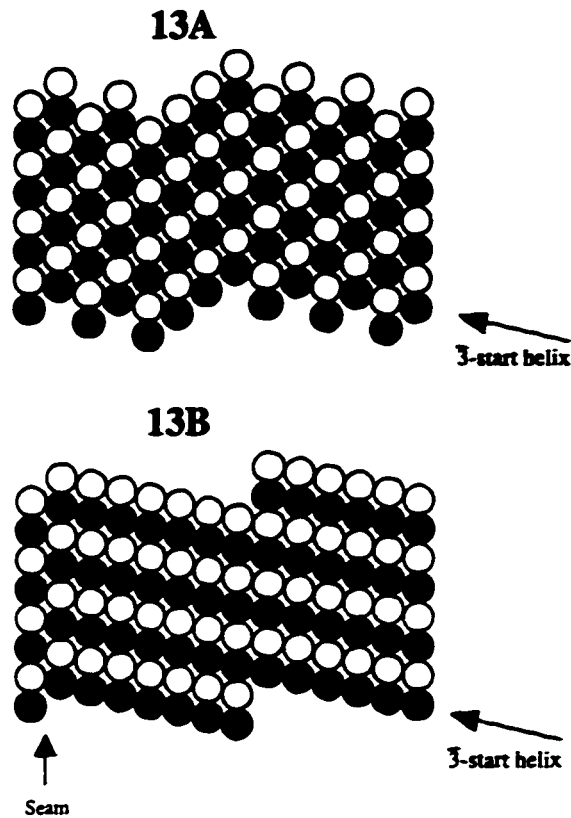


Figure 2.4: The A and B lattice types for a microtubule with 13 protofilaments.

occurs simply by adding dimers to the end of the tube. The second is where a sheet of protofilaments is formed. Once this sheet is wide enough, it can close to form the tube. In the first scenario, it is believed that hydrolysis occurs immediately after the dimer attaches itself to the microtubule. In the second picture, the closing of the sheet to form a tube causes hydrolysis to occur [11].

Microtubules are polar objects because of the way the dimers are organized into protofilaments. The end with the exposed β monomer is conventionally assigned as the (+) end and the α end is called the (-) end. The (+) end is the fast growing end and proves to be much more dynamic than the (-) end. The cell makes use of this fact and requires the (-) end to do very little. The (-) end is attached to the

MTOC and the (+) end always extends away. Thus assembly almost always takes place at the end which is able to grow the fastest. This growth is not monotonic, but dimers can be added on or taken off. The rate of growth is dependent on the tubulin concentration, but close examination of individual microtubules shows that while some are growing, other are shrinking. Even in a cell where the amount of assembled tubulin has reached a steady-state value, this is not a static state and there are still microtubules growing and shrinking. This behaviour has been termed *dynamic instability* [12, 13] and will be discussed more fully in the next chapter.

Objects interacting with microtubules

There are many factors which affect the assembly of microtubules. Aside from conditions within the buffer such as pH, temperature, etc. both drugs and other proteins can alter microtubule assembly. Several drugs prohibit the assembly of microtubules such as colchicine and nocadazole. These drugs bind to the dimers and prevent assembly [2]. Vinblastine causes assembled microtubules to fall apart into helically coiled protofilaments [8]. Other drugs such as taxol stabilize microtubules by binding to their ends, almost as a cap. Drugs such as vinblastine and taxol are used in the fight against cancer. If a cancerous cell would have one of these drugs added to it, it would be unable to divide and multiply since microtubules are required for mitosis.

A large group of proteins interact with microtubules and hence are given the name Microtubule Associated Proteins (MAPs). These types of proteins are very common and when one goes through the process of refining microtubules from solution, many MAPs co-purify with the tubulin. There is a wide variety of MAPs playing many different roles, but the general effect is to promote assembly [8]. The exact method in which MAPs could promote assembly is not known, but several possibilities exist. Some MAPs may bind and neutralize the acidic C-terminus of the tubulin dimer, thus reducing the repulsion between dimers. They may also reduce the electrostatic

repulsion at the interface between dimers [8]. Another possibility could be as simple as keeping the protofilaments straight to maintain the lateral bonds.

There are two basic classes of MAPs, lighter MAPs like tau with masses in the 50 kDa range and heavier MAPs such as MAP2 with masses closer to 300 kDa. Many MAPs are thought to have two main parts, one which binds to the microtubule and one which extends away from it [8]. Some of the heavier MAPs have binding domains of about 100 nm which means they are able to bind to about 12 dimers. This would correspond well with the periodic patterns that are observed in the binding of MAPs to microtubules.

Similar to the interaction between actin filaments and myosin, there are motor proteins associated with microtubules. These proteins, like MAPs, have a region which binds to the microtubule and a part which remains free to interact with other objects in the cytoplasm. There are two classes of microtubule motors: kinesins and dyneins. Both motors use ATP as their energy source, and they are able to move along microtubules or cause sliding between adjacent microtubules. There is polarity in the movement of each motor. Kinesin moves from the (-) end to the (+) end, ie. away from the centrosome. Dynein, on the other hand, has the opposite polarity and moves from the (+) to the (-) end [2]. Both motors are utilized in moving organelles and transporting materials within the cell. Apart from this linear movement, flagellar dynein can produce rotation [14] which is useful in cell motility.

Functions and arrangement of microtubules

As is implied by the name of the cytoskeleton, the main function of microtubules is to provide structure within the cell and give cell shape. In some cells, microtubules are the first structures to form. Materials are transported along them to the various parts of the cell, the other structures are assembled from these materials and the microtubules are dissolved [8]. Transport using molecular motors is obviously important,

but associated with transport is the microtubule involvement in mitosis. Here motors attach themselves to the end of a microtubule and a chromosome. The opposite end of the microtubule is embedded in one of the centrosomes. When the chromosomes align themselves along the mitotic spindle, the microtubules begin to disassemble at each end and the chromosomes are pulled to the two poles of the cell. Other types of movement include the rotary motion of flagella and the beating movement of cilia. Each process represents an important role played by these polymers.

It has been speculated that microtubules may play a role in signalling within the cell [6, 15]. To this point we have seen speeds from μm per minute to μm per second in both growth of microtubules and movement of motors. Signalling would require speeds much greater than this and must therefore be mediated by some other means. Sending signals along microtubules by using their dipole properties is a possibility [16, 17], but experiments are far from detecting such phenomena.

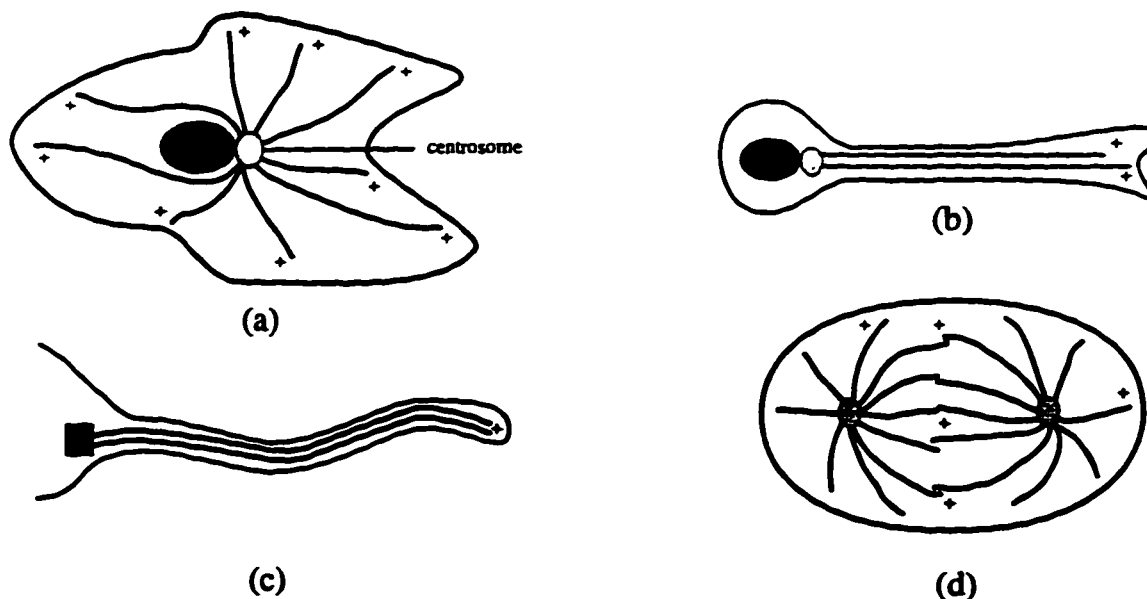


Figure 2.5: Illustration of different cell types with their microtubule arrangement: (a) interphase cell, (b) nerve cell, (c) ciliated cell and (d) a dividing cell.

The manner in which microtubules arrange themselves within the cell is dependent

on their function. Figure 2.5 shows several different types of cells and the microtubules within them. It goes without saying that these structures are vital to the function of the cell and indeed of the organism composed of such cells.

Chapter 3

Experimental Results and Previous Modelling

Although microtubules have been studied for the last half of this century, it is only within the past 15 years that the technology has really allowed scientists to view and manipulate individual microtubules. This chapter will summarize the experimental findings of researchers investigating the assembly of microtubules as well as theories that have been developed to attempt to explain these observations.

3.1 Experimental Results

As mentioned earlier, experimental groups were using the birefringence properties of microtubules to obtain images from within living cells [18]. Microtubules were able to be seen only when they occurred in large groups or bundles, such as the mitotic spindle of a dividing cell. In the 1970's, methods were developed whereby microtubules could be assembled *in vitro* from purified tubulin. During the next decade, microscopy was advanced enough that individual microtubules could be seen. Although the basic properties of these structures were known, a closer inspection of

microtubule assembly yielded quite a different picture than what was expected.

3.1.1 Dynamic instability

Mitchison and Kirschner [12, 13] were the first to use the term *dynamic instability*. They noticed that within a buffer containing microtubules, even though conditions were the same for all the polymers, some microtubules would be growing while other were shrinking. Shortly after this, Horio and Hotani [19] provided the plots of a single microtubule and its length as a function of time. These sharp, sawtooth-like plots (see Figure 3.1) were thought to be the result of the microtubule maintaining or losing a terminal GTP cap. When hydrolysis occurred faster than assembly did, the cap would be lost and the microtubule would become unstable and collapse. These ideas were expanded in later work by Kirschner and Mitchison [20] where they investigated the relationship between the physiochemical properties of microtubules and their dynamics. However, Walker et al. [21] showed how, if there was a GTP cap, it would have to be very small and its size would not depend on the growth rate of the microtubule. The one key finding which seems to dismiss the concept of a GTP cap is the fact that when microtubules are severed at their midpoint, the new (+) end rapidly disassembles, but the (-) end behaves as normal [8]. This would perhaps indicate that the $\alpha - \alpha$ and $\alpha - \beta$ bonds are not affected. Since the GTP bound at the N-site in the α monomer does not hydrolyze, the (-) end may remain stable. Because the (+) end is unstable, this would indicate that the $\beta - \alpha$ and $\beta - \beta$ bonds have been weakened, perhaps due to the hydrolysis at the E-site and the resulting conformational change. This interesting behaviour is not restricted to the laboratory. *In vivo* experiments have also shown that dynamic instability occurs within living cells [22].

Just as the reason for catastrophes is not known, the mechanism behind rescue events is also a mystery. It was originally thought that due to the large number of

Microtubule Associated Proteins (MAPs) that co-purify with tubulin, these proteins were able to stabilize shrinking microtubules and instigate a rescue. Recent work by Billger et al. [23] showed that with virtually MAP-free tubulin, rescues still occurred with normal frequency indicating that some other mechanism is the cause. In fact, this group found that assembly using MAP-free tubulin changed very few characteristics.

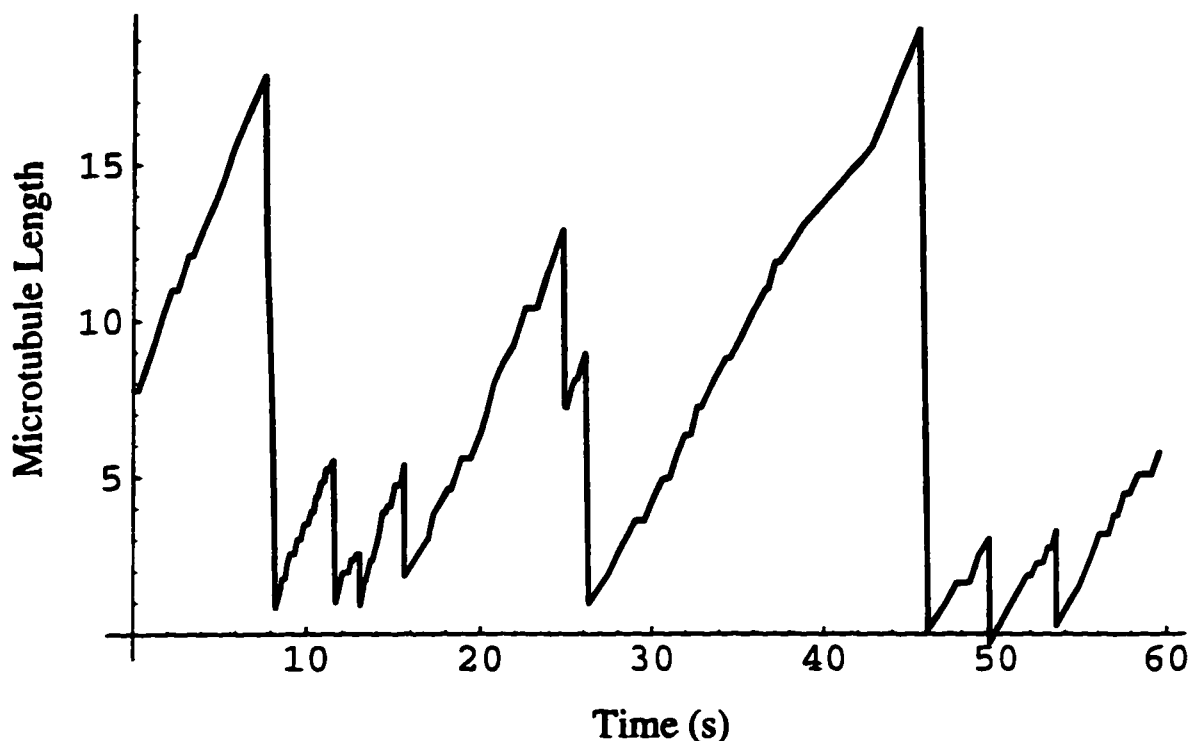


Figure 3.1: Experimental data of the growth of a single microtubule. Data courtesy of E. Mandelkow.

Many experiments are still being performed on this well researched subject. Recent reviews [24, 25] indicate that this problem is far from being well understood. There have also been investigations on whether there exists a GDP-P_i cap instead of a GTP cap [26, 27, 28, 29]. Perhaps the phosphorylation process may produce a conformational change that would make a microtubule unstable.

3.1.2 Microtubule Oscillations

Several years after the discovery of dynamic instability, a new type of behaviour was found by several groups at roughly the same time. When the buffer and temperature conditions were correct, it was found that the total amount of assembled protein would not simply grow to saturation as had been seen previously, but would instead oscillate around a steady-state value (see Figure 3.2). Depending on the experimental conditions, the oscillations would eventually be damped out and the system would assume its steady-state value.

Pirollet et al [30] discovered they could produce oscillations in a system with a mechanism that would regenerate GTP from the GDP given off in a microtubule collapse. As the oscillations would proceed, the average length of the individual microtubules would increase while the number would decrease. The key to this system seemed to be the amount and the production rate of GTP. If additional GTP was added to the system, the oscillations would decrease in size and eventually disappear. In the same respect, increasing the speed of GDP to GTP conversion decreased the amplitude of oscillations. If the acetate kinase responsible for the GTP production was decreased in concentration, oscillations would increase in size. Even if the tubulin concentration was dropped to a point where oscillations were not present, decreasing the amount of acetate kinase would cause them to reappear. This conclusion was supported by Melki et al. [31] who found that the rate of GDP/GTP exchange regulated the period of the oscillations. They stated that oligomers were not necessary for oscillations to occur, but the data supported either slow nucleotide exchange or slow oligomer breakup. They did consider it a possibility, however, that assembly competent tubulin may be blocked from the end of the microtubule by an excess of tubulin bound with GDP.

Carrier and her group [32] found that at tubulin concentrations of 25 - 30 μM , there was simply growth to saturation. At concentrations greater than 50 μM how-

ever, oscillations would arise following spontaneous nucleation. The amplitude and amount of damping varied, depending on the rate of nucleation. Also, by shearing microtubules they were able to determine that this behaviour was not simply due to large numbers of microtubules. Independent of the tubulin concentration (above the critical concentration), 35-40% of the available tubulin would be polymerized when oscillations ceased.

Wade et al. [33] had similar results to those of Carlier's group in that by increasing the free GTP concentration, they found that the system would shift from oscillations to monotonic polymerization. In contrast to previous authors, they postulated that the slow step in the process was the breakup of oligomers and not the regeneration of GTP. To support this they claimed that as they increased the concentration of GTP, the number of rings visible decreased and the oscillations were gradually removed.

This scenario involving the slow breakup of oligomers was also put forward by Caplow et al [34]. However, there was also the suggestion that the oligomers were formed in a side reaction not directly associated with microtubule assembly. They found the formation of oligomers increased sharply with GDP concentration and that the half-time for dissociation of GDP from an oligomer was about 6 times longer than from a single tubulin dimer.

Engelborghs [35] demonstrated how one slow step in the assembly process would not be enough to explain oscillations. According to Oosawa's theory of polymerization [36], the steady-state properties are purely determined by the rate constants. In this system however, constant turbidity is not a static situation but instead GTP is constantly being consumed and GDP produced.

A tremendous amount of work has been performed by the Mandelkow group in Hamburg. They have produced several papers in recent years dealing with microtubule oscillations [37, 38]. They distinguish between two different types of oscillations: 'high-GTP' and 'low-GTP' oscillations. The 'low-GTP' case is where GTP

is regenerated enzymatically so it is not in overabundance. The period of oscillation here tends to be about 10 minutes, much longer than in the 'high-GTP' case where the period tends to be in the 70-80 second range. With high GTP concentration, however, some type of destabilizing agent is required (Na^+ , K^+ or Ca^{2+}). In either case, there is a minimum number of polymers required for oscillations and the concentration of both polymers and free subunits determines the mode of assembly. Generating this minimum polymer concentration can be done through the addition of seeds or by self-nucleation.

There is one interesting aspect of microtubule oscillations that it seems has only been reported by the Mandelkow group [39]. Homogeneous oscillations do occur, but inhomogeneous oscillations are also common. These inhomogeneous oscillations often are adapted to the geometry of the vessel in which the experiment is taking place. In rectangular 'cells' one sees linear waves of assembly and disassembly passing through the medium and in circular vessels concentric waves form on the outside and move towards the center and disappear. These waves are not started by a jump in temperature, but it seems as if the nucleation barrier is lower at the periphery. The reaction is started at a nucleation site and then proceeds autocatalytically via diffusion coupling.

All of the above mentioned experiments took place *in vitro*. Just as there was evidence for dynamic instability within living cells, oscillations have also been seen. During metaphase in a dividing cell, chromosomes attached to microtubules have been seen to oscillate with oscillation periods in the 60 second range [40]. It is difficult to determine the mechanism behind these oscillations and whether it corresponds to the experiments done *in vitro*.

3.2 Previous modelling

As more and more experimental data became available, models have been developed to try to explain these two types of assembly within microtubules. Obviously some methods have been more successful than others. This section will briefly outline some previous attempts.

3.2.1 Dynamic instability

Immediately following Mitchison and Kirschner's discovery of dynamic instability, models were produced by Hill and Chen in a series of papers [41, 42, 43]. Their method was a Monte Carlo simulation on a 5-start helix where they assumed the presence of a GTP cap and a 13 protofilament A lattice. They had specific binding rules for new dimers on the end of a microtubule and a total of 24 hydrolysis rate constants. Similar methods were employed by Bayley and co-workers [44, 45, 46]. They also used a Monte Carlo approach, but considered two states for the microtubule: growing and shrinking. They again assumed the presence of a GTP cap and a coupled hydrolysis mechanism where the binding of an additional dimer would cause the hydrolysis of the dimer beneath it. If this terminal layer of GTP rich tubulin was lost, the microtubule would switch from growing to shrinking. This Monte Carlo technique was furthered by Gliksman et al. [47]. They again only considered assembly of the '+'-end. The predictions from this model were consistent with Bayley's group, including the population distributions that resulted from the simulations.

Much more recently, Flyvbjerg et al. [48] proposed a model involving stochastic GTP hydrolysis as opposed to the coupled hydrolysis mechanism. This model produces small GTP caps, but they are small enough to be consistent with experimental findings. Unfortunately, no plots of the growth profile of an individual microtubule were provided.

3.2.2 Microtubule oscillations

Just as in the case of dynamic instability, Chen and Hill were the first to attempt to produce a model for microtubule oscillations [49]. They only considered a single end of a polymer and assumed a growing and a shrinking phase. The transition rates between these two phases were dependent on the tubulin concentration. Their model did not allow for the disappearance of polymers and there was a very limited range of rate constants that produced “semi-satisfactory” results.

Marx and Mandelkow [50] produced a model for oscillations in the ‘high-GTP’ case. They considered growing and shrinking microtubules as separate entities and had a very complicated set of equations governing the transitions between free tubulin and microtubules and the binding of nucleotides. The rate constants in their model had a complicated exponential dependence and there was a total of 15 free parameters. They could produce reasonable oscillations, but only if they did not include the dependence of the catastrophe and nucleation rate on the concentration of GTP. They also stated that they required some additional effect of oligomers and tubulin on microtubule nucleation or catastrophe. They went on to perform Monte Carlo calculations with over 2000 coupled equations. They concluded that the nonlinear dependence of nucleation, catastrophes and rescues on the concentration of GTP rich tubulin was not enough to produce oscillations. They also stated that it seemed likely that the presence of GDP rich tubulin could significantly increase the catastrophe rate.

A recent paper by Houchmanzadeh [51] considered growing and shrinking microtubules. With these two species, they set up two coupled reaction equations in (1+1) dimensions. Very high concentrations were required to produce oscillations and they would disappear if the GDP to GTP conversion rate was increased or decreased. As written in a paper by Mandelkow et al. [38], ‘All models are unsatisfactory in some respect, either in curve shape, amplitude or damping factor’. This is the problem which we will attempt to address.

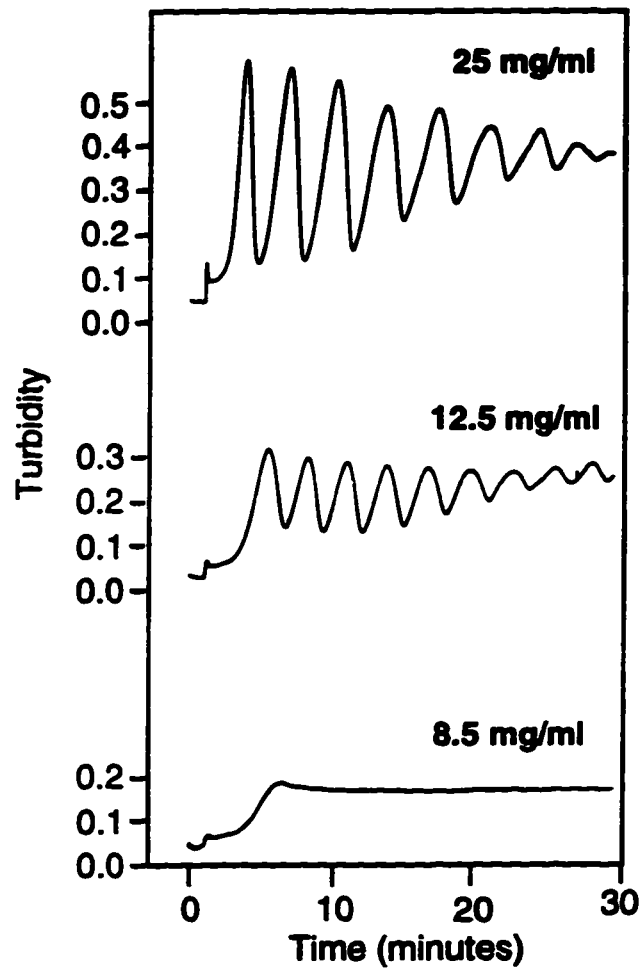


Figure 3.2: Experimental data showing the oscillations of an ensemble of microtubules. The amount of oscillation varies with the tubulin concentration (given in the inset). Data courtesy of E. Mandelkow.

Chapter 4

Modelling Single Microtubule Growth

As described in the previous section, several authors have modelled dynamic instability in microtubules, mostly by Monte Carlo methods. In these simulations, sets of rules are set up and the system simply evolves according to these rules. The factors controlling microtubule assembly are many and their effect is not always well understood. The obvious controlling factors are temperature, tubulin concentration and the supply of GTP, but there are also large effects from pH, assembly promoting elements such as DMSO or Mg^{2+} and assembly inhibiting factors like Na^+ , K^+ or drugs such as taxol. The basic elements of growth are known, the process of shrinkage and the reason for collapse, however, are not well understood. Originally, it was speculated that a microtubule collapsed due to the loss of a GTP cap, a feature known to exist in actin filaments. No evidence has been found for this cap and the actual destabilizing mechanism is not known.

4.1 Statistical Analysis

The irregularity of the growth and shrinkage patterns observed in experiments suggest a complicated behaviour. In most of the biophysical and biological literature, two main modes of behaviour have been identified and termed: (a) catastrophes, a sudden change from growth to shrinkage, and (b) rescues, a sudden change from shrinkage to growth. The implication is that these are two distinct phases that the system must choose between. These phases are very different from each other and it seems likely that they are in fact independent. The overall tendency is for microtubules to grow. It is perhaps more plausible that there is one stable phase (growth) that provides the dynamical background. The smooth and largely linear behaviour of this growth phase is occasionally interrupted by stochastic, unpredictable events (catastrophes).

The question of the degree of randomness in terms of frequency and size of catastrophes has not been answered. Several authors have examined the statistical properties of these events [52, 53] and have found limited results. It appears as if the power spectrum of microtubule length life histories has an exponent of 1.1-1.2, but conclusions are difficult to draw from this. We will examine the growth profiles using a different method. First for interest's sake, using standard Fourier analysis, we can find the Fourier transforms for the different assembly plots. No dominant frequency can be distinguished. Also, no characteristic features of period doubling or transitions to chaos can be detected in these plots (see Figure 4.1(b)).

Another method of looking for order within a seemingly random system is to calculate the Hurst exponent [54]. Hurst developed a statistical method for dealing with series of observations which he called 'rescaled range analysis'. To perform this analysis we require several definitions. Following Feder [54], we assume that we are measuring a variable ξ as a function of time. The average value of ξ at a given time

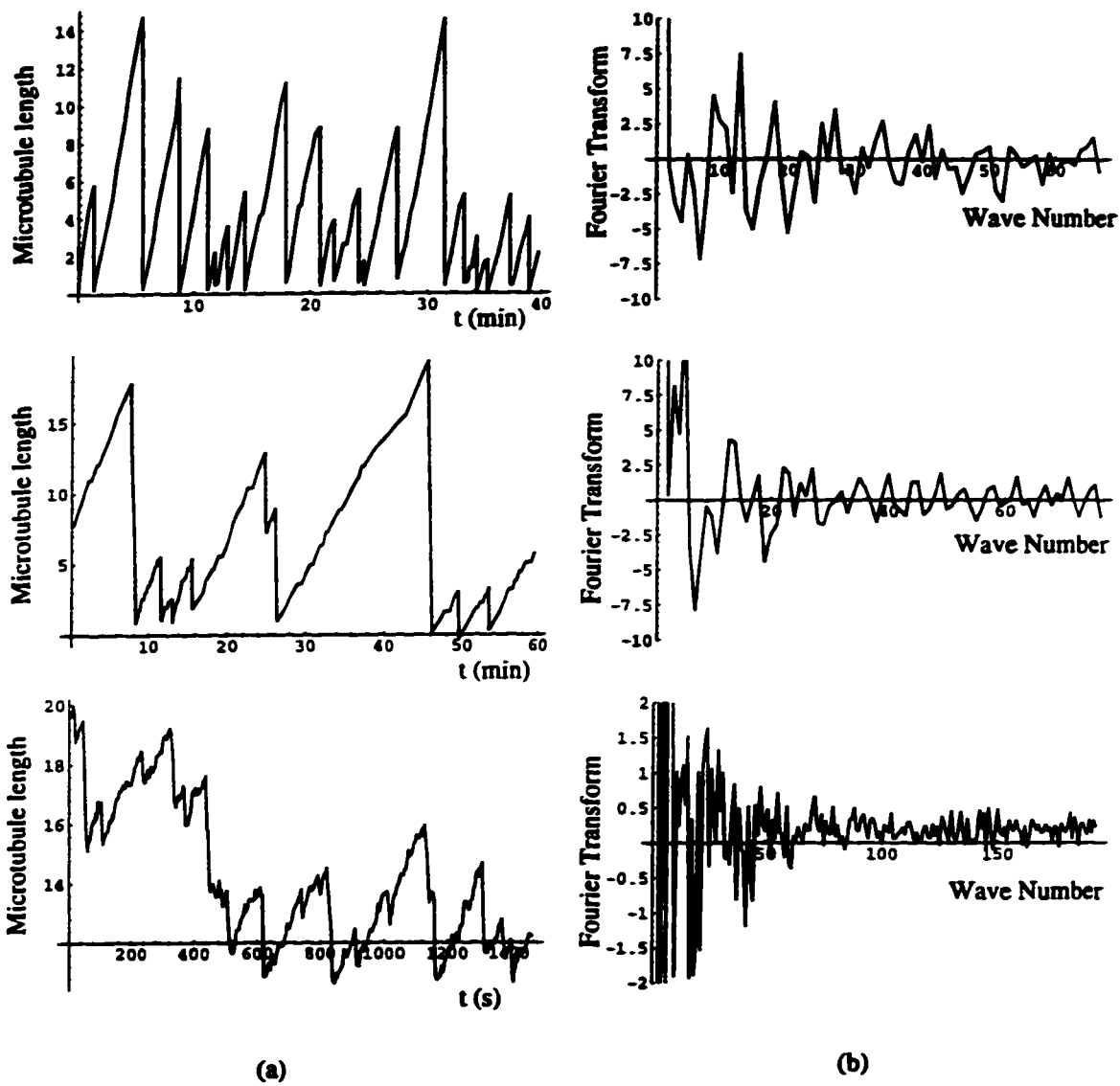


Figure 4.1: Three sets of experimental data for single microtubule growth and their Fourier transforms. Top two set of data courtesy of E. Mandelkow and the bottom data courtesy of S. Pedigo.

τ is

$$\langle \xi \rangle_\tau = \frac{1}{\tau} \sum_{t=1}^{\tau} \xi(t). \quad (4.1)$$

The accumulated departure of $\xi(t)$ from the mean value $\langle \xi \rangle_\tau$ is defined as

$$X(\tau, t) = \sum_{u=1}^t (\xi(u) - \langle \xi \rangle_\tau). \quad (4.2)$$

The range R is the difference between the maximum and minimum values of $X(\tau, t)$, namely

$$R(\tau) = \max_{1 \leq t \leq \tau} X(\tau, t) - \min_{1 \leq t \leq \tau} X(\tau, t). \quad (4.3)$$

The range R will be rescaled by the standard deviation S defined by

$$S = \left(\frac{1}{\tau} \sum_{t=1}^{\tau} (\xi(t) - \langle \xi \rangle_\tau)^2 \right)^{1/2}. \quad (4.4)$$

So for a time series of recorded observations, the rescaled range should the relationship

$$\frac{R}{S} = \left(\frac{\tau}{2} \right)^H \quad (4.5)$$

where H is the Hurst exponent which is bounded between 0 and 1. A Hurst exponent of 0.5 indicated a purely random process or 'white noise'. A process with $H > 0.5$ indicates persistence or a correlation between the past trend and future behaviour. This means if a variable was increasing in the past, it should continue to increase. $H < 0.5$ implies antipersistence or anticorrelated behaviour. Most natural phenomena follow Hurst statistics, usually displaying persistence. This is not surprising since most naturally occurring events depend to some extent on past history (eg. rainfall, temperature, etc.).

We have three different data sets to work with, each one for a microtubule undergoing a series of catastrophes and rescues (as shown in Figure 4.1(a)). These data look similar to one another to a certain extent, but they differ with respect to growth velocity, frequency of catastrophes and rescues, and the general smoothness of the

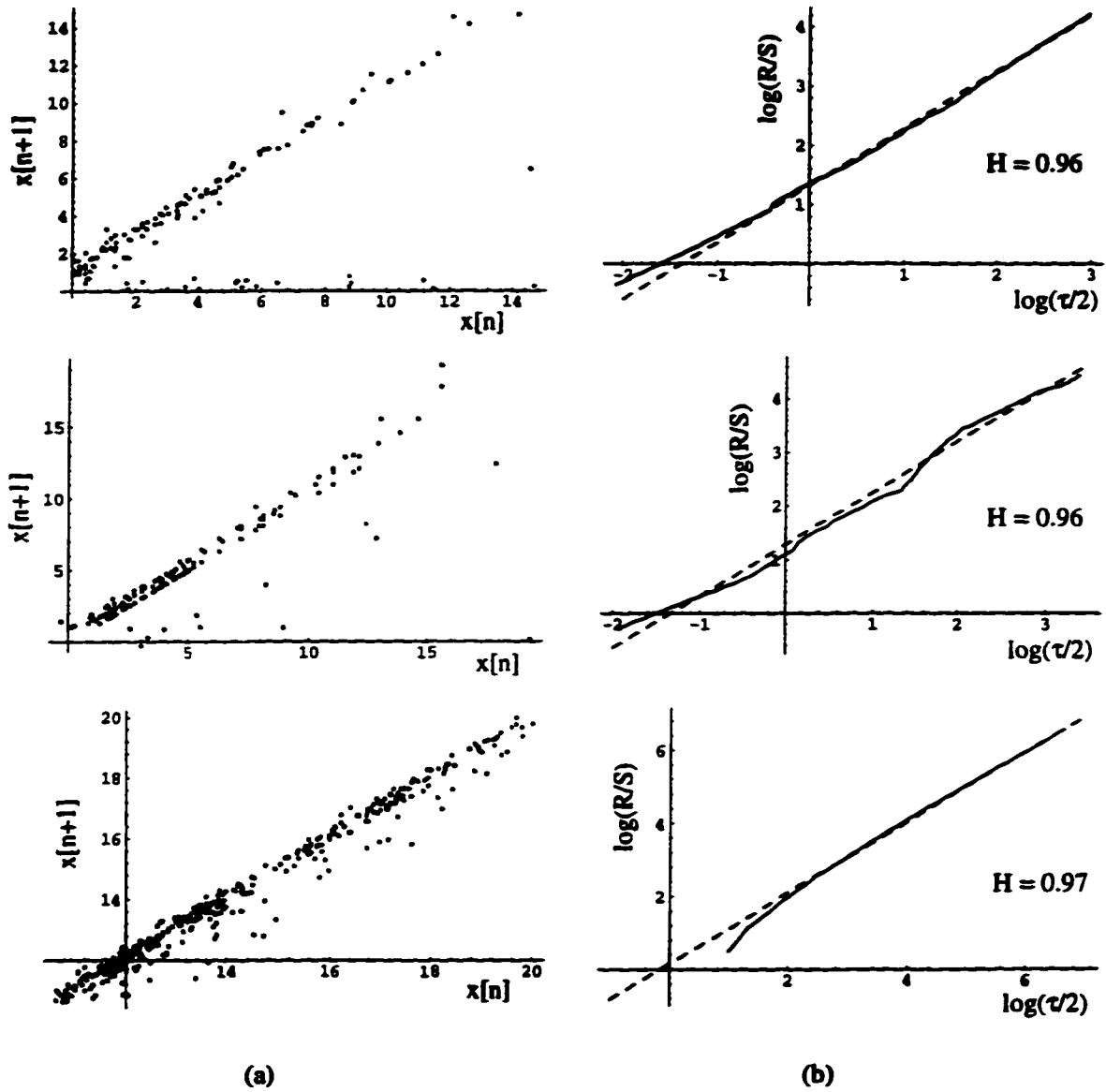


Figure 4.2: Recursive maps and Hurst analysis for the three sets of experimental data given in Figure 4.1.

plots is different. Instead of the usual time series representation of the experimental data, let us represent it as a recursive map where we plot the length of a microtubule at time t_n versus the length at time t_{n+1} . These plots show a predominantly linear nature with another branch near the x-axis (Figure 4.2(a)). This again supports our postulate of a steady growth phase interrupted by catastrophes. If we perform rescaled range analysis and plot $\log(R/S)$ versus $\log(\tau/2)$ we get the plots shown in Figure 4.2(b). Despite the differences in the data, the Hurst exponents are 0.96, 0.96 and 0.97, respectively, for the three plots above. This indicates a process that is highly persistent and strongly supports the idea that this dynamic behaviour is the result of a growth phase being stochastically interrupted by catastrophes. This may also demonstrate that the mechanism causing this instability is the same in all three systems. This rescaled range analysis will prove useful in differentiating between various models that we will develop next.

4.2 Recursive Maps

With these statistical aspects in mind, we can try to develop our own system for modelling dynamic instability. We can model this using a very simple stochastic map:

$$x_{n+1} = r(x_n + a) \quad (4.6)$$

where a is the amount of growth, x_i the length of the microtubule at time t_i and r is a random number chosen as

$$\begin{aligned} r &= 0 \text{ with probability } P \\ r &= 1 \text{ with probability } 1-P. \end{aligned} \quad (4.7)$$

$1 - P$ is the probability that the microtubule will grow by an amount a and thus P is the probability that the microtubule will collapse to length zero. We can get a value

for a from experiments since it simply represents the growth velocity multiplied by the time interval between t_n and t_{n+1} .

What is obvious from looking at the experimental plots is that quite often the collapse of a microtubule is not complete. To represent this, we can modify our linear map to a more general form

$$x_{n+1} = r(x_n + b)c + (1 - r)(x_n + d)e. \quad (4.8)$$

If we choose $b = 1$ (ie. one unit of addition), $c = 1$, $d = 0$ and $e = 0.3$ (microtubule collapses to 30% of original length), we can produce more realistic maps. The parameter e can easily be found by taking the slope of the branch near the x-axis on the recursive map plots. A plot of the growth profiles in Figure 4.3(a) and the accompanying recursive maps in Figure 4.4(b) agree well with the experimental picture. They were done for two choices of the probability $P = 0.10$ and $P = 0.05$. The plots in Figure 4.3(a) and (b) look very similar to each other. Note that by changing the value for e we can move the lower branch of the recursive map closer to the x-axis or closer to the diagonal line in the center of the graph. If we calculate the Hurst exponents, we find that $H = 0.69$ for the choice of $P = 0.10$ and $H = 0.96$ for $P = 0.05$. The rescaled range plots along with the linear fits are given in Figure 4.3(c). This added analysis gives us a method of selecting one choice of P over another.

To this point, we have assumed the probability of collapse to be constant. Experiments show that with rising tubulin concentration, the probability of a microtubule collapsing goes down. As well, we would expect that as the amount of assembly competent tubulin is decreased (simply because it is assembly into a microtubule) the catastrophe probability should increase. Thus we can make the adjustment as

$$P = P_0 + P_1 \frac{s}{\text{units}} \quad (4.9)$$

where P is still the probability of collapse, s is the length of the microtubule and units is the total number of tubulin subunits available for assembly. The base probability

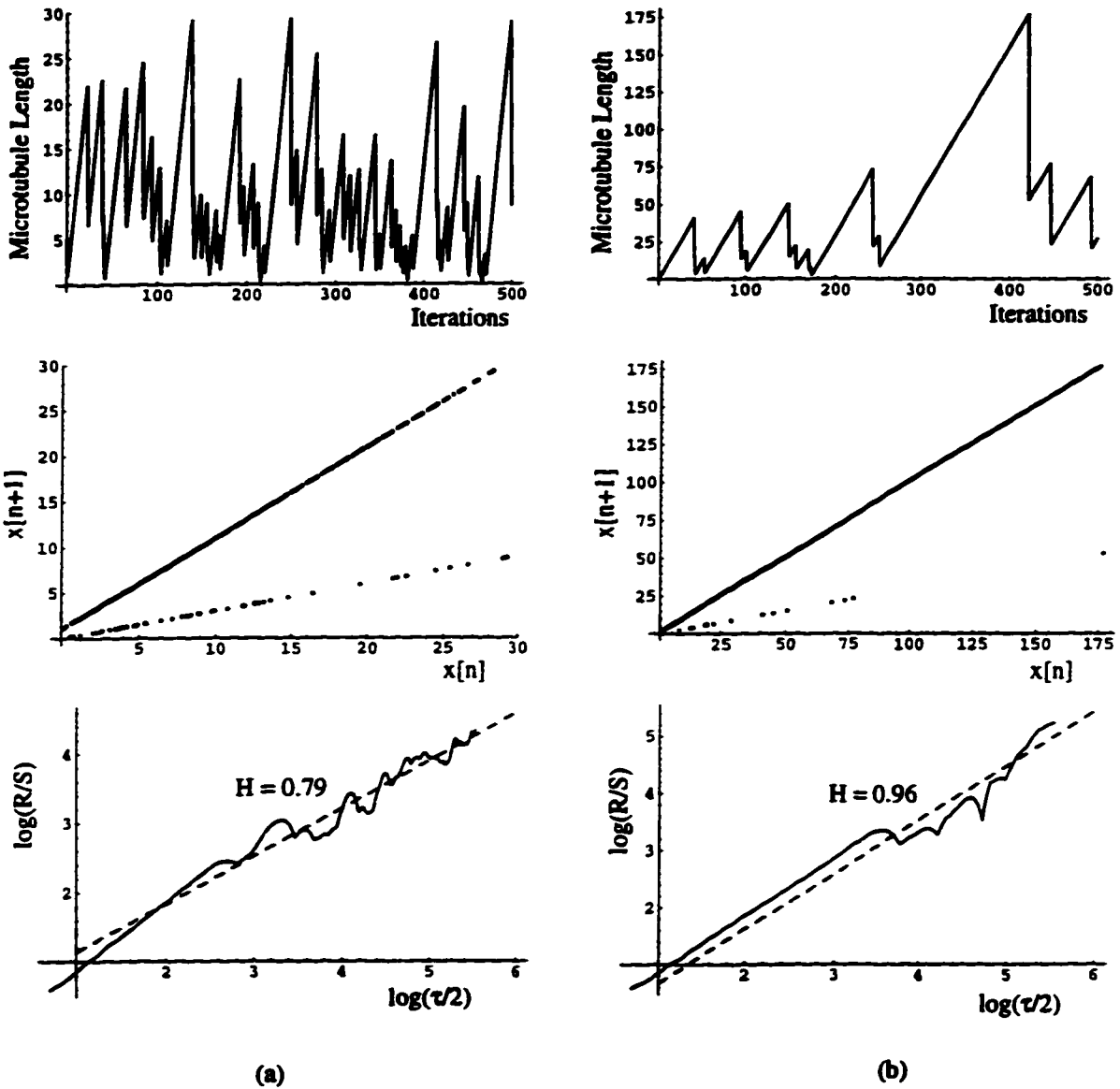


Figure 4.3: Growth profiles, recursive maps and Hurst analysis for two simulations with: (a) $P = 0.10$ and (b) $P = 0.05$. The resulting Hurst exponents are given in the inset.

is $P_0 = 0.05$ as was determined in our initial analysis. Figure 4.4 shows the plots, recursive maps and Hurst analysis for two cases: $P_1 = 0.5$ and 0.9 . The Hurst exponents for these two case were 0.73 and 0.65 , respectively. Other cases have been investigated, but the transition behaviour is smooth down to the point $P_1 = 0$ where once again $H = 0.96$.

This increase in collapse probability due to the tubulin concentration is not the only effect we need to consider. Figure 4.5(a) shows a schematic presentation of the growth of an individual microtubule from nucleation to a steady state as adapted from Alberts et al. [2]. The time derivative of such a plot would give the rate of microtubule growth. We can fit the plot quite well with the function

$$L = 0.4(1 + \tanh(t - t_1)). \quad (4.10)$$

L is the length of the microtubule which goes from 0 to 0.8 and the time t is in arbitrary units. If we take the derivative we get

$$\frac{dL}{dt} = 0.4 \operatorname{sech}^2(t - t_1). \quad (4.11)$$

If we invert eq.(4.10) we can write

$$t - t_1 = \tanh^{-1}\left(\frac{L}{0.4} - 1\right) \quad (4.12)$$

which substituted into eq.(4.11) gives us

$$\frac{dL}{dt} = 0.4 \operatorname{sech}^2\left(\tanh^{-1}\left(\frac{L}{0.4} - 1\right)\right) = 0.4\left(1 - \left(\frac{L}{0.4} - 1\right)^2\right). \quad (4.13)$$

Thus the rate of growth varies with the length as shown in Figure 4.5(b), reaching a maximum rate when the microtubule is roughly half of its steady-state value. It is logical to assume that as the probability of binding a dimer goes up, the rate of growth would be higher. Thus we assume an additional component to the collapse probability

$$P = P_0 + P_1 \frac{s}{\text{units}} - P_2 \left(0.4\left(1 - \left(\frac{s}{0.4 \text{ units}} - 1\right)^2\right)\right). \quad (4.14)$$

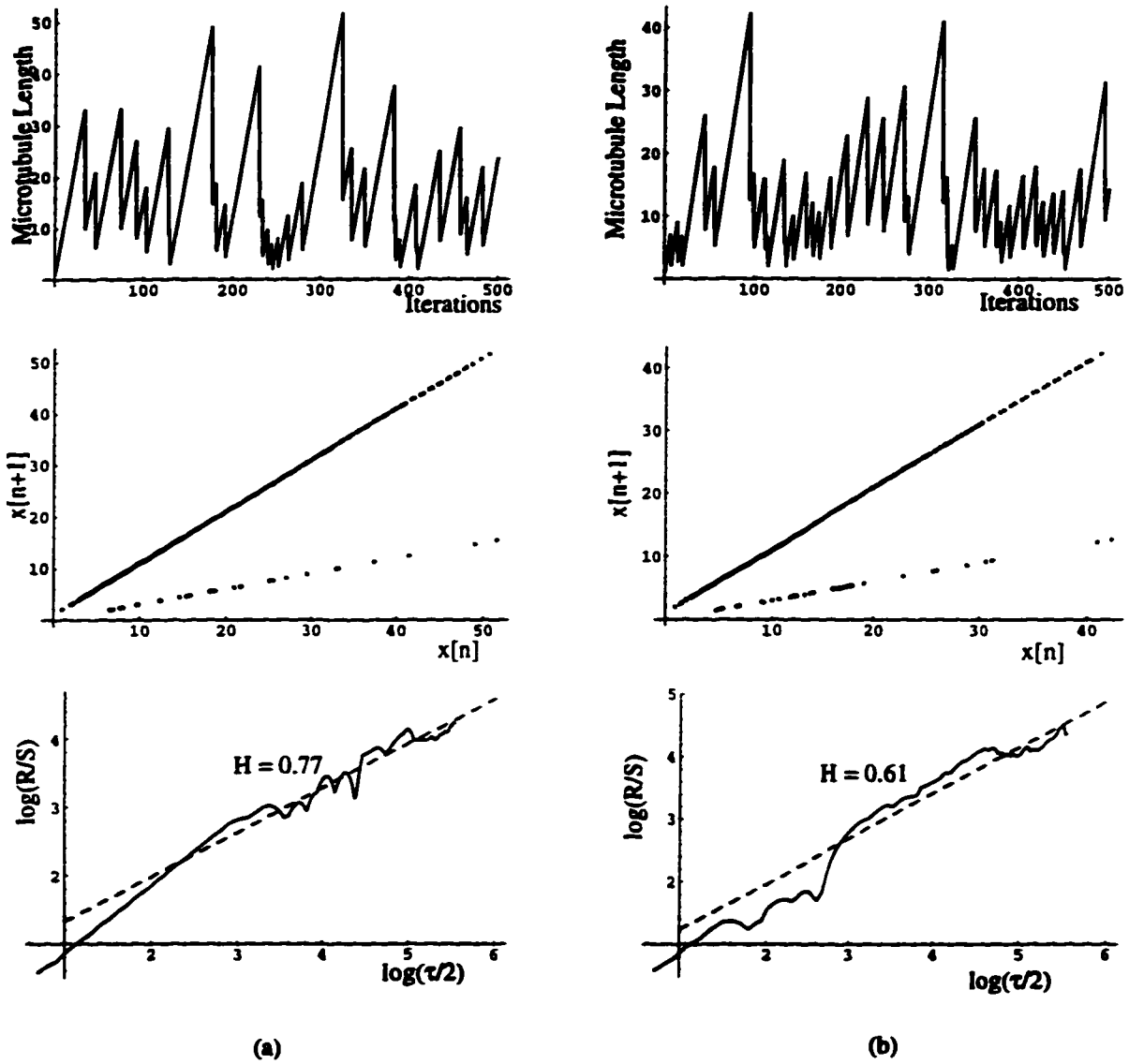


Figure 4.4: Growth profiles, recursive maps and Hurst analysis for two simulations with: (a) $P_1 = 0.5$ and (b) $P_1 = 0.9$. The resulting Hurst exponents are given in the inset.

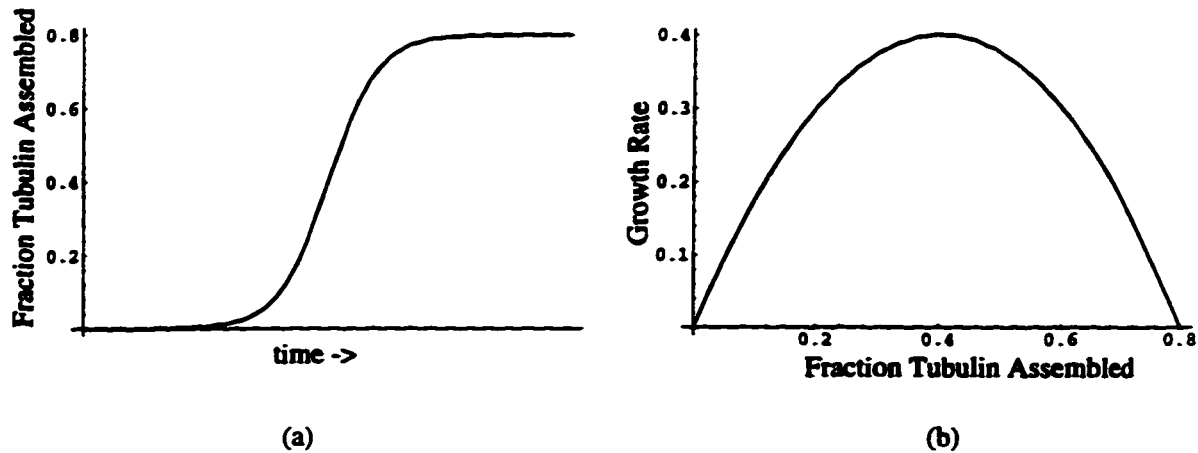


Figure 4.5: (a) Schematic representation of the growth of a microtubule (adapted from Alberts et al. [2]) and (b) the derivative of this plot showing rate of growth.

Once again we fix $P_0 = 0.05$, but P_3 must not be chosen too large to avoid our probability P becoming negative. A reasonable choice proves to be $P_2 = 0.7$ and $P_3 = 0.2$. Figure 4.6 shows all the plots for these choices of parameters.

We have included two pieces of information as to how the collapse probability is affected by the tubulin concentration and the length of the microtubule. With this, we have managed to reproduce plots that reasonably agree with the picture from experiments. As well, our simulations produce similar recursive maps and Hurst exponents. The ultimate goal, however, is to explain the transition from the stochastic behaviour of a single microtubule to the smooth oscillations of an ensemble. By coupling many of these recursive maps together, we hope to achieve that end.

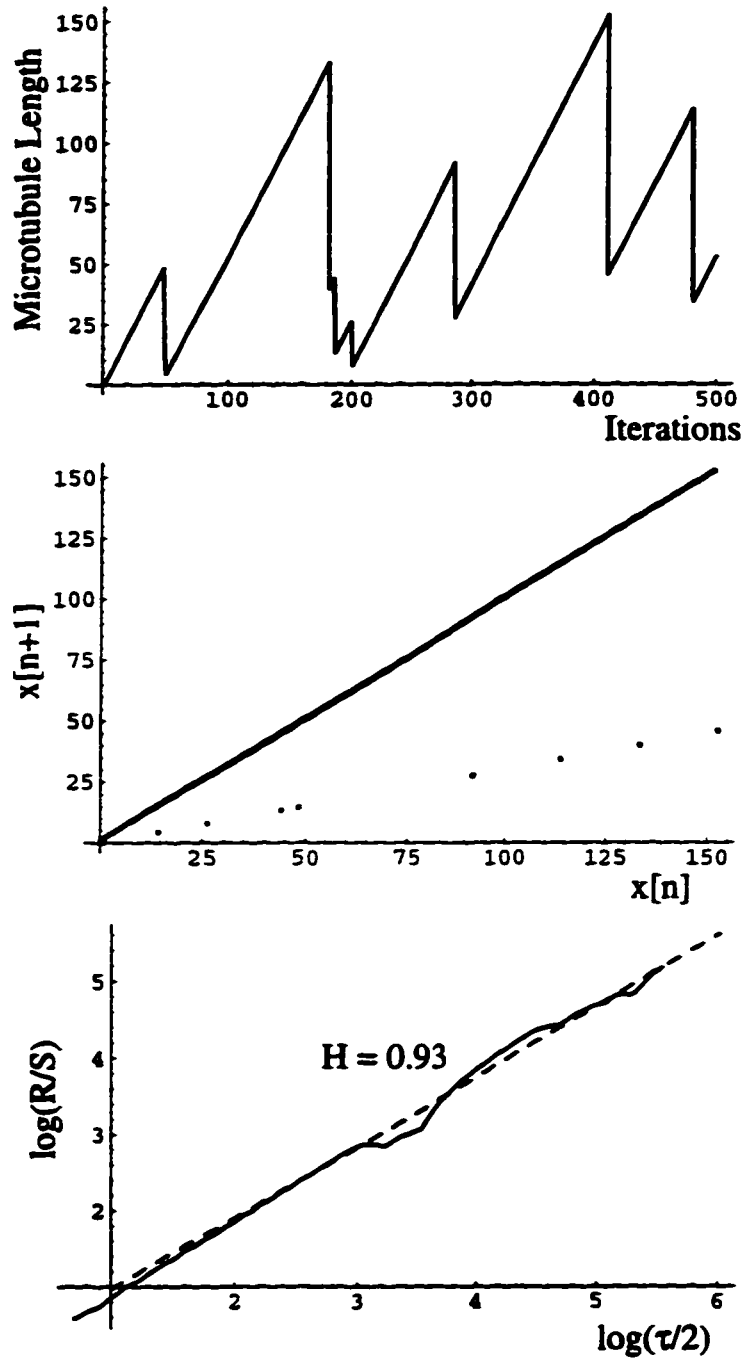


Figure 4.6: Growth profiles, recursive maps and Hurst analysis for a simulation with $P_0 = 0.05$, $P_1 = 0.7$ and $P_3 = 0.2$. The resulting Hurst exponent is given in the inset.

4.3 Coupled Recursive Maps

The transition from the stochastic growth of a single microtubule to the coherent oscillations of an ensemble of microtubules is as of yet not well understood. It is postulated that the microtubules begin in a synchronized state and evolve, eventually losing this synchrony due to dynamic instability. This seems plausible in experiments where the onset of nucleation and oscillations comes from a fast temperature jump. In this situation, the entire microtubule ensemble begins in the same state. In other cases where oscillations are seen, there is no known mechanism that starts the ensemble out under such controlled conditions.

There is a need for microtubules within an ensemble to be able to communicate with one another. This may occur via dipolar interactions, but what we will consider will be communication via some biochemical means. The microtubules are growing within the same buffer and this may be their point of interaction. All of the models derived here have given realistic results in terms of the growth profiles for single microtubules, even of different types. By coupling several of these recursive maps together, we can gain some idea of the ensemble behaviour. The coupling in this case is simply due to the fact that all the microtubules are growing from a common pool of tubulin.

A note is in order here on the computational methods employed. Each microtubule obeys a recursive map as given by eq.(4.14). We must choose a reasonable number of microtubules for the amount of available tubulin dimers. For 500 dimers, any number of microtubules between 1 and 50 gives good results. If the number of subunits were increased, the number of microtubules would also need to be increased to gain the same results. It is easily demonstrated that for 500 dimers and 30 microtubules, the results are identical to a choice of 5000 dimers and 300 microtubules in terms of the fraction of tubulin that assembles. In each case, roughly 50% of the tubulin forms

microtubules, which is consistent with experimental data. The results for the larger simulations are smoother since the collapses constitute a smaller percentage of the overall ensemble, however the number of coupled equations and hence the required computational time increases. A further refinement of this model must be made. We cannot permit all microtubules to evolve at each time step in the simulation. This effectively allows all the polymers to access the same individual tubulin dimers at the same time. By taking smaller time steps and allowing only one microtubule (chosen randomly) to grow or shrink, the process would more resemble an actual experiment. When this modification is done, the changes in the total amount of assembled tubulin are not so drastic.

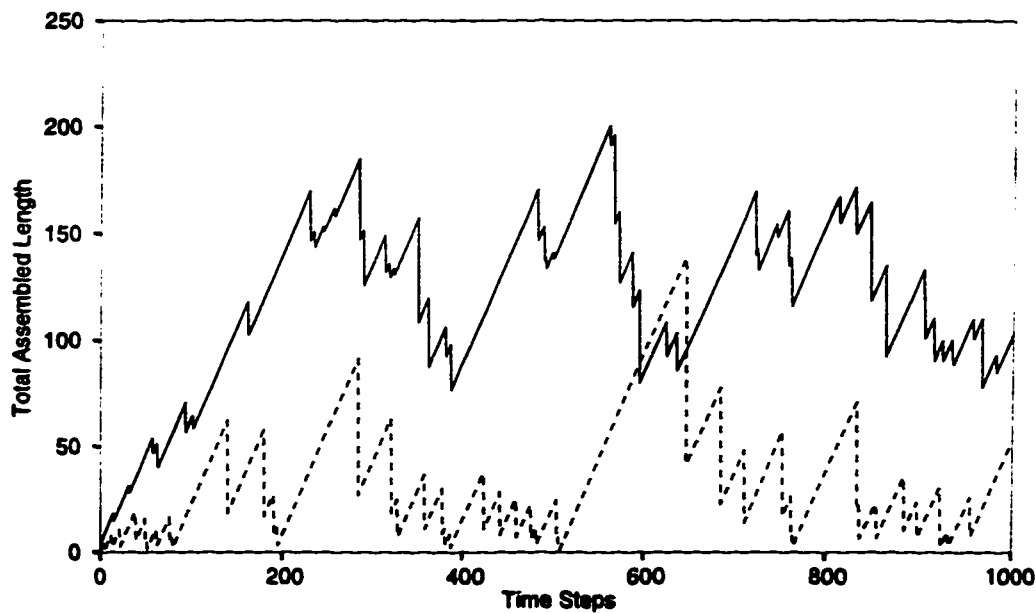


Figure 4.7: Plot of total assembled tubulin for 5 coupled microtubules (top curve) and a single microtubule.

We begin with 500 subunits available and 5 microtubules. Figure 4.7 shows the total amount of assembled tubulin as the simulation progresses. For comparison, the

plot of a single microtubule following the same recursive map is included. The curve that emerges is still very choppy and erratic. We know from Obermann et al. [37] that a minimum number density of microtubules is required for oscillations. Figure 4.8 shows the same simulations for both 30 and 50 microtubules. In this case, as the number of microtubules is increased, the system simply evolves towards a steady-state value. Increasing the number beyond 50 has very little effect and too high a number causes the situation of many short microtubules, none of which are able to grow effectively.

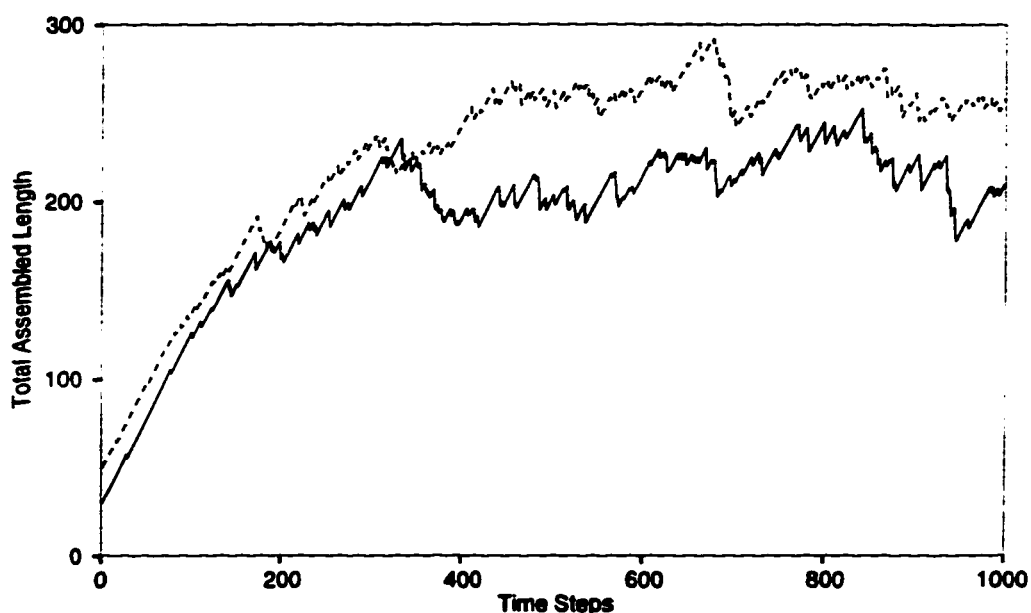


Figure 4.8: Plot of total assembled tubulin for 30 coupled microtubules (bottom curve) and 50 coupled microtubules.

One factor we have ignored is that the dimers freed in a microtubule collapse are GDP rich, not GTP rich. In order for them to be able to reassemble they must be able to exchange their bound nucleotide. If there is no mechanism for regenerating GTP from the GDP that is released, eventually all the GTP will be consumed and



Figure 4.9: Plots of the fraction of assembled tubulin for 300 microtubules. The rate of GDP to GTP conversion at each time step is: 0.3% (top curve), 0.1% (middle curve) and 0.05% (bottom curve).

all of the microtubules will disassemble. If instead we include a process for regenerating GTP from GDP, there will always be the possibility of assembly. A small rate of GDP→GTP conversion (1-2%) at each time step in the simulation proves to be sufficient to generate an overshoot in the amount of assembled tubulin. If the rate is increased, the system behaves as before and grows to saturation (see Figure 4.9). This is consistent with the experimental findings presented in Chapter 2. There it was found by several authors that increasing the concentration of the enzyme responsible for this conversion removed oscillations from the system or conversely decreasing the concentration introduced oscillations into the system [31]. We do not see the oscillations here, but the behaviour does change with different conversion rates. Figure 4.10 shows three different simulations for 200, 300 and 500 microtubules. The number of tubulin dimers was 5000 and at each step in the simulation 0.3% of the GDP in solu-

tion was converted to GTP. The result was once again saturation with the possibility of a small overshoot. Despite trying many combinations of parameters and constants, oscillations could not be produced using such a methodology.

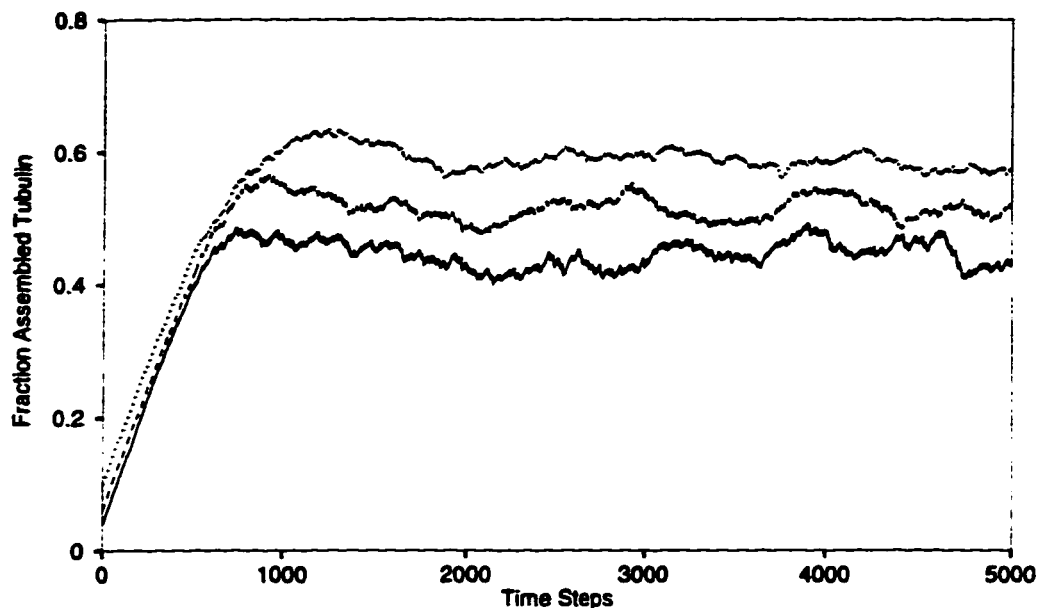


Figure 4.10: Plots of the fraction of assembled tubulin for 200 (bottom), 300 and 500 (top) microtubules. The rate of GTP to GDP conversion at each time step is: 0.3%.

What seems to be the limiting factor in the effectiveness of these simulations is that the number of microtubules, while able to be changed, is fixed for the duration of each simulation. We know from experiment [37, 30] that the number of microtubules change from the start to finish of oscillations with fewer and longer microtubules being the result. It has also been determined that self-nucleation of microtubules is required for oscillations [37]. The next chapter deals with the case of microtubule nucleation in a different formalism.

Chapter 5

Modelling using a Landau-Ginzburg Approach

It seems plausible for us to view the process of microtubule formation as a liquid-solid phase transition. The parallels between inhomogeneous nucleation in a first order phase transition and that of microtubule nucleation and growth are sufficient for us to follow this line of reasoning. We can directly equate the liquid phase with that of free tubulin. This is the regime where the solid phase, ie. microtubules, are unstable. Similarly the solid phase would correspond to free tubulin being the unstable solution and microtubules being stable. In this regime, we would see self-nucleation of microtubules just as in standard nucleation phenomena. In experimental situations, we can find ourselves in any three of these regions. When the buffer conditions are not correct, the temperature too low or perhaps the tubulin concentration insufficient, microtubules are unstable. This would correspond to the liquid phase. As conditions are altered so that microtubules can form, the system would enter the coexistence region. Once the tubulin concentration is raised beyond a certain level, microtubules would begin to self-nucleate within the solution. This is the solid phase. Figure 5.1 shows a phase diagram constructed using data points from Fygenon et al. [55] which

depicts these three regions of the phase diagram..

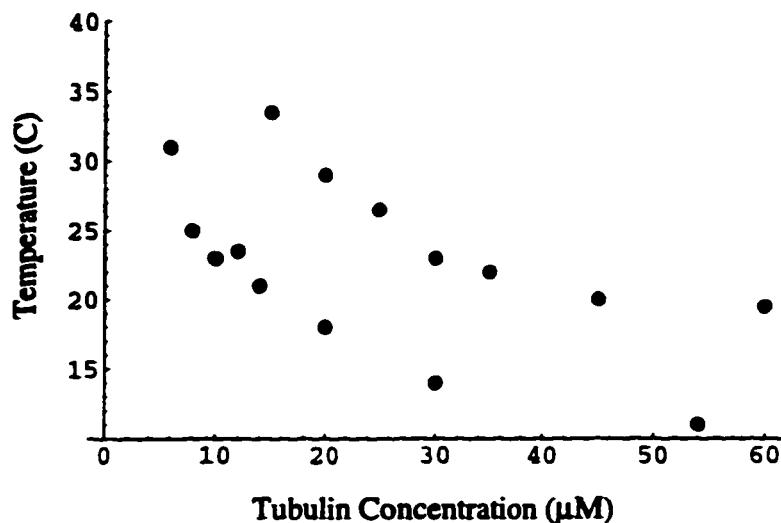


Figure 5.1: A phase diagram for microtubules. Data points taken from Fygenon et al, 1994.

5.1 Landau-Ginzburg Free energy expansion

One preferred method of dealing with such a phase transition is using a Landau-Ginzburg approach. In this case we would expand the free energy in terms of some order parameter. Temperature is a natural choice for a control parameter in our system, but the concentration of tubulin will also control the phase dynamics. This parallels once again liquid-solid transitions where temperature and pressure (density) control the phase of the system. From the phase diagram, we see that upon raising the temperature and/or the concentration of tubulin, we move from the state of free tubulin to the coexistence region. As for the order parameter, experiments tend to measure the turbidity which is basically the amount of assembled tubulin. This will also be our choice of an order parameter since it is zero in the disordered state (free tubulin) and non-zero in the ordered state (assembled tubulin). Since we have no

symmetry requirements for the order parameter, we choose the expansion for the free energy as:

$$F(\phi) = A\phi^2 + B\phi^3 + D\phi^4 \quad (5.1)$$

where

$$\begin{aligned} A &= A(C, T) \\ B &< 0 \\ D &> 0 \end{aligned} \quad (5.2)$$

A physical interpretation of these expansion coefficients in terms of the underlying processes will be given in Chapter 7. For the control parameter in our expansion, A , we choose it to be a function of the concentration C and the temperature T . The requirement that $B < 0$ is simply so that the ordered phase appears at $\phi > 0$. What makes this formulation different from standard Landau phenomenology is that instead of approaching the ordered phase as we lower the control parameter (T for example), in our case we approach the ordered phase by raising either the temperature or the tubulin concentration. This point must be kept in mind when we choose a particular form for A . Taking the form of the free energy expansion given in eq.(5.1), we want to solve the equilibrium condition

$$\frac{\partial F}{\partial \phi} = 0 \quad (5.3)$$

which gives us the non-zero solutions:

$$\phi_{\pm} = \frac{-3B \pm \sqrt{9B^2 - 32AD}}{8D}. \quad (5.4)$$

In order for ϕ_{\pm} to be real roots, we require that

$$9B^2 - 32AD \geq 0. \quad (5.5)$$

The point at which this is equal to zero is exactly the point at which the solid phase (ie. a microtubule) begins to appear. If we continue to raise the control parameter(s)

(which in our formulation causes A to become smaller), we eventually reach the point $A = 0$ which defines the solid transition point. Beyond this point, the liquid (free tubulin) state is unstable (see Figure 5.2 for clarification).

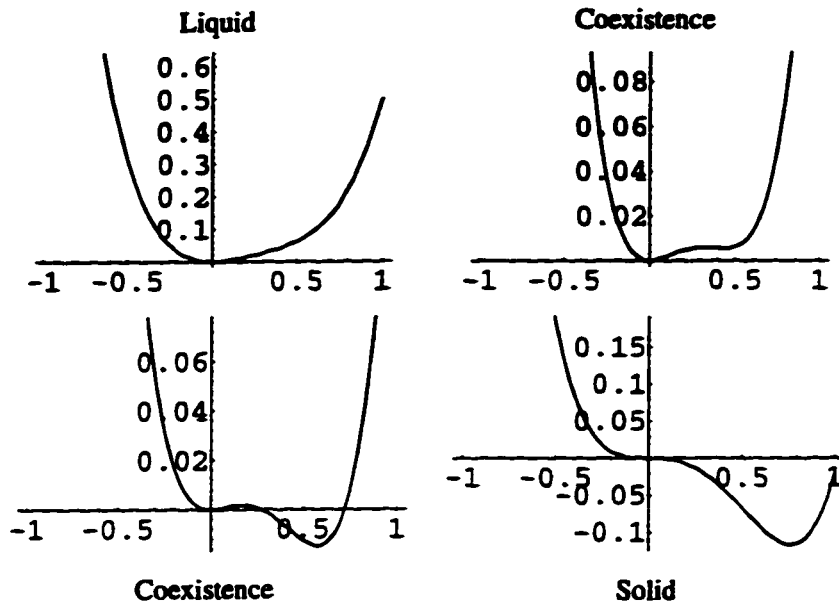


Figure 5.2: Plots of the free energy potential showing the three phase regions in our theory.

We have several unknowns in our free energy expansion. We can gain some information about the value of the expansion coefficient by looking at the experimental phase diagram Figure 5.1. We can perform a fit to the data for the top curve (solid transition line). This line has the basic characteristic

$$(T - T_c) \propto (C - C_c)^{-0.5} \quad (5.6)$$

where roughly $T_c = 4^\circ C$ and $C_c = 1.5 \mu M$. This curve corresponds to the point where $A = 0$, therefore we postulate that

$$A \propto (T - 4)(C - 1.5)^{0.5} - 105 \quad (5.7)$$

or adding in a constant of proportionality

$$A = a[105 - (T - 4)(C - 1.5)^{0.5}] \quad a > 0. \quad (5.8)$$

Recall the requirement that we approach the ordered phase as we *raise* the control parameter(s). Thus we must choose the particular form given above for A . For small temperatures and/or concentrations, $A > 0$. As we raise one or both of the control parameters, A approaches zero which is what we required. The bottom curve in Fig. 5.1 is the point where the coexistence region begins. As shown before, at this point

$$A = \frac{9B^2}{32D} \quad (5.9)$$

which directly leads to

$$(T - 4) = \frac{105 - \frac{9B^2}{32aD}}{(C - 1.5)^{0.5}}. \quad (5.10)$$

If we assume a , B and D to be constants, we can best fit the data by choosing

$$\frac{9B^2}{32aD} \simeq 48. \quad (5.11)$$

Plots of both eq. (5.8) and eq. (5.10) are shown in Figure 5.3. It is possible that a better fit may be obtained by assuming that one or more of the coefficients depend on one or both of the control parameters, but this would needlessly complicate our calculations. Our model certainly fits the data points from experiment very well. Aside from the phase diagram, Landau-Ginzburg theory can make predictions for order parameter solutions which is our next step.

5.2 Mean Field Dynamics

5.2.1 Adding surface energy

We want to extend our model to include the so-called Ginzburg term. This in turn brings in surface energy, due to the interface between the two phases, and kinetic

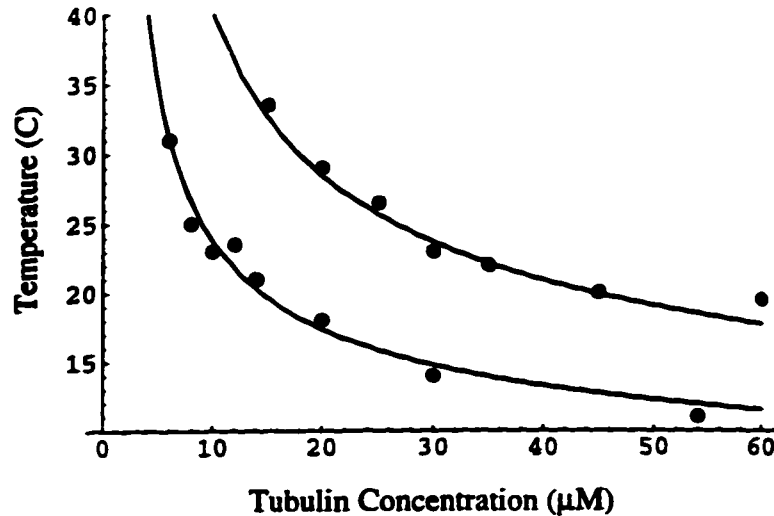


Figure 5.3: Plots of eqs. (5.8) and (5.10) along with the experimental data points.

energy of the floating microtubules' interface motion. This last addition corresponds to the kinetics of growth and shrinkage of the microtubules. We will treat our system as one-dimensional and thus our free energy expansion is now a functional of the form

$$F = \int dx \left[\frac{d}{2} (\nabla \phi)^2 + \frac{m}{2} \left(\frac{\partial \phi}{\partial t} \right)^2 + A\phi^2 + B\phi^3 + D\phi^4 \right]. \quad (5.12)$$

This gives rise to the equation of motion for the solid-liquid boundary

$$m\ddot{\phi} - d\phi'' + \gamma\dot{\phi} + 2A\phi + 3B\phi^2 + 4D\phi^3 = 0 \quad (5.13)$$

where a 'friction' term $\gamma\dot{\phi}$ has been added in by hand. This equation represents the motion of the phase front, ie. the leading edge of the microtubule. The friction term is representative of the fact that the microtubule can only grow when there is tubulin around. The less tubulin that there is, the slower the microtubule grows. Also, as the tubulin becomes used up, the rate of growth will slow. Therefore, it seems natural that γ will depend on the tubulin concentration. This follows the ideas suggested in papers by Melki et al. [31] and Mandelkow et al. [38] where they put forward the concept that tubulin bound with GDP may block the ends of microtubules for

tubulin bound with GTP. Although we are not considering GDP and GTP in this formulation, as the assembly competent tubulin becomes used up, there will be more GDP-tubulin in the solution and hence more friction.

If we assume a traveling wave type solution so that our order parameter has the functional dependence $\phi = \phi(\xi)$ where $\xi = x - vt$ is our moving coordinate, our equation of motion can be written

$$(mv^2 - d)\phi'' - \gamma v\phi' + 2A\phi + 3B\phi^2 + 4D\phi^3 = 0 \quad (5.14)$$

where $' = \partial/\partial\xi$. The solutions to this nonlinear ordinary differential equation will give us our order parameter patterns in terms of the moving coordinate ξ .

5.2.2 Solving the equation of motion

Solving the equation of motion (5.15) is quite straightforward. The choice of initial conditions is really the key to the behaviour. We know that the critical parameters are the concentration of seeds and the concentration of GTP [37]. Our order parameter represents the amount of assembled tubulin. The concentration of seeds for microtubule growth is essentially an amount of pre-assembled tubulin, therefore it is natural to choose $\phi(0)$ according to this criterion. The amount of available GTP is indicative of the potential growth and hence could be thought of as defining the initial derivative $\phi'(0)$. These choices are certainly open to question and revision, but as we shall see, they produce acceptable results.

The coefficient of the 'friction' term should depend on the tubulin concentration C . This is because the more tubulin there is, the higher the number of tubulin molecules that may encounter the end of the microtubule. With this in mind, we will assume that γ depends on C as $\gamma \propto C^{-1}$ so that low concentration means high 'friction' and vice versa.

In order to compare our results to those from experiments, we need to have similar

conditions. Thus we are basically required to fix our temperature T at 37°C and only work with one control parameter, C the tubulin concentration. From looking at the phase diagram, we see that this gives us a critical concentration for microtubule growth of $C = 4.7\ \mu\text{M}$ and a critical concentration of $C = 13\ \mu\text{M}$ for microtubule self-nucleation. Using the initial conditions stated above, the equation of motion was solved using *Mathematica*. The results are shown in Figure 5.4 and 5.5.

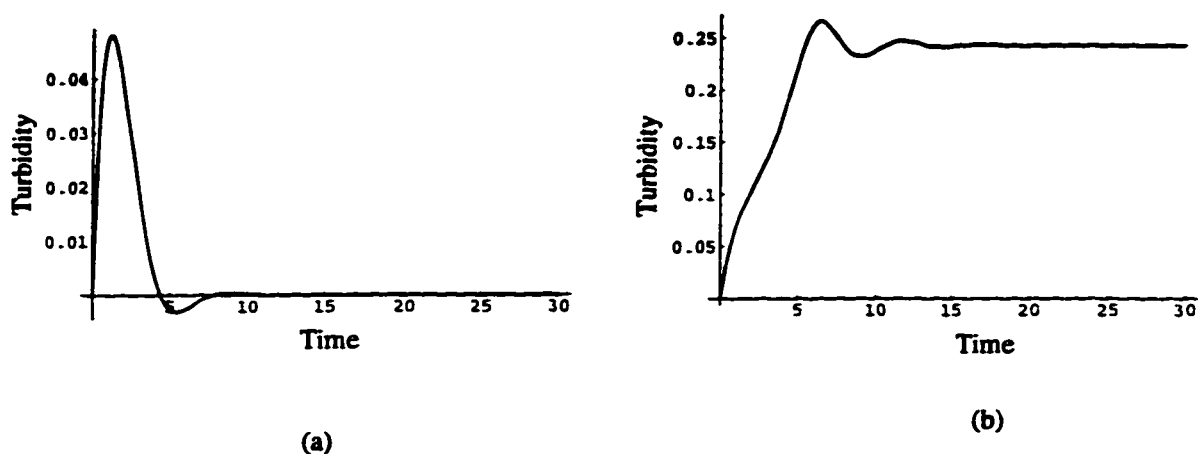


Figure 5.4: The amount of assembled tubulin versus time for (a) $3\ \mu\text{M}$ and (b) $6\ \mu\text{M}$ tubulin concentration. Both solutions performed at 37°C .

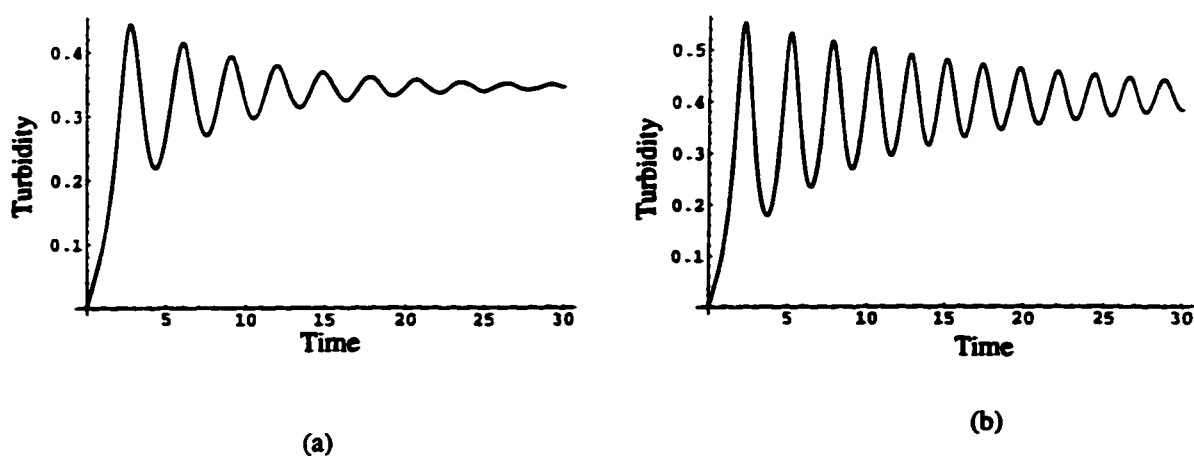


Figure 5.5: The amount of assembled tubulin versus time for for (a) $15\ \mu\text{M}$ and (b) $25\ \mu\text{M}$ tubulin concentration. Both solutions performed at 37°C .

The solutions that we acquire show a transition that occurs as we raise the tubulin concentration. First we see that at low concentrations microtubules form, become unstable and collapse. At slightly higher concentrations, the system grows to saturation, perhaps with a small overshoot. Then, at even higher tubulin concentrations, oscillations enter in, increasing in size as we raise C . In comparing these solutions with the oscillations seen in experiments we find several similarities. First, the tubulin concentrations at which growth begins and oscillations occur are in agreement with experiment. In this sense we can only look at the order of magnitude since there are many additional factors that we have not included in this theory. Second, as we raise the tubulin concentration, the steady-state value that the system works towards increases. Unfortunately, we cannot estimate what fraction of the tubulin is assembled. Lastly, the form of the oscillations looks very much like the experimental patterns. Aside from these points, the oscillations were produced using the parameter fits from the phase diagram in Figure 5.1. The phase diagram and the experimental data were acquired separate from one another and it is nice to see that this simple theory can explain them both.

5.3 Other predictions from the model

Because we have a simple expression for the free energy of our system, we can determine other properties of the system such as specific heat. The specific heat is found using

$$C = -T \frac{\partial F(\phi)}{\partial T} \quad (5.15)$$

where F is the free energy expression given in eq.(5.1). We would initially expect to see a change in the specific heat when the new solid phase is introduced into the system. This is in fact the case as seen in Figure 5.6. What is different in this system is that the ordered phase is the high-temperature phase and thus the plots of specific

heat may appear to be 'backwards'. Because this is a first-order phase transition,

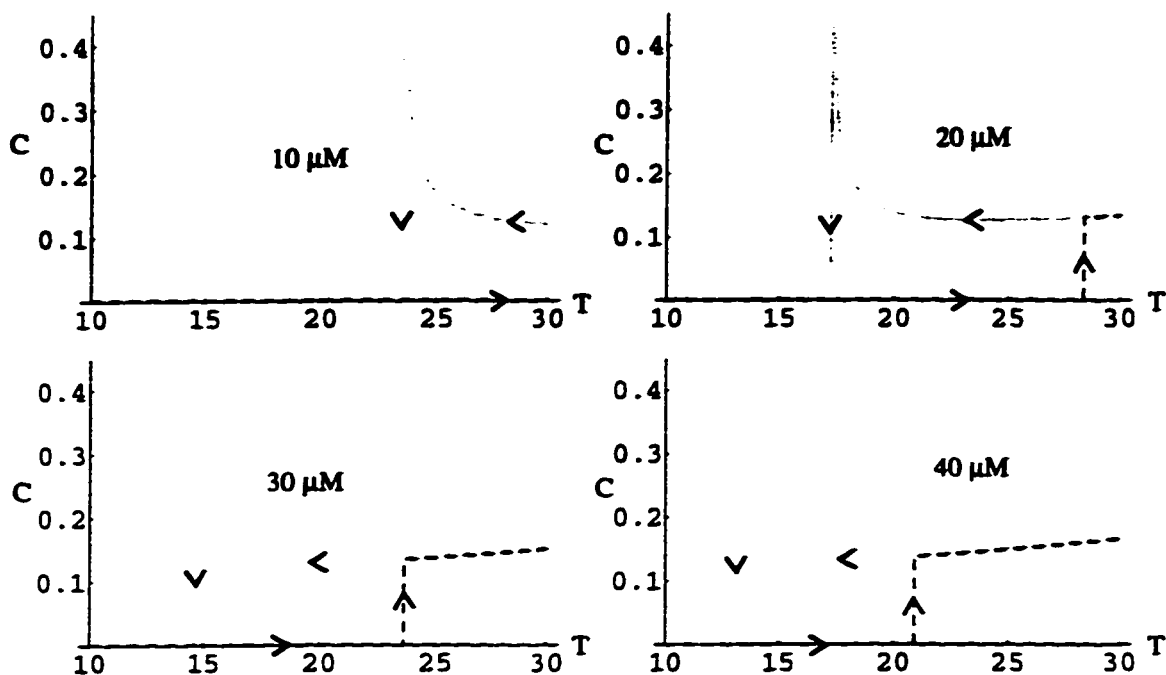


Figure 5.6: Specific heat predicted by our model as a function of temperature and tubulin concentration.

there is thermal hysteresis present. As the tubulin concentration is increased, the transition lines between the three regions become closer together and the hysteresis region becomes smaller. It is conceivable that at high enough tubulin concentrations these two lines would meet at a triple point. Beyond this point, the monotonic growth region would not exist and we would simply have a second order transition from no growth to oscillations. It would be interesting to test this experimentally. Using a method such as Differential Scanning Calorimetry we could find the contribution to the specific heat from the phase transition without any of the background effects. This would also be a prime method for determining the order of the transition. The effect on the specific heat due to the phase transition may also be observable via other means. Since the dimers and the microtubules are polar objects, there may be

a change in the dielectric constant or the polarization of the system. To detect this, the phase transition would perhaps need to be carried out with an applied electric field.

Chapter 6

Reaction Kinetics Model

In the preceding chapter, it was demonstrated how a Landau-Ginzburg phenomenology could give rise to oscillations in a system undergoing a phase transition. This treatment considered tubulin and microtubules as two different phases of the same substance. Although at high tubulin concentrations this assumption is quite adequate, this is only partially correct. The actual phase dynamics are more complicated, and we need to treat free dimers and microtubules as interacting entities. The method now will be that of chemical kinetics and it is expected to offer a more accurate formalism.

6.1 Chemical Kinetics

Imagine that we have a simple chemical reaction



where the reactants A and B are consumed to form the product C . The rate at which the reactants are consumed must be the same as the rate at which the product C is

produced. This means

$$\frac{d[C]}{dt} = -\frac{d[A]}{dt} = -\frac{d[B]}{dt} \quad (6.2)$$

where we have denoted the concentration of each species by $[A]$, etc.. The rate at which such a reaction proceeds is often proportional to the concentration of the reactants to some power. [56]. If our reaction were first order in both reactants, the rate would be $k[A][B]$ where k is the rate constant. Thus we can write down the rate laws for each component in the reaction as

$$\frac{d[A]}{dt} = -k[A][B] = \frac{d[B]}{dt} \quad (6.3)$$

$$\frac{d[C]}{dt} = k[A][B]. \quad (6.4)$$

By solving these differential equations with appropriate initial conditions, we can find the concentrations as functions of time. The rate constants are usually determined experimentally and many are found to follow the Arrhenius equation [56]

$$k = Ae^{-\Delta E/(RT)} \quad (6.5)$$

where A is a constant, ΔE is the activation energy required for the reaction, R is the universal gas constant and T is the temperature in degrees Kelvin. This will be the basic methodology followed in the next sections.

6.2 Oscillations in (Bio)chemical Systems

In certain situations, reactions described using chemical kinetics do not proceed in a simple monotonic manner, but exhibit oscillations. Oscillations are not an indication of the system moving between multiple stable states, but instead represent a kind of dynamical instability [57] referred to in the context of nonlinear dynamics as limit cycles. One of the first systems in which oscillations were observed was in the Belousov-Zhabotinskii reaction [58]. Since then, many such examples have been

found, including many in biological systems. Such examples include circadian clocks [59], biochemical processes like the glycolytic pathway [60] and the biosynthesis of some proteins [61].

In writing down a set of chemical kinetic equations, how can we tell whether or not oscillations will be admitted? This can be done from a purely mathematical approach. Suppose we have a set of reaction equations

$$\dot{\vec{X}} = \vec{v}(\vec{X}). \quad (6.6)$$

where $\vec{v}(\vec{X})$ is a vector of the various elements and products of the components of \vec{X} . Two criteria must be met for undamped oscillations to occur within such a system [62].

1. The divergence of the potential $\vec{\nabla} \cdot \vec{v} = \partial v_i / \partial X_i$ must change sign on the domain of $\{X_i\}$. This is equivalent to saying that the trace of the Jacobian matrix, $\text{Tr } J$, where J is

$$J = \begin{pmatrix} \frac{\partial v_1}{\partial X_1} & \frac{\partial v_1}{\partial X_2} & \dots \\ \frac{\partial v_2}{\partial X_1} & \dots & \\ \vdots & & \\ \vdots & & \end{pmatrix} \quad (6.7)$$

must change sign. This can also be interpreted as a negative condition of Bendixson's criterion [63].

2. The determinant of the Jacobian, $\text{Det } J$, evaluated at the steady state values must be positive at the point when $\text{Tr } J = 0$.

The second criterion is only required for undamped oscillations. In our case, the situation is slightly different and we can modify this requirement. To get damped oscillations, we require that the eigenvalues of J have a negative real part. At the

critical point, when $\text{Tr } J$ changes sign, at least two eigenvalues will develop an imaginary part giving rise to oscillatory solutions. We will apply these criteria to our model to check for the solutions that we require.

6.3 Models for Microtubule Oscillations

The approach using chemical kinetics treats the system as a bulk system, just as the Landau method did. Although we are not modelling individual microtubules, we can easily include reactions which we know are true of single microtubules. The first such reaction is the growth of a microtubule by the simple addition of a dimer. This can be expressed as



where MT_i is a microtubule containing i dimers, T is a tubulin dimer and k_+ is the reaction rate constant for this reaction. We also know that microtubules collapse, releasing tubulin back into solution. This we can write as



where we have assumed that the microtubule will completely collapse releasing all of its dimers. These two reactions represent the basis of the recursive map formulation presented in Chapter 4 where we simply had the possibility of growth and collapse. What was added in Chapter 5 was the nucleation of microtubules. We will include the same idea here as the reaction



For simplicity we may assume that only one tubulin dimer ($n = 1$) is required to start a microtubule. This may seem simplistic, but this choice does not have a large effect on the overall dynamics. Several different experiments have given different values

for n . These values range from $n = 12$ [64] to assembly in the presence of assembly promoters such as MAPs where as few as two dimers may be required [65].

These three reactions represent the simplest scheme we can write down. We now need to develop the associated reaction equations. Before we do this, however, we must make one observation. Although it is convenient to use the notation MT_i in writing down our reactions, what we are really concerned with is the amount of assembled tubulin and the number density of microtubules. In our reactions, MT_i represents both of these things. In the growth reaction, the amount of assembled tubulin, T_a , increases but N , the number of microtubules, remains constant. In the collapse reaction, both T_a and N decrease and in the last reaction both increase. The equations that we arrive at are:

$$\dot{T}_f = -k_+ T_f N + k_c N - k_n T_f \quad (6.11)$$

$$\dot{N} = -k_c N + k_n T_f \quad (6.12)$$

$$\dot{T}_a = k_+ T_f N - k_c T_a + k_n T_f \quad (6.13)$$

where we have denoted the free tubulin as T_f . Since the total mass of tubulin is conserved, $C = T_a + T_f$, we can eliminate T_f from the equations which leaves us with

$$\dot{N} = -k_c N + k_n (C - T_a) \quad (6.14)$$

$$\dot{T}_a = k_+ C N + k_n C - (k_c + k_n + k_+ N) T_a. \quad (6.15)$$

The Jacobian for this system is

$$J = \begin{pmatrix} -k_c & -k_n \\ k_+ C - k_+ T_a & -(k_c + k_n + k_+ N) \end{pmatrix}. \quad (6.16)$$

Applying Bendixson's criterion shows us that

$$\text{Tr } J = -k_c - (k_c + k_n + k_+ N) \quad (6.17)$$

which is always negative. Since $\text{Tr } J$ does not change sign, we cannot have oscillations. Perhaps this is not that surprising since this simple system is not really an extension over the previous models.

One addition we can make is to recognize the difference between tubulin bound with GDP versus GTP. Our reaction scheme is now



where we have now ignored the i subscript. Our system will never be able to work towards a non-zero steady-state value unless we provide a sufficient number of assembly competent dimers. We can add a process which produces GTP-rich dimers from the GDP-rich dimers that are released in a collapse:



With this added reaction and the inclusion of the difference in nucleotides, our equation set is

$$\dot{N} = -k_c N + k_n T_t \quad (6.22)$$

$$\dot{T}_a = k_+ N T_t - k_c T_a + k_n T_t \quad (6.23)$$

$$\dot{T}_d = k_c T_a - k_r T_d \quad (6.24)$$

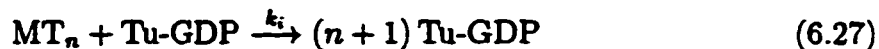
$$\dot{T}_t = -k_+ N T_t - k_n T_t + k_r T_d \quad (6.25)$$

where T_d represents Tu-GDP and T_t represents Tu-GTP. The trace of our Jacobian in this case is

$$\text{Tr } J = -2k_c - k_r - k_+ N - k_n. \quad (6.26)$$

Since all the rate constants are positive and $N \geq 0$, once again $\text{Tr } J$ cannot change sign and we cannot have oscillations. Even though we have 'completed the circle' in our set of reactions, we require something more.

Instead of the mathematical criterion previously discussed, we can give physical requirements for oscillations to occur. What is needed is that one element of the system catalyzes its own production [62]. Recall two papers discussed in Chapter 2. Both Melki [31] and Marx [50] suggested that microtubule collapse may be brought on by a high concentration of GDP-rich tubulin, especially around the ends of a microtubule. Since the collapse of a microtubule produces Tu-GDP, such a process would qualify as an autocatalytic step. Thus we add one more reaction



where k_i is the rate constant for this ‘induced collapse’. The addition of this autocatalytic step gives us the following set of reaction equations:

$$\dot{N} = -k_c N + k_n T_t - k_i N T_d \quad (6.28)$$

$$\dot{T}_a = k_+ N T_t - k_c T_a + k_n T_t - k_i T_a T_d \quad (6.29)$$

$$\dot{T}_d = k_c T_a - k_r T_d + k_i T_a T_d \quad (6.30)$$

$$\dot{T}_t = -k_+ N T_t - k_n T_t + k_r T_d. \quad (6.31)$$

From this set of equations, we find that

$$\text{Tr } J = -2k_c - k_+ N - k_n - k_r - k_i(2T_d - T_a). \quad (6.32)$$

Now because of the last term, $\text{Tr } J$ can change sign and oscillations should appear in this system of equations.

6.4 Determining the Rate Constants

Since most of the reactions in our theoretical model are observed in experiments, we can estimate many of the rate constants from analyzing data in the literature. It should be stressed that the reaction rates are strongly dependent on numerous

T(°C)	k_+ ($\mu\text{M}^{-1} \text{s}^{-1}$)
25	3
30	4
35	7
37	9

Table 1: Values for the rate constant k_+ at different temperatures. See text for references.

experimental factors. Temperature is one of the major controlling elements, but tubulin concentration, ionic concentrations etc. vary from experiment to experiment and their effects are difficult to accurately quantify [66, 67]. For this reason, we have assumed reactions involving one reactant are first order and reactions involving two reactants are second order. We will also assume constant rates or include temperature effects where warranted.

The first reaction we will consider is the growth reaction given in eq. (6.18). The rate constant k_+ has been measured in many experiments, but mainly at 37° C. Table 6.1 lists four measurements at four different temperatures [68, 69, 70, 66] If we assume an Arrhenius like behaviour such that

$$k \sim Ae^{-\frac{\Delta E}{RT}}$$

we can plot $\log(k_+)$ versus $(1/T)$ as shown in Figure 6.1. We see that ΔE is not completely temperature independent, but a linear fit to the data will suffice. Thus we arrive at an expression for k_+ as

$$k_+ = 5.14 \times 10^{13} \exp\left(-\frac{75.7 \text{ kJ/mol}}{RT}\right) \mu\text{M}^{-1} \text{s}^{-1} \quad (6.33)$$

where T is the temperature in degrees Kelvin and R is the universal gas constant.

The rate constant k_c for microtubule collapse has also been studied by many groups. Measurements with varying temperature indicate that collapse frequency

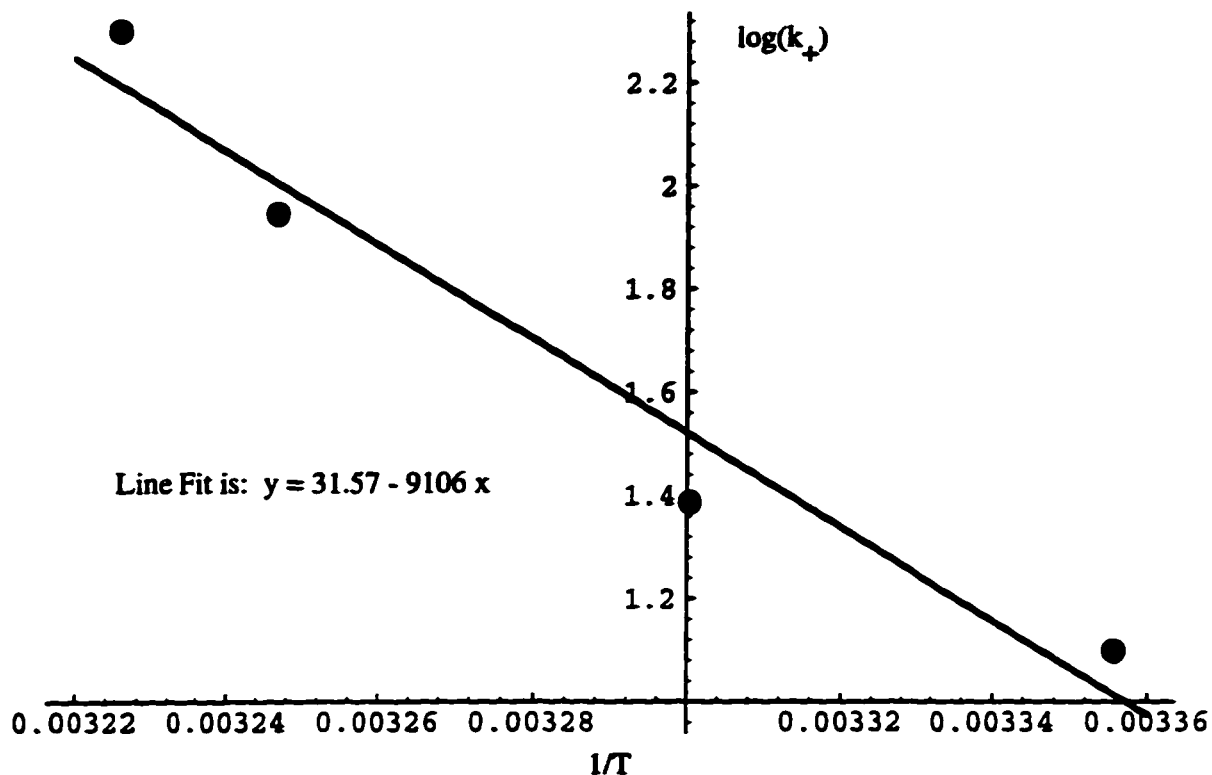


Figure 6.1: Arrhenius plot of $\log(k_+)$ vs. $(1/T)$ to determine the values of A and ΔE .

rises with decreasing temperature [35]. Walker et al. [66] found $k_c = 0.001 \text{ s}^{-1}$ at 37°C . If we estimate that this rate will grow as we lower the temperature according to the Arrhenius equation, we can write k_c as

$$k_c = 4.32 \times 10^{-8} \exp\left(-\frac{25.9 \text{ kJ/mol}}{RT}\right) \text{ s}^{-1}. \quad (6.34)$$

In determining k_n , we again have more experimental data. An Arrhenius behaviour is again found and the rate constant has the form [71]

$$k_n = 8 \times 10^7 \exp\left(-\frac{78.3 \text{ J/mol}}{RT}\right) \text{ s}^{-1} \quad (6.35)$$

such that at 37°C , $k_n \simeq 4 \times 10^{-6} \text{ s}^{-1}$. We know that nucleation is one of the slower processes in the reaction cycle and this rate is in accordance with that.

The actual reaction for regenerating GTP and exchanging the nucleotide at the E-site in a tubulin dimer is not as straightforward as we have presented it. The actual process is mediated by enzymes and requires several steps. In the same sense, the process given in eq.(6.21) is quite general and simply represents GDP-rich dimers being turned into GTP-rich dimers. Hence, this process may or may not involve the breakup of oligomer rings [50]. It is difficult to assign a rate constant to such a process and we will try several possibilities when generating solutions. As a rule, k_r will be on the order of $2 s^{-1}$.

The last rate constant we have to determine is k_i for the autocatalytic reaction (6.27). No experimental data for this reaction exist. We will leave this rate constant open to try and fit the phase diagram shown previously in Chapter 5.

6.5 Phase Diagram of Microtubule Assembly

The phase diagram we presented in Chapter 5 showed three regions of microtubule assembly. We had made the connection between the region of spontaneous nucleation and microtubule oscillations. Like the axes on the diagram, we have temperature and tubulin concentration as the control parameters in our system. The temperature will affect the rate constants and the tubulin concentration will determine the dynamics since we require total tubulin concentration: $C = T_a + T_d + T_t$. In order to find the transition point to oscillations, we must find the eigenvalues of our Jacobian matrix

$$J = \begin{pmatrix} -k_c - k_i T_d & 0 & -k_i N & k_n \\ k_+ T_t & -k_c - k_i T_d & -k_i T_a & k_n + k_+ N \\ 0 & k_c + k_i T_d & k_i T_a - k_r & 0 \\ -k_+ T_t & 0 & k_r & -k_n - k_+ N \end{pmatrix} \quad (6.36)$$

evaluated at the steady-state values for T_a, T_d, T_t and N . We find the steady-state values by solving our reaction equations (6.28-31) with $\dot{T}_a = \dot{T}_d = \dot{T}_t = \dot{N} = 0$. This

leads to the following

$$N = \frac{k_n T_t}{k_c + k_i T_d} \quad (6.37)$$

$$T_a = N \left(1 + \frac{k_+}{k_n} N\right) \quad (6.38)$$

$$0 = k_+ T_t N + k_n T_t - k_r T_d \quad (6.39)$$

$$C = T_a + T_d + T_t. \quad (6.40)$$

After much algebra, we find that N is a root of the quartic algebraic equation

$$\begin{aligned} k_+^2 k_i N^4 + 2k_+ k_i k_n N^3 + (-k_+ k_c k_n - C k_+ k_i k_n + k_i k_n^2 - k_+ k_n k_r) N^2 \\ + (-k_c k_n^2 - C k_i k_n^2 - k_c k_n k_r - k_n^2 k_r) N + C k_n^2 k_r = 0 \end{aligned} \quad (6.41)$$

and the other solutions are then found as

$$T_a = N \left(1 + \frac{k_+}{k_n} N\right) \quad (6.42)$$

$$T_d = \frac{(k_n + k_+ N)(C - N - \frac{k_+}{k_n} N^2)}{k_n + k_r + k_+ N} \quad (6.43)$$

$$T_t = \frac{k_r (C - N - \frac{k_+}{k_r} N^2)}{k_n + k_r + k_+ N}. \quad (6.44)$$

Despite the quartic equation for N , it can be determined numerically that there is only one positive root for N that gives positive results for T_a , T_d and T_t . These values are all found numerically and substituted into the Jacobian. The eigenvalues of the resulting matrix can easily be found using *Mathematica* [72]. Thus for a given temperature (or tubulin concentration) we can find the tubulin concentration (or temperature) at which oscillations appear. This will be the point when two of the eigenvalues develop imaginary parts. This change always occurs in pairs of eigenvalues. Since the determinant must be real, if we have one complex eigenvalue, we must have another which is its complex conjugate. We still have freedom in choosing our rate constant k_i . A choice which proves to give us the best fit to the phase diagram

is

$$k_i = 13.0 \exp\left(-\frac{-10.75 \text{ kJ/mol}}{RT}\right) \mu\text{M}^{-1} \text{s}^{-1} \quad (6.45)$$

which at 37°C and a Tu-GDP concentration of 0.1 μM has a value of 0.02 s^{-1} . The second curve on the phase diagram is the transition line from no assembly to monotonic growth. Although we do not consider it in our reaction scheme, just as a single dimer can be added to a microtubule, a single dimer may come off. The ratio of the off and on rates for a single dimer determines the critical concentration for assembly [36]. The off rate k_- has a wide range of values in the literature, between 7 s^{-1} and 89 s^{-1} [66, 11, 73, 50]. This discrepancy is mostly due to different buffer conditions. To best fit the data, we chose a value of $k_- = 28 \text{ s}^{-1}$ so that the critical concentration for assembly has the form

$$C_c = \frac{k_-}{k_+} = \frac{28 \text{ s}^{-1}}{5.14 \times 10^{13} \exp\left(-\frac{75.7 \text{ kJ/mol}}{RT}\right) \mu\text{M}^{-1} \text{s}^{-1}}. \quad (6.46)$$

The plots of C_c and the transition line predicted for oscillations are shown in Figure 6.2. The fit between both experimental and theoretical curves is very favourable. It is also noteworthy that most of our rate constants have an experimental basis. Now using these same rate constants, we can find solutions to the set of eqs.(6.28-31) to see how microtubule assembly proceeds in time.

6.6 Solving the Reaction Equations

We would now like to solve the reaction equations (6.28-31). The equations are all first order in time and we simply require initial conditions for all the variables. The solutions are found using a fourth-order Runge-Kutta method. This method also incorporates a variable step size which can be reduced if the fifth-order term exceeds a user-defined threshold. In this system, the solutions were very smooth in their evolution and the step size actually remained constant. The initial conditions

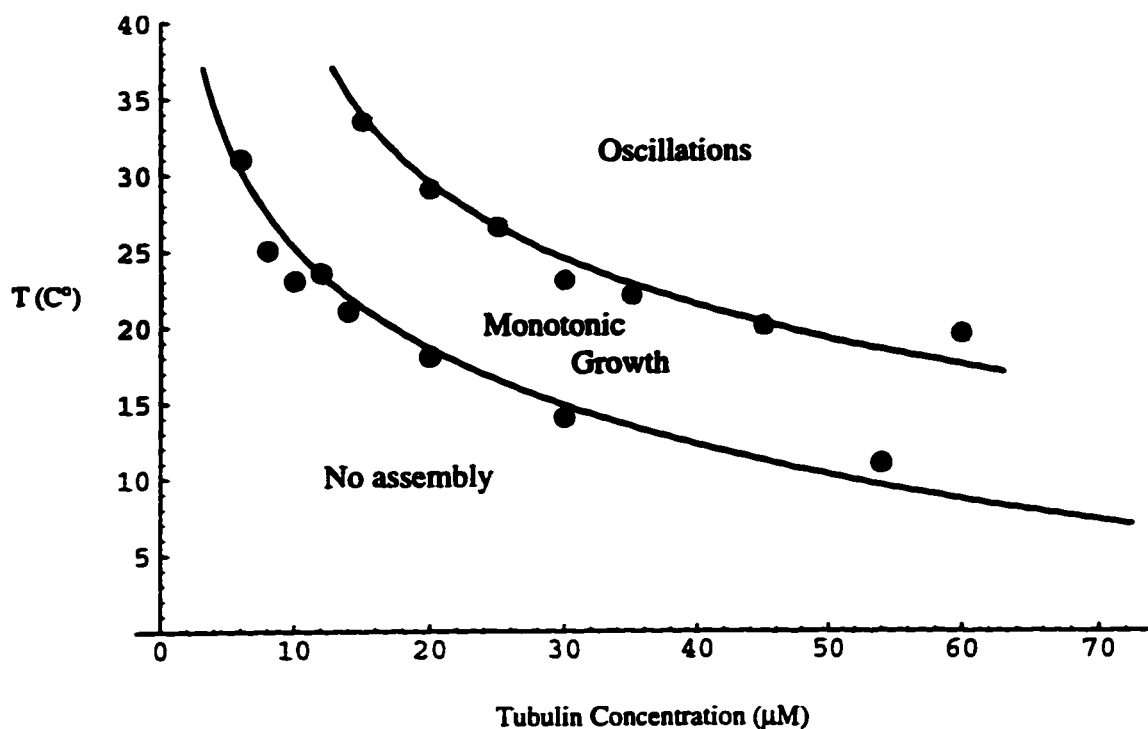


Figure 6.2: Theoretical predictions and experimental data points for the two transition lines from no assembly to assembly and from assembly to oscillations.

proved to be quite arbitrary. The steady-state value that the system works towards is only based on the choice of temperature and tubulin concentration. These two values determine the rate constants which define the steady-state value. Figure 6.3 shows typical plots for T_a , T_d , T_t and N for the initial conditions $T_t = 40 \mu\text{M}$ and $T_a = T_d = N = 0$. If we would instead begin with $T_d = 40 \mu\text{M}$ and $T_t = 0$, there is an initial lag when there is not enough GTP for assembly to occur (see Figure 6.4). This deficit is soon overcome and the system proceeds as in the first case. In order to make this somewhat easier, a graphical user interface was constructed on top of the ODE solver. This enabled immediate results for a choice of temperature and tubulin concentration, making an exploration of all the possibilities of the set of equations very straightforward. With all of the parameters established, we can investigate the

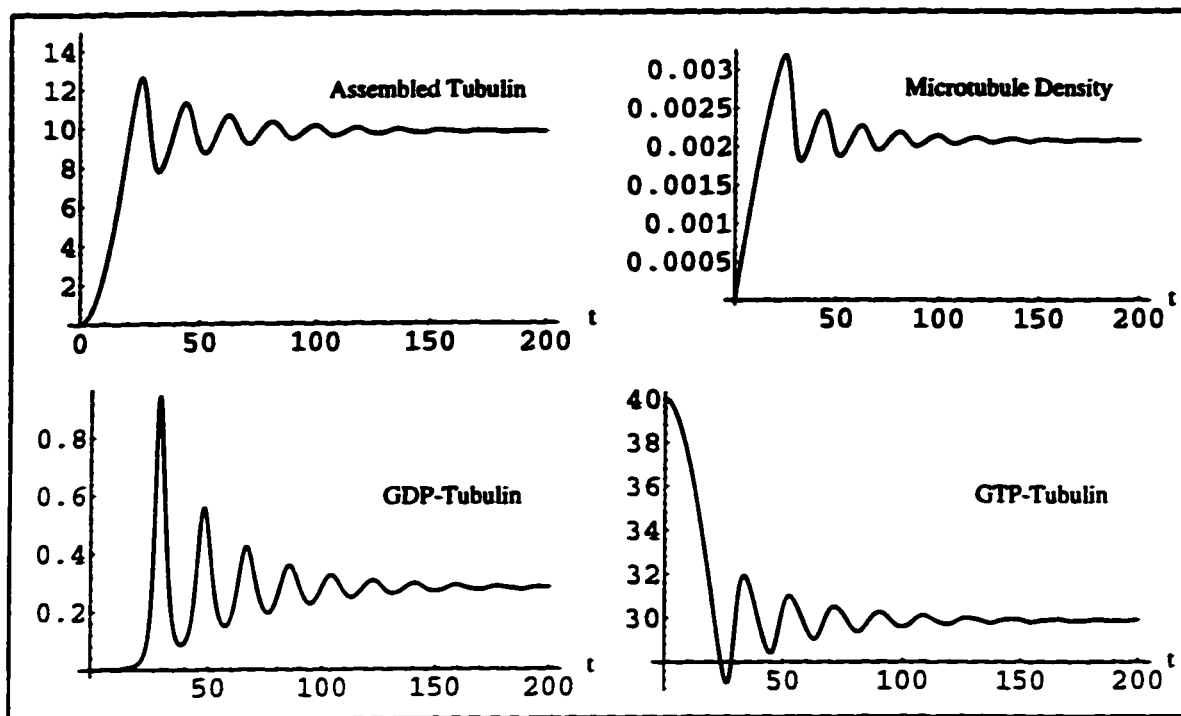


Figure 6.3: Solutions for T_a , T_t , T_d and N as functions of time. Simulations were performed for $T = 37^\circ C$ and $C = 40 \mu M$.

possibilities of the system and compare the results to experiment.

6.7 Comparison with Experimental Results

The most basic of all results in microtubule oscillations is that with increasing tubulin concentration, monotonic growth gives way to oscillations which continue to grow in size with rising concentration. Figure 6.5 shows the simulation results from our model for four different tubulin concentrations. The results agree well with one another and similar experimental findings [32]. It is interesting to note the overshoot which occurs between the stages of monotonic and oscillatory growth. This feature also appears when measured in the laboratory.

A second similar effect is seen when assembly is performed at different temper-

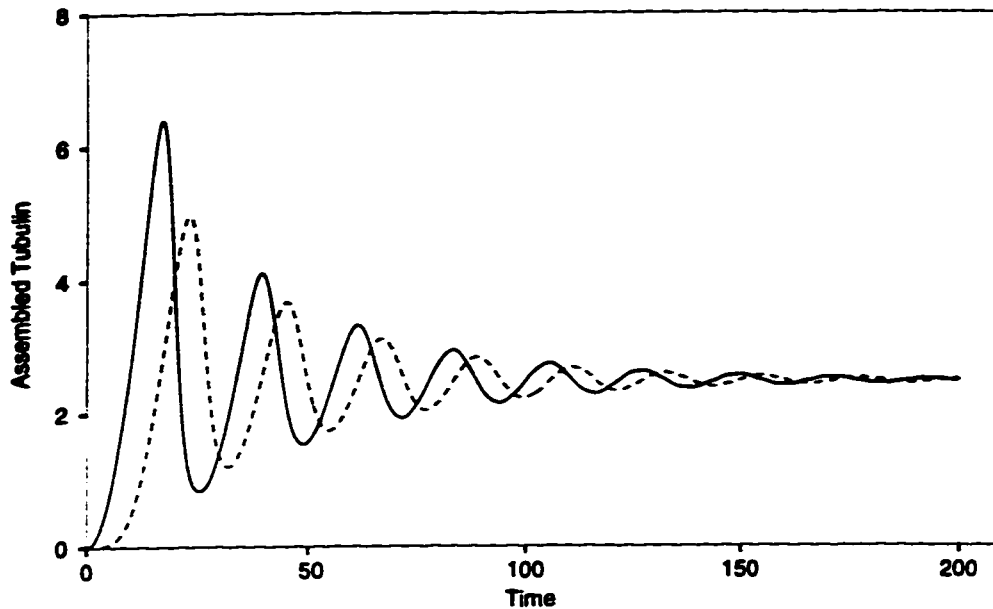
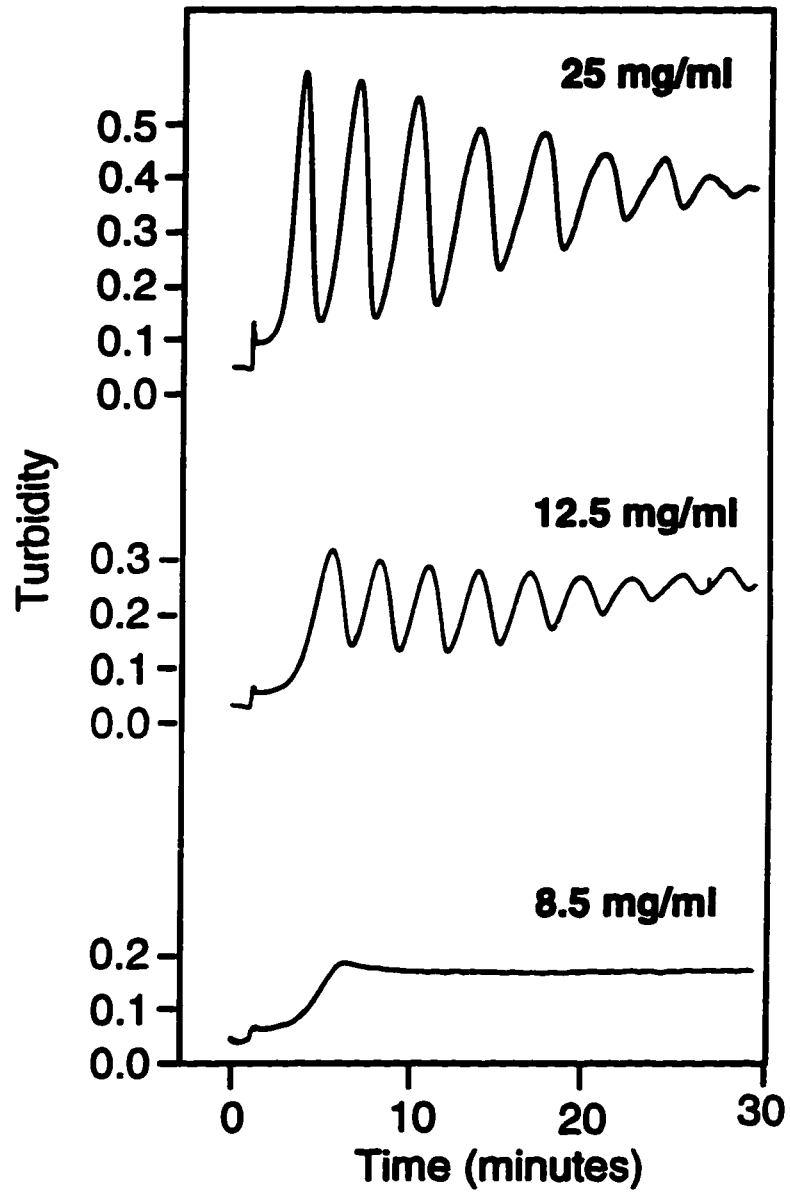


Figure 6.4: Solutions for T_a as a function of time for two sets of initial conditions. The solid line is for $T_t = 40 \mu\text{M}$ with all other variables initially set to zero and the dashed line is for $T_d = 40 \mu\text{M}$ and all others set to zero.

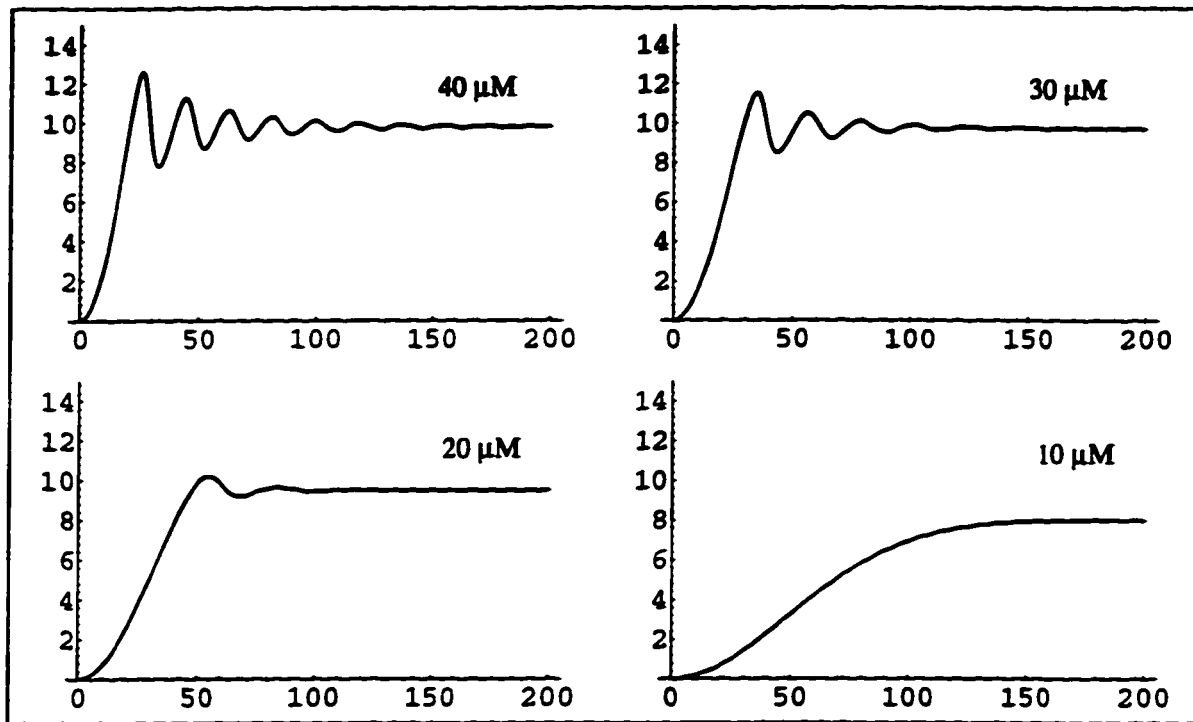
atures. Figure 6.6 shows the theoretical and experimental results. Although more evident in experiment [37], lowering the temperature produces a slower rise time and less pronounced oscillations with a greater period.

The temperature jump studies that are often performed involve quickly raising the temperature from 4°C to 37°C . If the temperature is raised slowly, it has a large effect on nucleation and the oscillations that result [37]. The same is found in this theoretical model (Figure 6.7). The more slowly that the temperature is raised, the more time the system has to adapt before oscillations enter in. This gives a slower rise time and smaller oscillations.

As was seen in the last section, the amount of assembled tubulin is not the only quantity which exhibits oscillations. It has also been observed that the free tubulin that is GTP-rich oscillates, although out of phase with the assembled tubulin [74].

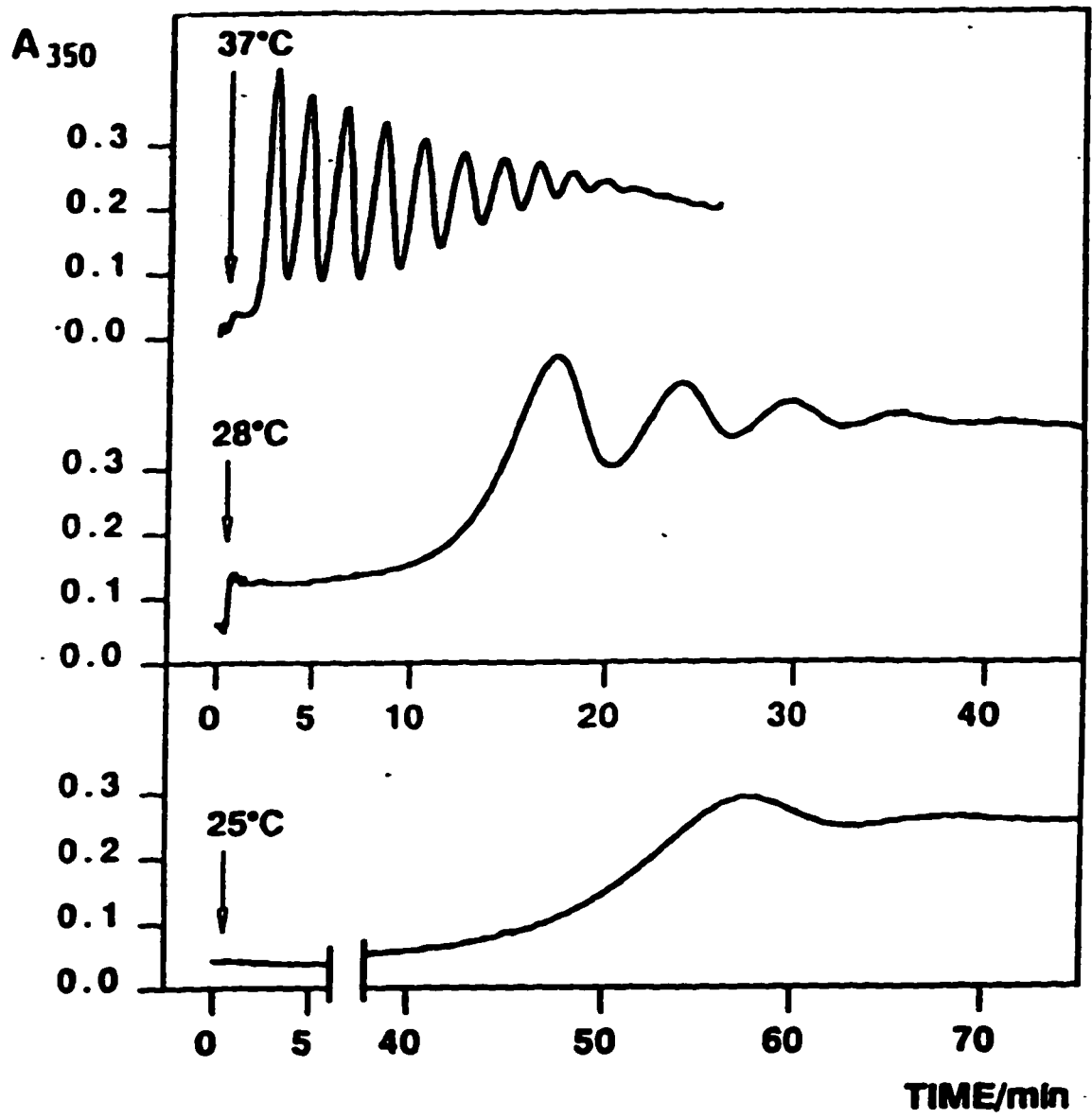


(a)

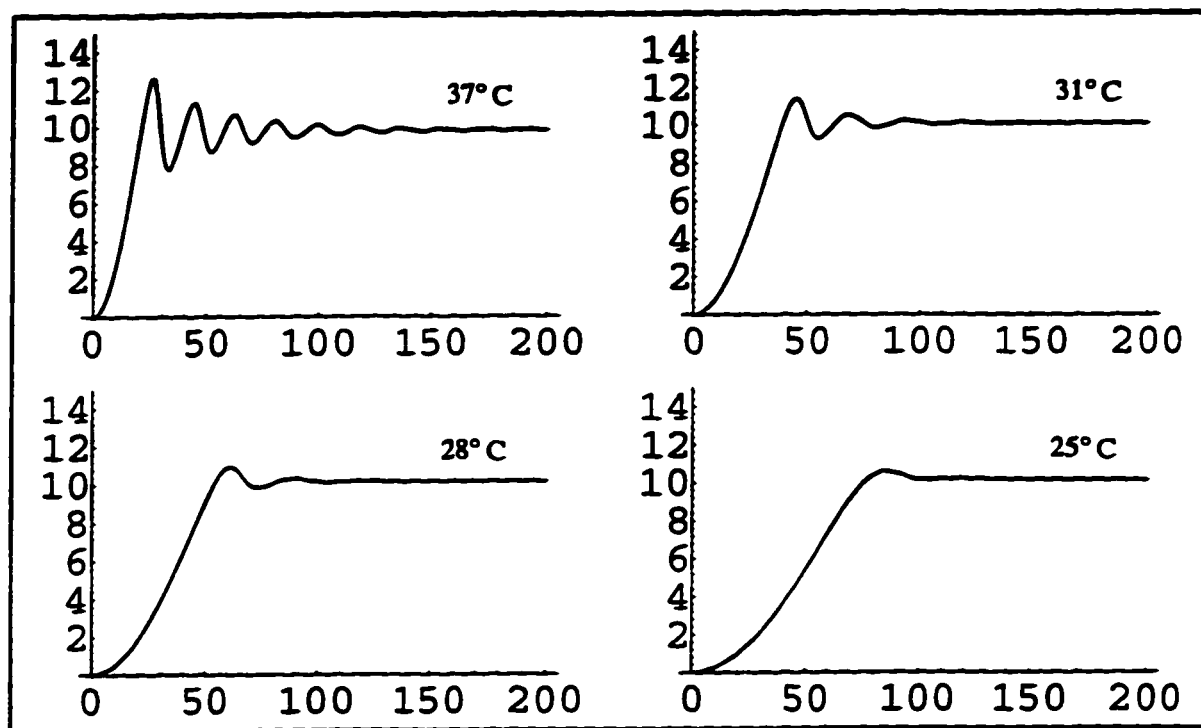


(b)

Figure 6.5: Plots of (a) experimental (previous page) and (b) theoretical results for microtubule oscillations at various tubulin concentrations. The results are both for 37°C. Experimental data courtesy of E. Mandelkow.



(a)



(b)

Figure 6.6: Plots of (a) experimental [37] (previous page) and (b) theoretical results for microtubule assembly at different temperatures. Simulations are for a tubulin concentration of $40 \mu\text{M}$.

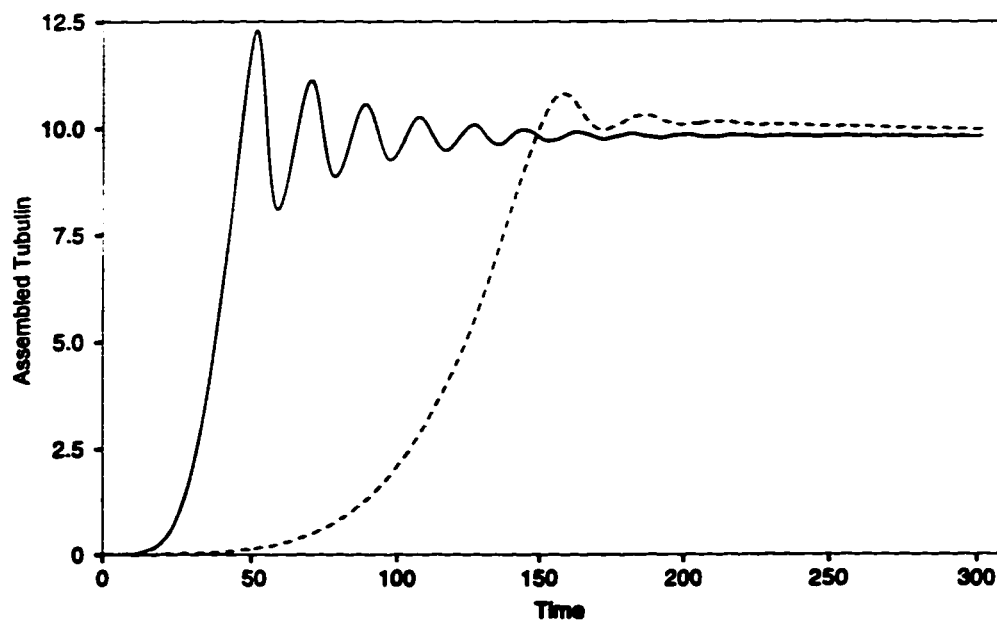
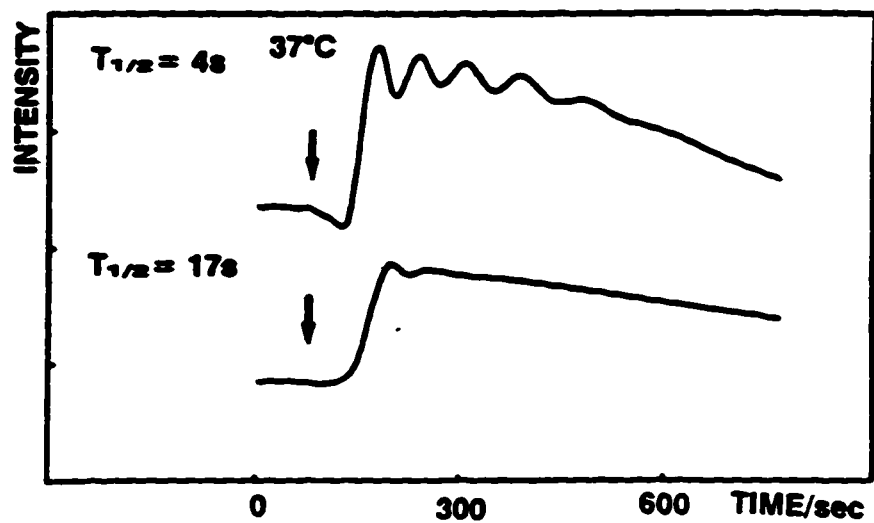


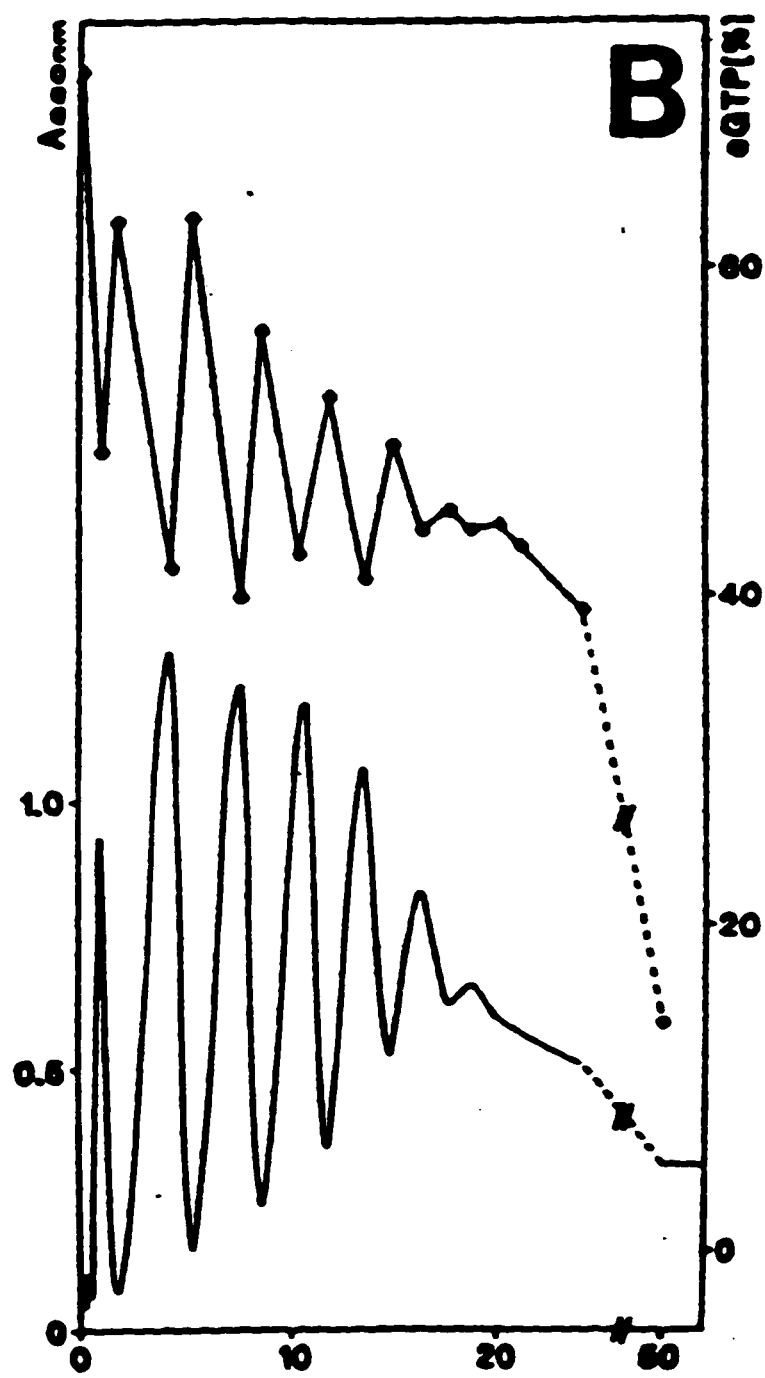
Figure 6.7: Experimental [37] (top) and theoretical (bottom) results showing the effect of slowly raising the temperature on oscillations and nucleation. For the theoretical results, in each case the temperature was raised from 0 – 37°C with a half time of 10 (solid curve) and 80 (dashed curve). The time units are the same as the units of the x-axis.

The same results occur in the theoretical model and are shown in Figure 6.8.

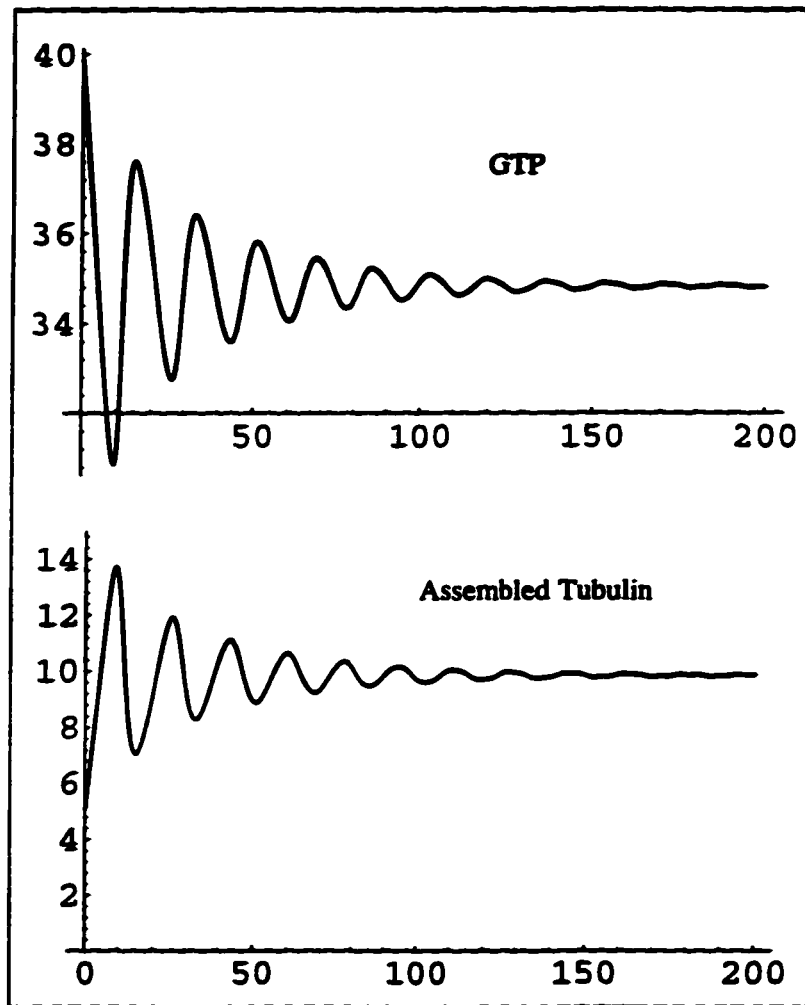
The amount of GDP or GTP-rich tubulin is a strong determining factor in the dynamics of the microtubule ensemble. In experiments, if GTP is added after the system has reached its steady-state value, oscillations are started once again. Figure 6.9 shows these results in both the experimental and theoretical case.

The rate at which GTP is regenerated in the theoretical model plays an important role in the dynamics. If the rate is elevated to a sufficiently high level, eventually all oscillations disappear and the system returns to monotonic growth (see Figure 6.10). Melki et al. [31] reported that the rate of GTP regeneration controlled the period of the oscillations. Their experimental data along with the theoretical results are shown in Figure 6.11.

One final experimental result that we can model is for an experiment performed by Carlier et al. [32]. In order to investigate the effect of microtubule number density on microtubule oscillations, they sheared the microtubules in the sample at the peak of the second oscillation. This in effect gives twice as many microtubules within the sample. Amos [8] noted how, when a stable microtubule was sheared at its midpoint, the new '-' end was stable while the new '+' end tended to shrink. This is consistent with measurements indicating that up to 75% of the assembled polymer would disassemble upon shearing [75]. If we attempt to simulate the same situation, we set $N = 2N$ and $T_a = 0.5T_a$ at the peak of the second oscillation. Reducing the amount of assembled tubulin at this same point takes the collapse of the new '+' end into account. The theoretical and experimental results are shown in Figure 6.12.



(a)



(b)

Figure 6.8: (a) Experimental findings [74] (previous page) and (b) theoretical plots for GTP-rich tubulin (top curves in each case) and the amount of assembled tubulin (bottom curves). Note how in each case the oscillations are in antiphase.

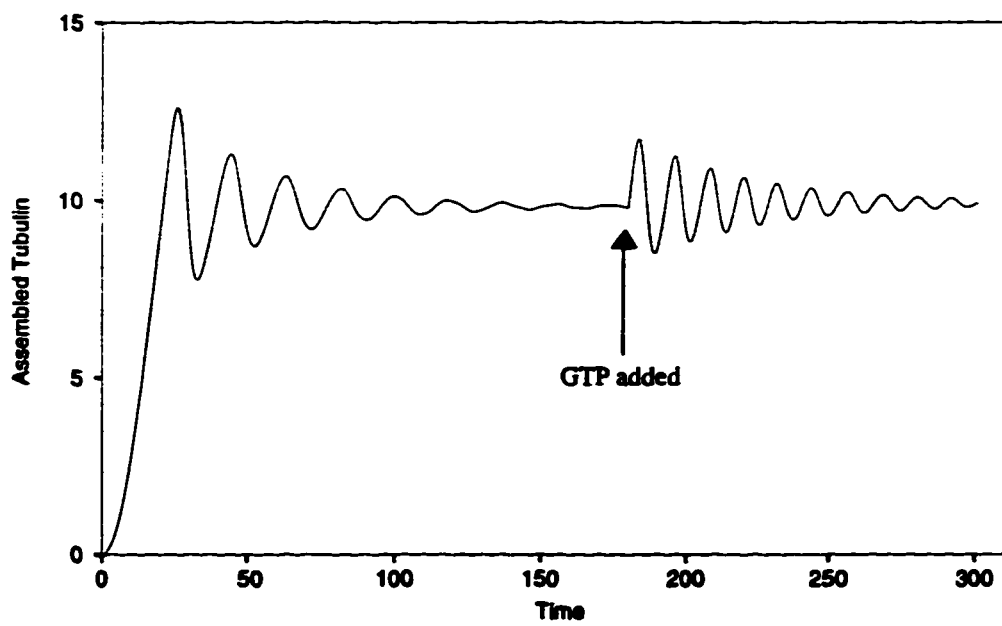
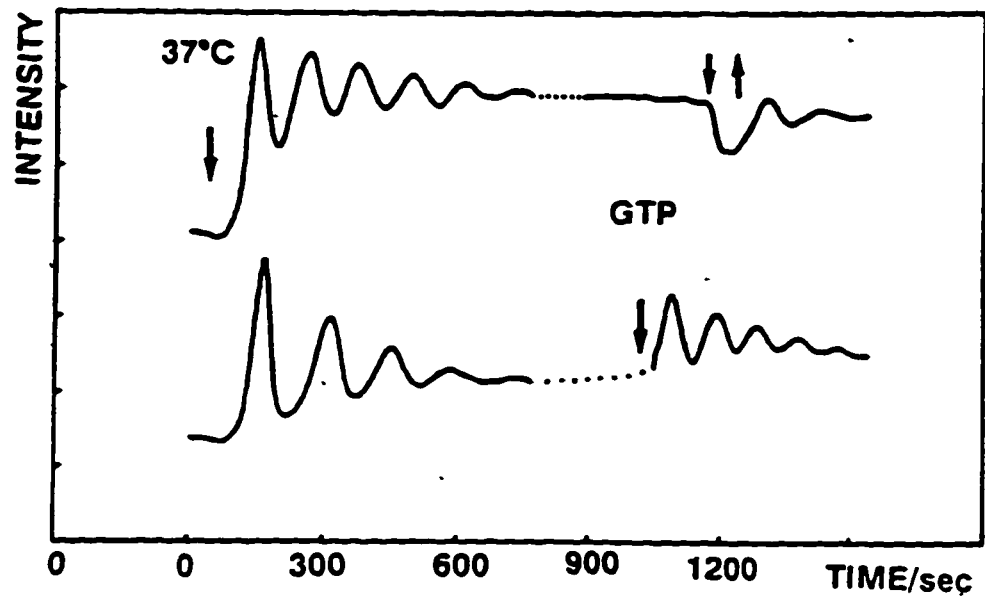


Figure 6.9: Plots of experimental [37] (bottom curve in top plot) and theoretical results (bottom plot) for adding GTP to a microtubule ensemble after reaching a steady-state.

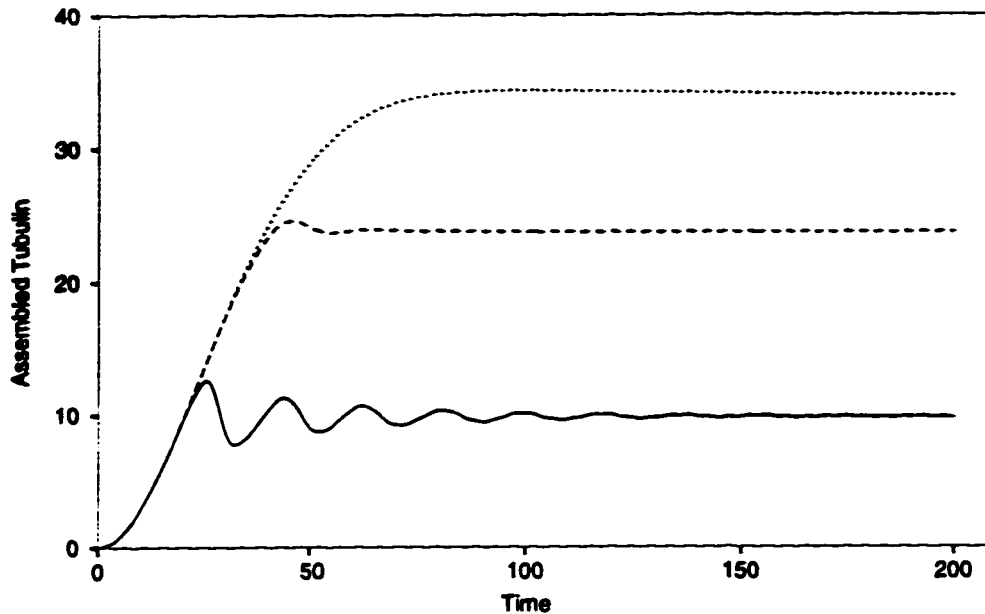


Figure 6.10: Plots of the total amount of assembled tubulin for various values of k_r . The values are $k_r = 2 \text{ s}^{-1}$ (solid curve), 5 s^{-1} (dashed curve) and 8 s^{-1} (dotted curve). All simulations are for a temperature of 37°C and a tubulin concentration of $40 \mu\text{M}$.

6.8 Additional Results

Aside from trying to reproduce existing experimental results, we can make predictions for potential new experiments. We have demonstrated how the rate of GTP regeneration controls the period of oscillations and at elevated values can make oscillations disappear. It would be interesting to see a phase diagram similar to Figure 6.2, but with k_r as a control parameter instead of temperature. Figure 6.13 shows the predicted phase diagram from the model where tubulin concentration and k_r are the control parameters. From looking at the diagram we see that if we begin in the oscillation region with a fixed tubulin concentration, by increasing k_r we move into the region of monotonic growth.

The temperature at which experiments are carried out had proved to be quite

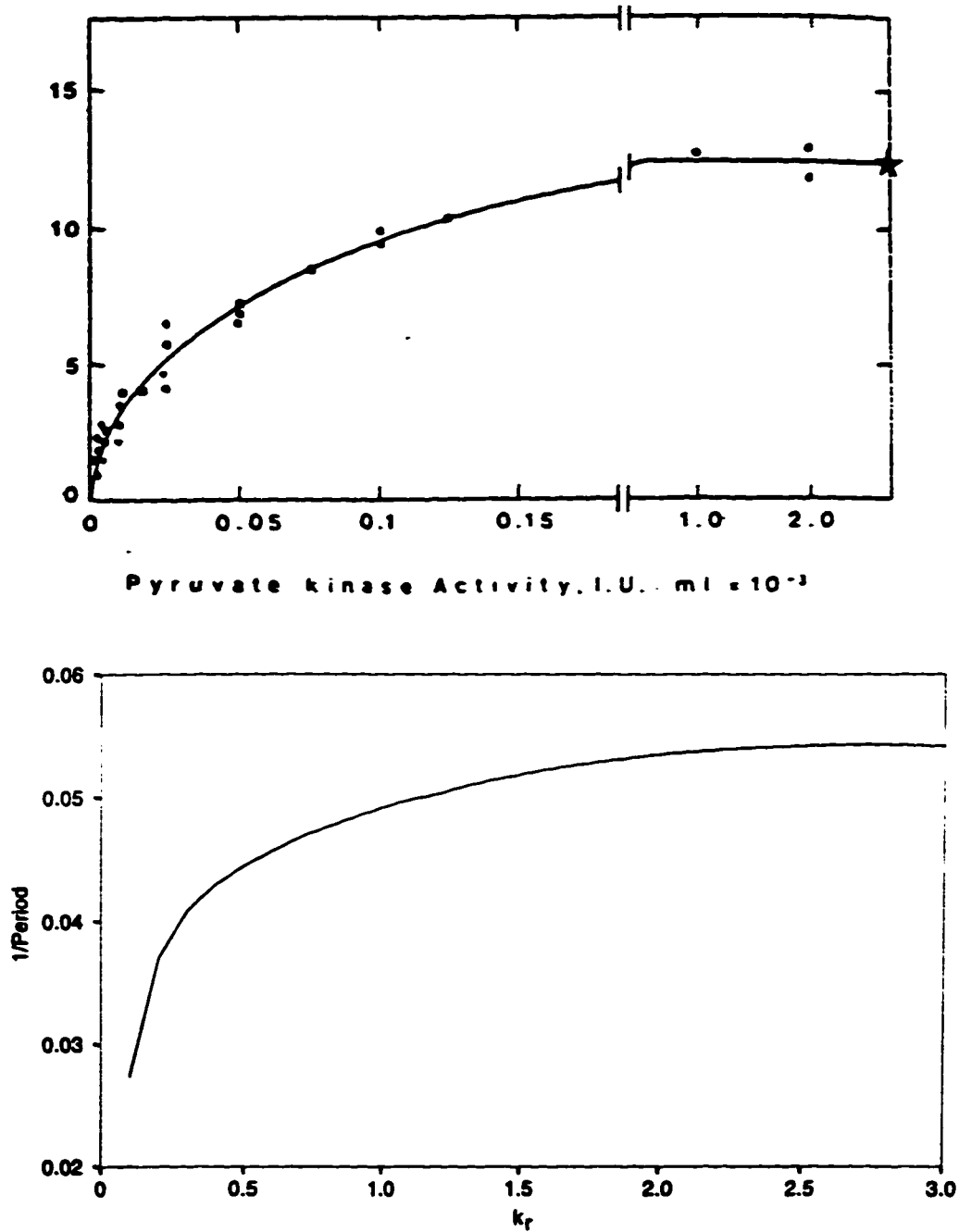


Figure 6.11: The period of microtubule oscillations as a function of the rate of GTP regeneration from experimental work [31] (top) and as predicted from the theoretical model (bottom).

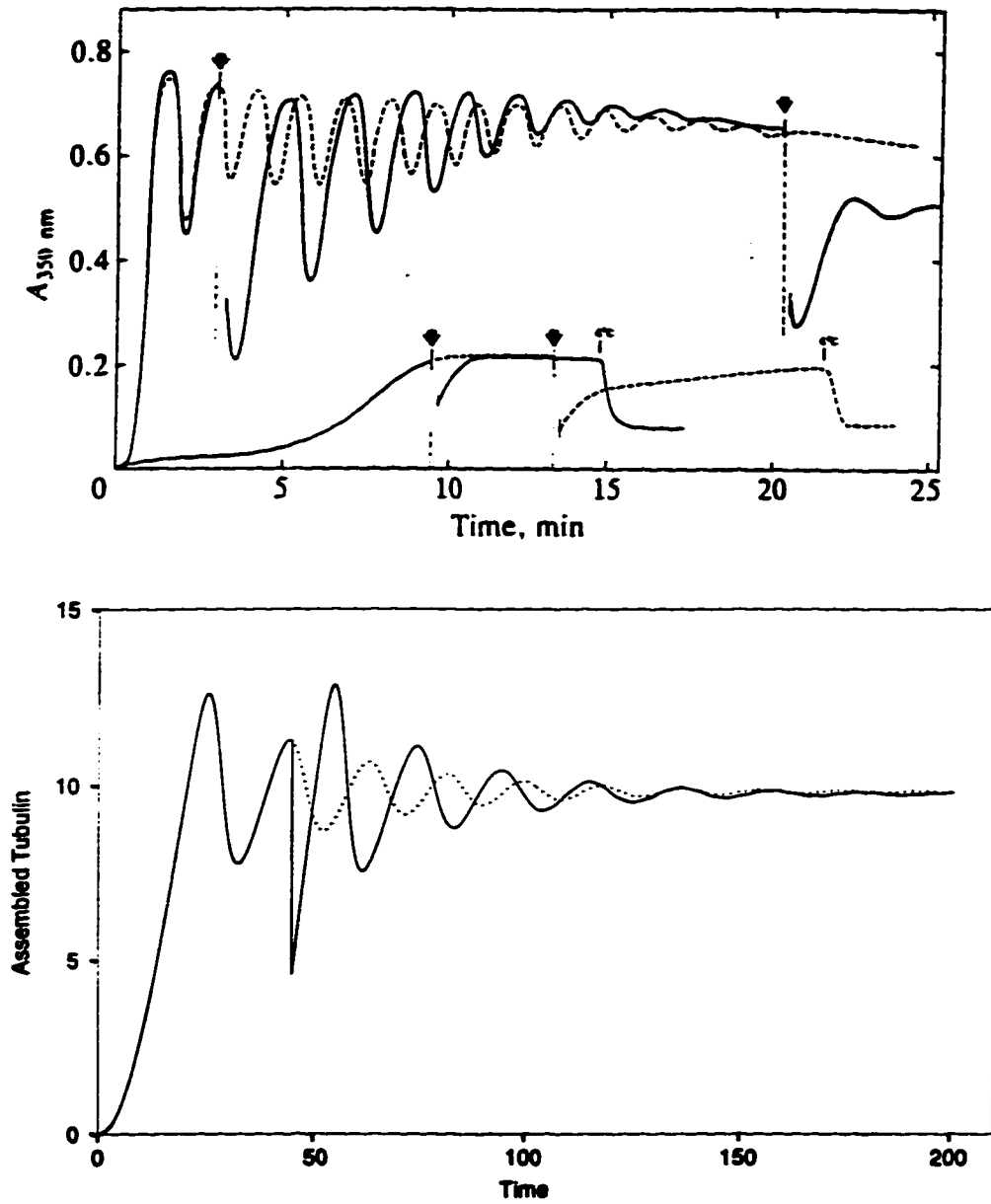


Figure 6.12: Experimental [32] (top) and theoretical (bottom) results for shearing of the microtubule ensemble. See text for explanation.

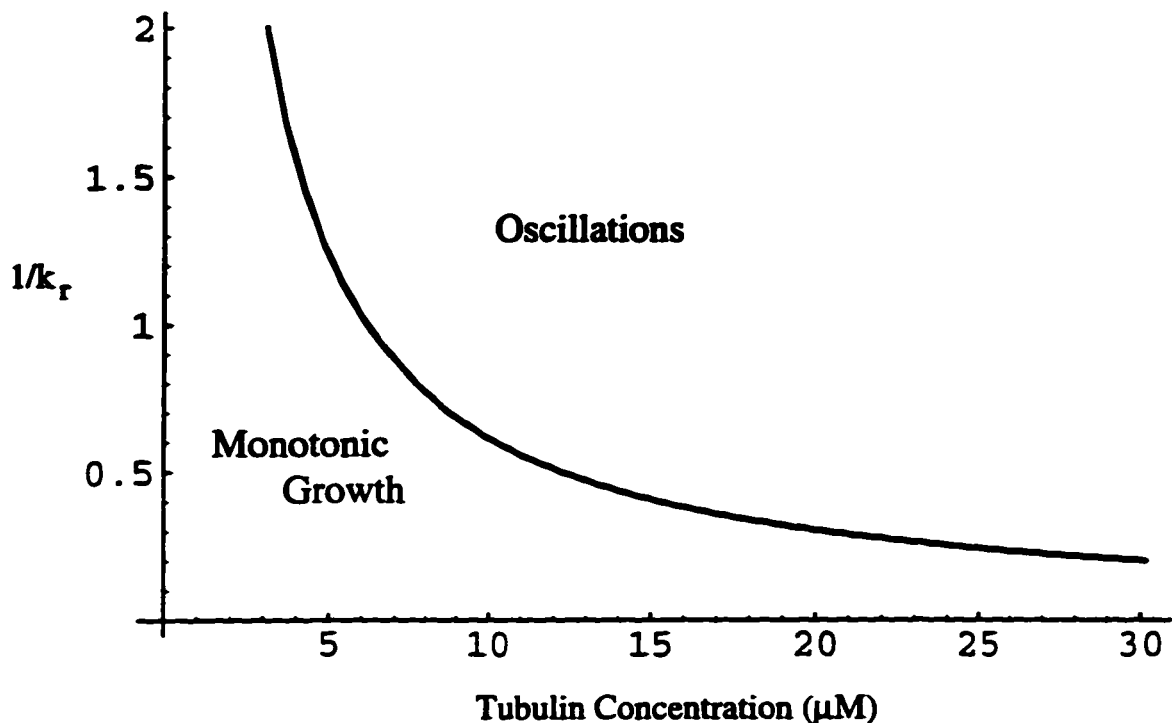


Figure 6.13: Phase diagram showing the different regions of microtubule assembly for different values of k_r and C . The temperature is fixed at 37°C .

important. It was also seen how raising the temperature had an effect on microtubule nucleation. We can perform similar simulations, but this time we will lower the temperature of the system after it has reached a steady-state. Figure 6.14 shows four plots for lowering the temperature at different rates. In the cases where the temperature is lowered more slowly, it almost appears as if oscillations would re-emerge, but inefficient nucleation seems to prevent the system from achieving this.

All of our results in this chapter have been based on the assumption that we are dealing with a homogeneous system. In terms of chemical kinetics, this is viewed as a system which is continuously stirred. In the lab however, regions of higher and lower concentration can occur which can give rise to inhomogeneous oscillations. As mentioned in Chapter 3, these oscillations produce both temporal and spatial

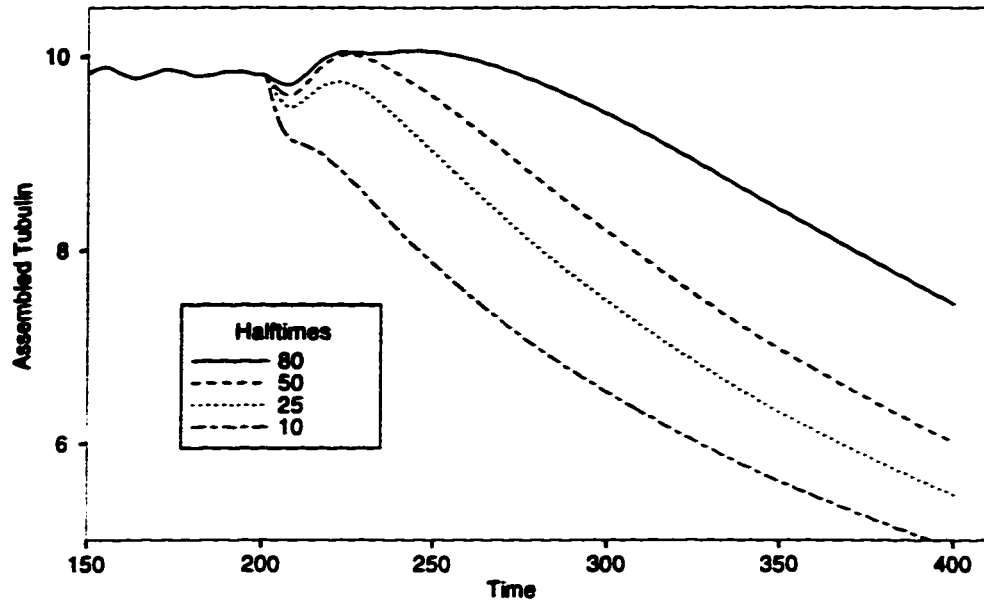


Figure 6.14: Plots showing the effect of lowering the temperature after the system has reached a steady-state. The halftimes listed are in the same units as the time on the x-axis.

patterns. To incorporate this possibility into our system we need to include spatial dependence in our variables. It also is natural at this stage to extend our model to include diffusion. Thus, the chemical reaction model will now become a set of reaction-diffusion equations. This is the topic of the next chapter.

Chapter 7

Reaction-Diffusion Modelling

Our system to this point has been assumed to be homogeneous. This is certainly true in some cases, but very often the reacting species are not uniformly distributed throughout the sample. If we take this inhomogeneity into account, it is also natural to allow the species to diffusively move through the cell. Thus, we arrive at a set of reaction-diffusion equations of the form

$$\dot{\vec{X}} = \vec{v}(\vec{X}) + D\nabla^2\vec{X} \quad (7.1)$$

where D is a diagonal matrix of diffusion constants. Such a system now allows us to investigate a much wider range of possibilities.

7.1 Connection with the Landau-Ginzburg Formulation

Before we concern ourselves with solving equations such as (7.1), it is most interesting to note the relationship between a reaction-diffusion approach and the Landau-Ginzburg method from Chapter 5. Imagine that we begin with a set of eqs. (7.1). We will denote the steady-state solution of our system as \vec{X}_0 and expand our system

of equations in a Taylor series around this point [76]

$$\dot{\phi} = D\nabla^2\phi + A\phi + B\phi\phi + C\phi\phi\phi + \dots \quad (7.2)$$

where $\vec{\phi} = \vec{X} - \vec{X}_0$. In this expansion, A is our Jacobian matrix given by

$$A_{ij} = \frac{\partial v_i}{\partial X_j} \quad (7.3)$$

and the other vectors are given by

$$(B\phi\phi)_i = \frac{1}{2!} \sum_{jk} \frac{\partial^2 v_i}{\partial X_j \partial X_k} \Big|_{X_0} \phi_j \phi_k \quad (7.4)$$

$$(C\phi\phi\phi)_i = \frac{1}{3!} \sum_{jkl} \frac{\partial^3 v_i}{\partial X_j \partial X_k \partial X_l} \Big|_{X_0} \phi_j \phi_k \phi_l. \quad (7.5)$$

For a simpler notation, we have dropped the vector notation and to make the calculations more straightforward we will assume that our chemical system has only second order and lower reactions so that $C = 0$. Suppose that we are dealing with a system involving microtubules. We know that for a fixed temperature, there exists a critical tubulin concentration C_c at which oscillations appear. With this in mind, we define

$$\mu = \frac{C - C_c}{C_c} \quad (7.6)$$

and expand our Jacobian in powers of μ as

$$A = A_0 + \mu A_1 + \dots \quad (7.7)$$

At criticality, we know from Chapter 6 that a pair of eigenvalues of A become complex. We choose one of these eigenvalues λ and expand it in the same manner

$$\lambda = \lambda_0 + \mu\lambda_1 + \dots \quad (7.8)$$

For convenience, we define a small parameter ϵ as [76]

$$\delta\epsilon^2 = \mu \quad \delta = \text{sgn } \mu \quad (7.9)$$

and expand ϕ in terms of ϵ

$$\phi = \epsilon\phi_1 + \epsilon^2\phi_2 + \dots \quad (7.10)$$

where $\phi_0 = 0$ since at the critical point the system remains at X_0 . Now our Taylor expansion coefficients become

$$A = A_0 + \delta\epsilon^2 A_1 + \epsilon^4 A_2 + \dots \quad (7.11)$$

$$B = B_0 + \delta\epsilon^2 B_1 + \epsilon^4 B_2 + \dots \quad (7.12)$$

We also want to introduce slow time and space coordinates, namely

$$\tau = \epsilon^2 t \quad (7.13)$$

and

$$\xi = \epsilon x. \quad (7.14)$$

Thus in terms of ξ and τ we will be looking at large scale, slow moving excitations. This choice of expansion also agrees with Landau-Ginzburg and diffusion theory in that

$$x \propto t^{1/2}.$$

So now we replace

$$\frac{d}{dt} \longrightarrow \frac{\partial}{\partial t} + \epsilon^2 \frac{\partial}{\partial \tau}$$

and

$$\nabla_x \longrightarrow \epsilon \nabla_\xi$$

so that our equation set becomes

$$\left(\frac{\partial}{\partial t} + \epsilon^2 \frac{\partial}{\partial \tau} - \epsilon^2 \nabla_\xi^2 - A_0 - \delta\epsilon^2 A_1 + \dots \right) (\epsilon\phi_1 + \epsilon^2\phi_2 + \dots) \quad (7.15)$$

$$= \epsilon^2 B_0 \phi_1 \phi_1 + \epsilon^3 2B_0 \phi_1 \phi_2 + O(\epsilon^4) \quad (7.16)$$

Matching powers of ϵ gives us:

$$\epsilon^1 : \left(\frac{\partial}{\partial t} - A_0 \right) \phi_1 = 0 \quad (7.17)$$

$$\epsilon^2 : \left(\frac{\partial}{\partial t} - A_0 \right) \phi_2 = B_0 \phi_1 \phi_1 \quad (7.18)$$

$$\epsilon^3 : \left(\frac{\partial}{\partial t} - A_0 \right) \phi_3 = - \left(\frac{\partial}{\partial \tau} - \delta A_1 - D \nabla_{\xi}^2 \right) \phi_1 + 2B_0 \phi_1 \phi_2 \quad (7.19)$$

⋮

$$\epsilon^i : \left(\frac{\partial}{\partial t} - A_0 \right) \phi_i = \Lambda_i \quad (7.20)$$

By examining eq.(7.20) it seems appropriate to express both ϕ_i and Λ_i in a Fourier series as

$$\phi_i(t, \tau) = \sum_l \phi_i^{(l)}(\tau) e^{il\beta_0 t} \quad (7.21)$$

$$\Lambda_i(t, \tau) = \sum_l \Lambda_i^{(l)}(\tau) e^{il\beta_0 t} \quad (7.22)$$

where β_0 is the imaginary part of $\lambda_0 = \alpha_0 + i\beta_0$, the eigenvalue which approaches criticality. Thus for each value of l we get an equation

$$(il\beta_0 - A_0) \phi_i^{(l)} = \Lambda_i^{(l)}. \quad (7.23)$$

If we apply the left eigenvector of A_0 corresponding to λ_0 , ie.

$$U_L A_0 = \lambda_0 U_L,$$

and take $l = 1$ we get

$$\begin{aligned} (i\beta_0 - \lambda_0) U_L \phi_i^{(1)} &= U_L \Lambda_i^{(1)} \\ -\alpha_0 U_L \phi_i^{(1)} &= U_L \Lambda_i^{(1)} \\ U_L (\Lambda_i^{(1)} + \alpha_0 \phi_i^{(1)}) &= 0. \end{aligned} \quad (7.24)$$

We will come back to eq.(7.24) later since we first need to solve for ϕ_1 and ϕ_2 . From eq.(7.17) we can easily determine that

$$\phi_1 = \eta(\tau) U_R e^{i\beta_0 t} + \bar{\eta}(\tau) \bar{U}_R e^{-i\beta_0 t} \quad (7.25)$$

where η is a complex amplitude, U_R is a right eigenvector of A_0 , again for the eigenvalue λ_0 and we have denoted the complex conjugate with a bar. Substituting this solution into (7.18) gives us [76]

$$\phi_2 = F_+ \eta^2 e^{2i\beta_0 t} + F_- \bar{\eta}^2 e^{-2i\beta_0 t} + F_0 |\eta|^2 + \gamma \phi_1 \quad (7.26)$$

where

$$F_+ = \bar{F}_- = -(A_0 - 2i\beta_0 \mathcal{I})^{-1} B_0 U_R U_R \quad (7.27)$$

$$F_0 = -2A_0^{-1} B_0 U_R \bar{U}_R \quad (7.28)$$

where \mathcal{I} represents the identity matrix. These two solutions can now be substituted into (7.19) so we can find an expression for Λ_3 . We are really interested in solving (7.24) which requires knowing $\phi_3^{(1)}$. From (7.23) we see that

$$\phi_3^{(1)} = -(A_0 - i\beta_0 \mathcal{I})^{-1} \Lambda_3^{(1)} \quad (7.29)$$

so (7.24) becomes

$$U_L \left([\mathcal{I} - \alpha_0 (A_0 - i\beta_0 \mathcal{I})^{-1}] \Lambda_3^{(1)} \right) = 0 \quad (7.30)$$

The expression for $\Lambda_3^{(1)}$ is just the right-hand side of (7.19) with the solutions (7.25) and (7.26) substituted and taking on the terms with the factor $e^{i\beta_0 t}$:

$$\Lambda_3^{(1)} = -\left(\frac{\partial}{\partial \tau} - \delta \lambda_1 - D \nabla_\xi^2 \right) U_R \eta + 2B_0 (U_R F_0 + \bar{U}_R F_+) |\eta|^2 \eta. \quad (7.31)$$

Thus, eq. (7.30) becomes a Landau-Ginzburg equation

$$\frac{\partial \eta}{\partial \tau} = \delta \lambda_1 \eta - \Delta |\eta|^2 \eta + D' \nabla_\xi^2 \eta \quad (7.32)$$

where the constants Δ and D' are defined as

$$\Delta = \frac{U_L (\mathcal{I} - \alpha_0 (A_0 - i\beta_0 \mathcal{I})^{-1}) 2B_0 (U_R F_0 + \bar{U}_R F_+)}{U_L (\mathcal{I} - \alpha_0 (A_0 - i\beta_0 \mathcal{I})^{-1}) U_R} \quad (7.33)$$

$$D' = U_L D U_R. \quad (7.34)$$

If instead we write $\eta = \psi(\xi, \tau)e^{i\theta(\tau)}$, eq. (7.32) separates into two equations

$$\frac{\partial \psi}{\partial \tau} = \delta \alpha_1 \psi - \Delta_r \psi^3 + D'_r \nabla_\xi^2 \psi \quad (7.35)$$

$$\frac{\partial \theta}{\partial \tau} = \delta \beta_1 - \Delta_i \psi^2 + D'_i \nabla_\xi^2 \psi \quad (7.36)$$

where we have written $\lambda_1 = \alpha_1 + i\beta_1$, $\Delta = \Delta_r + i\Delta_i$ and $D' = D'_r + iD'_i$. Thus we have an amplitude which satisfies a Landau-Ginzburg equation. Similar interpretations relating to the nonlinear diffusion equation and Landau-Ginzburg theory have shown how the envelope of an oscillating wave satisfies an equation such as (7.32). We, however, are not interested in simply defining the envelope of solutions, but finding the solutions themselves.

7.2 The Reaction-Diffusion Model

Our model has been extended to include diffusion, but not all quantities will diffuse to the same extent. Assembled microtubules are much larger than their constituent dimers and would diffuse much more slowly. For this reason, we will only consider the diffusion of free tubulin, T_d and T_t . With these added terms, eqs. (6.28-31) become

$$\dot{N} = -k_c N + k_n T_t - k_i N T_d \quad (7.37)$$

$$\dot{T}_a = k_+ N T_t - k_c T_a + k_n T_t - k_i T_a T_d \quad (7.38)$$

$$\dot{T}_d = k_c T_a - k_r T_d + k_i T_a T_d + D \nabla^2 T_d \quad (7.39)$$

$$\dot{T}_t = -k_+ N T_t - k_n T_t + k_r T_d + D \nabla^2 T_t. \quad (7.40)$$

where the diffusion constant D is the same for all dimers, independent of their bound nucleotide. Just as we had experimental data to determine our rate constants, the diffusion of tubulin within the cytoplasm has been measured. Salmon et al. [77] found an *in vivo* value of $D = 5.9 \times 10^{-8} \text{ cm}^2/\text{s}$. From this they also estimated a value of $D = 56 \times 10^{-8} \text{ cm}^2/\text{s}$ for tubulin in an *in vitro* buffer.

With all of the constants determined, we can solve the system of equations. However, we can no longer use the Runge-Kutta method from the last chapter. For a solution in one spatial dimension, we discretize each quantity (T_a , T_d , T_t and N) on a (x, t) grid. To avoid having to invert very complicated matrices and to maintain all of the nonlinear terms, an explicit method was selected. The second derivative was calculated using a five-point central difference formula

$$\frac{\partial^2 T_i^n}{\partial x^2} \approx \frac{1}{3} \left[\frac{4(T_{i+1}^n - 2T_i^n + T_{i-1}^n)}{\Delta x^2} - \frac{T_{i+2}^n - 2T_i^n + T_{i-2}^n}{(2\Delta x)^2} \right] + O(\Delta x^4). \quad (7.41)$$

In this formula, the subscript i and superscript n denote the grid point (x_i, t_n) and T represents one of the reactant concentrations. We want to solve this system subject to particular boundary conditions. Since we have a closed vessel, we choose no-flux boundary conditions

$$\frac{\partial T_i^n}{\partial x} = 0 \text{ for } i = 1, N. \quad (7.42)$$

This can easily be incorporated into our central difference formula by artificially making each concentration profile symmetric around each boundary. If T_1 represents one of the edges, then we assume $T_0 = T_2$, $T_{-1} = T_3$, and so on. Care must be taken in doing the time discretization. Since we have a diffusion term, a standard leap-frog method cannot be used since it is unconditionally unstable. The next highest order explicit method is the third order Adams-Bashforth method [78]. If we have an equation of the form

$$\frac{\partial T}{\partial t} = F$$

the temporal difference is

$$T^{n+1} = T^n + \Delta t \left(\frac{23}{12} F^n - \frac{16}{12} F^{n-1} + \frac{5}{12} F^{n-2} \right) \quad (7.43)$$

where F^n represent the function F evaluated at time t_n . This scheme is accurate to $(\Delta t)^3$. The initial conditions can be set identically into the first three time steps. This causes the first iteration to be simply forward difference, the second to be a

combination of leap-frog and second order Adams-Bashforth, but all subsequent iterations to be third order accurate. Linear stability analysis is extremely difficult for a coupled nonlinear system like ours. To ensure stability, we will simply choose a Δt that is 'small enough'.

We are now ready to find solutions. Once again a graphical user interface was constructed on top of the solver so that parameters could easily be manipulated. After selecting a temperature, tubulin concentration and diffusion constant, the user could watch all the solutions develop in time for a given set of initial conditions.

7.3 Results of the model

The free parameters we now have to work with are the temperature, tubulin concentration and the diffusion coefficient for T_d and T_t . We have one additional freedom compared to the previous modelling in that we may choose inhomogeneous initial conditions for the concentrations. If we would choose constant profiles for T_d and T_t , the diffusion term would contribute nothing since the Laplacian would be zero. For non-constant profiles, each part of the system will evolve based on local concentrations but would be coupled to the rest of the cell by the diffusion of the free tubulin. Systems such as this have long been known to be important in pattern formation phenomena. Turing [79] proposed reaction-diffusion models as the basis for pattern formation in chemical systems. Later, models involved gradients of the concentrations to produce patterns in biological systems [80]. In any case, the basis of all pattern formation either in chemical or biological systems is inhomogeneity in either the initial conditions, diffusion coefficients or the rate constants. For steady-state patterns to emerge in systems with diffusion, patterns must be due to spatially inhomogeneous rate or diffusion constants since diffusion will eventually remove patterns simply due to initial conditions.

In our system, the diffusion constant is very small on the scale of the other variables. Because of this, instabilities arising from diffusion are unlikely. Figure 7.1 shows the effect that diffusion has on the solutions. The initial conditions were such that the neighbouring grid points to the point which was plotted have zero tubulin concentration and thus diffusion was maximal. The effect is a longer period with more damping of the oscillations. The steady-state value does not depend on D and is the same in each case.

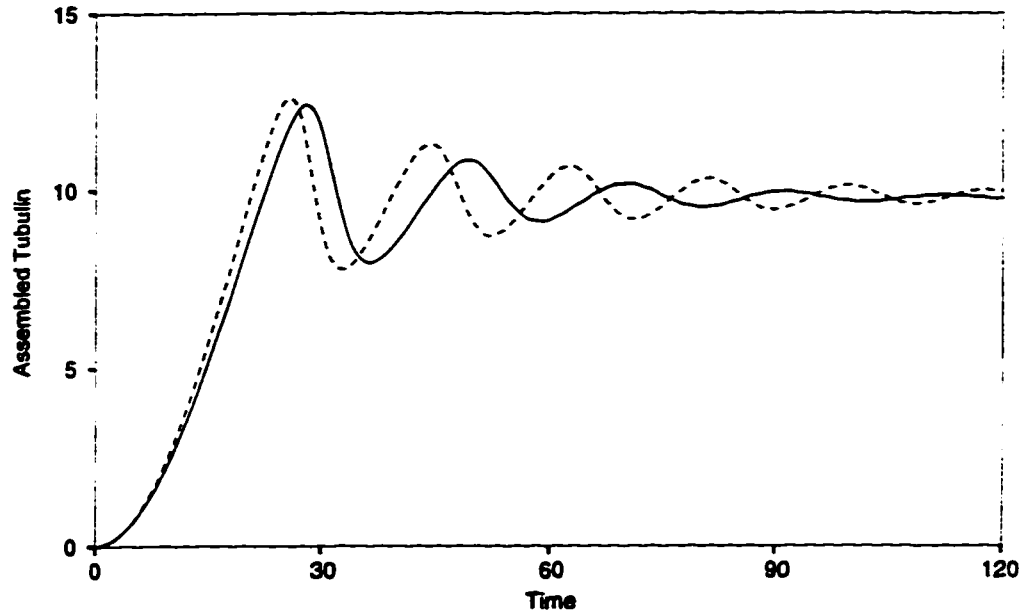


Figure 7.1: Plot showing the effect of diffusion on the solutions. The dashed line is for $40 \mu\text{M}$ without diffusion and the solid line with diffusion. See text for details.

We know that increasing the concentration of GTP rich tubulin increases the size of the oscillations. If we introduce an initial gradient of T_t across the cell, we would expect interesting dynamics. Figure 7.2 shows the results for a linear gradient of T_t from $20 \mu\text{M}$ on one edge to $60 \mu\text{M}$ on the other. The spatial dimension was discretized into 160 points.

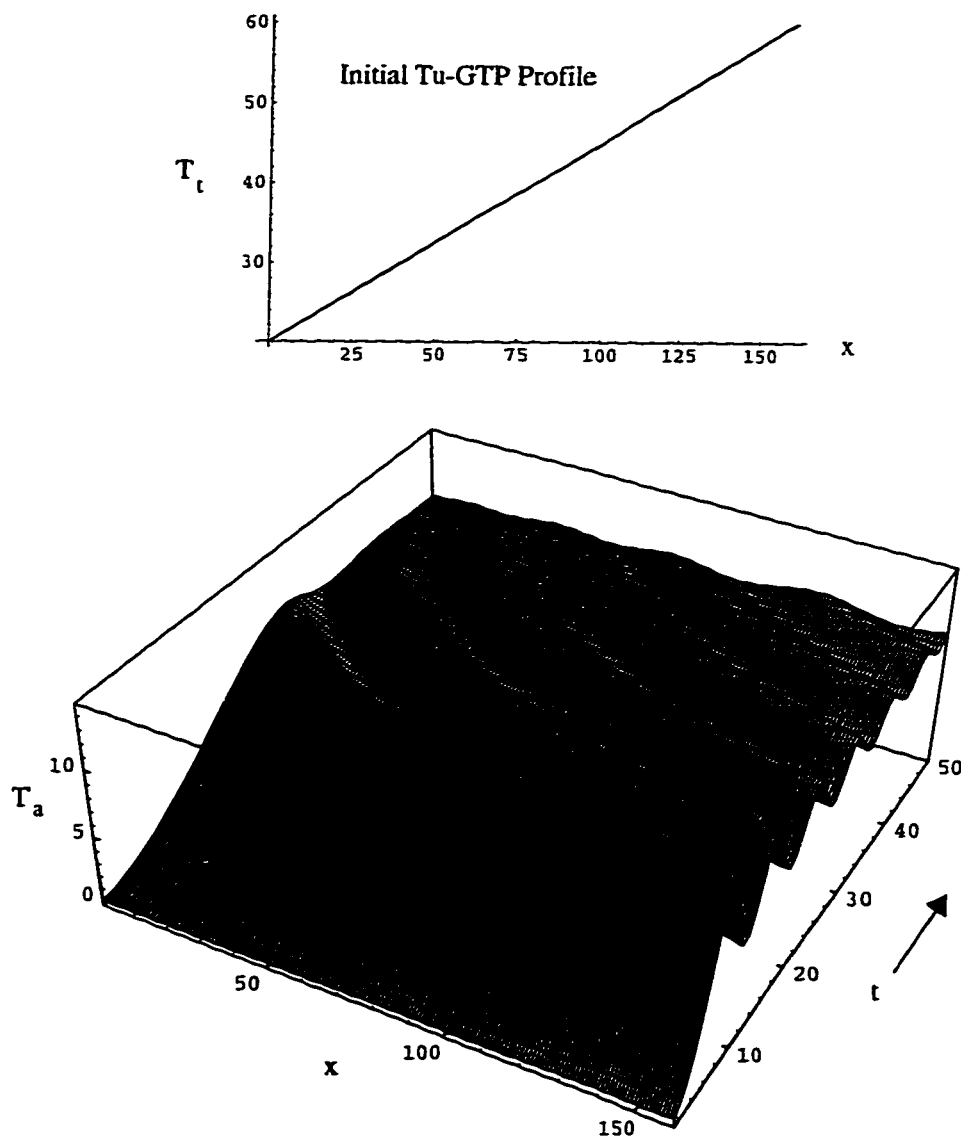


Figure 7.2: Simulation for an initial gradient of Tu-GTP as shown in the top plot. All other variables are initially set to zero.

Apart from the effect of tubulin concentration, we know that temperature also has a large effect. Figure 7.3 shows a simulation for a temperature gradient of 5°C across the cell. The result is once again a higher rate of oscillation at the high temperature end. Although these plots only run for a short time, it can easily be seen how initial conditions cannot produce stable patterns. At the last time step, each plot is very nearly flat. To change this result, we must assume some constant(s) to be spatially inhomogeneous.

Recall the finding of the Mandelkow group discussed in Chapter 2. In systems where they observed waves crossing the vessel, they concluded that the barrier for nucleation was somehow lower at the boundaries. Since most of the experiments were started using a temperature jump, we can safely assume that the buffer was well mixed to begin with. They also stated that temperature gradients were virtually absent from the experiment. To try and produce such waves in our system, we assume a nucleation rate which is highest at the edge of the cell and decays exponentially to the interior of the cell. Figure 7.4 shows the spatial dependence of k_n along with the plot of T_a . The simulation was performed for a tubulin concentration of $40\ \mu\text{M}$. After nucleation at the boundary, a wave of assembled tubulin propagates into the cell center. This is in fact not a single wave, but a series of waves.

If the tubulin concentration is raised to $100\ \mu\text{M}$, the size of the waves does not change, but they persist further into the cell. As well, if the GTP regeneration rate is lowered from $2\ \text{s}^{-1}$ to $0.3\ \text{s}^{-1}$, the height difference between the crests and troughs is increased and the spacing between adjacent waves is greater. Both these effects are shown in Figure 7.5.

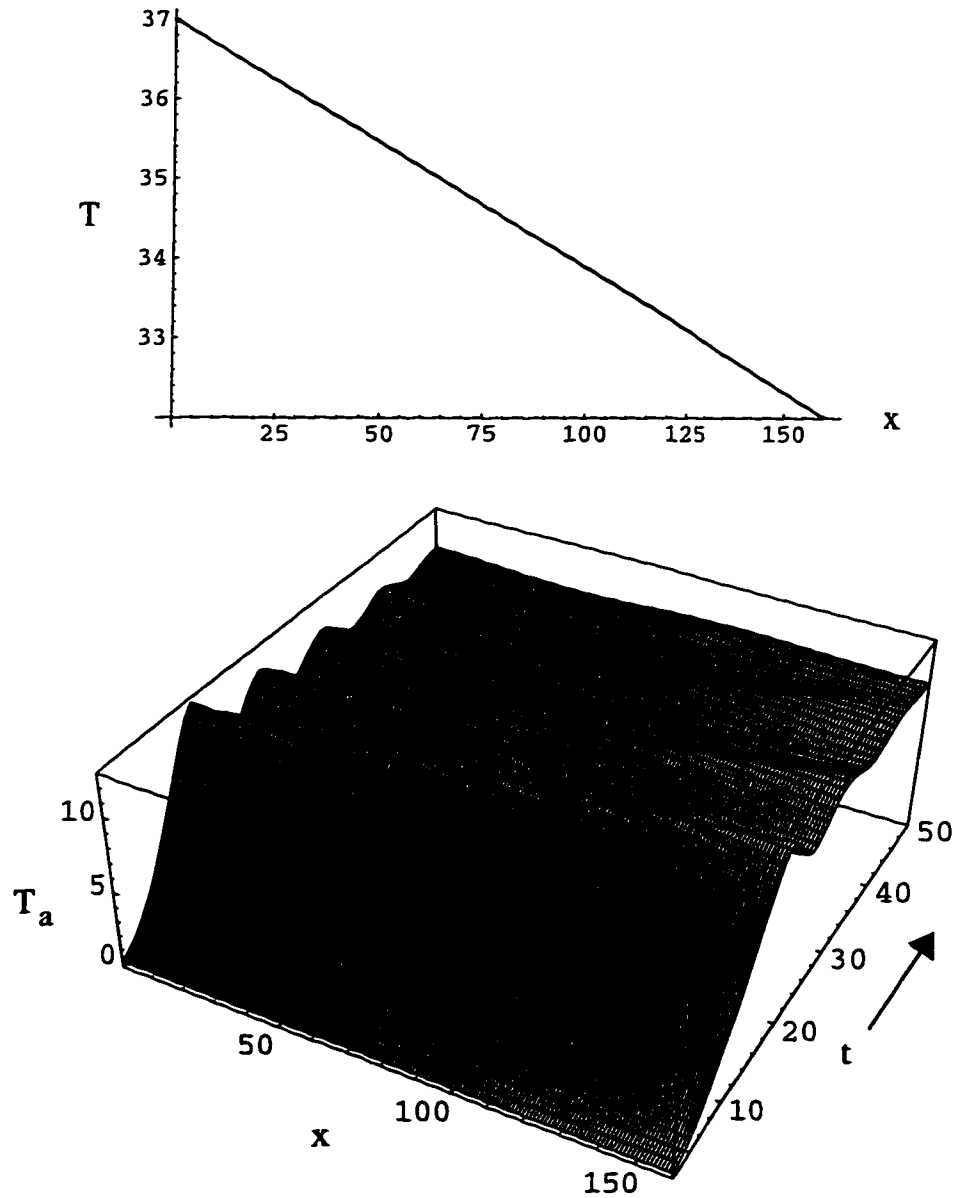


Figure 7.3: Simulation for a temperature gradient across the cell as shown in the top plot. Initially, $T_t = 40 \mu\text{M}$ and all other variables are set to zero.

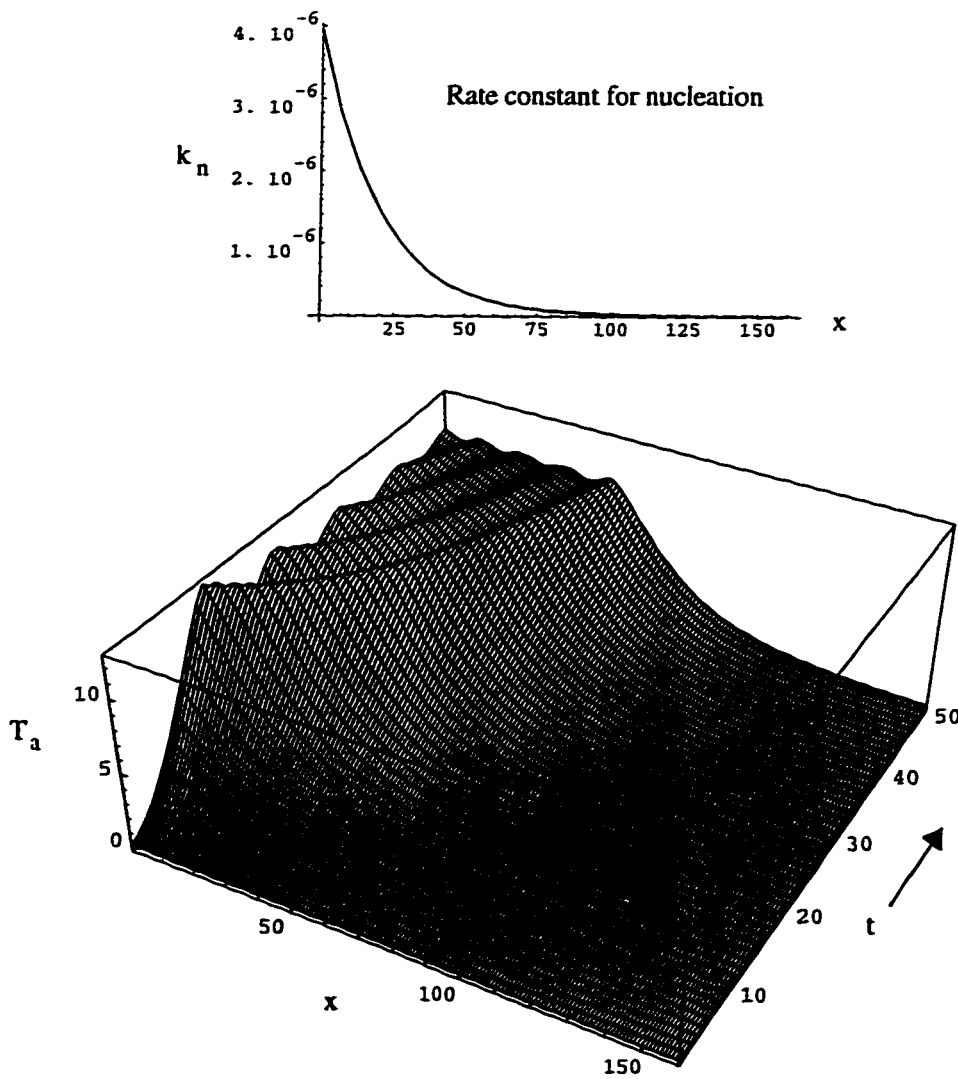


Figure 7.4: Simulation for an inhomogeneous nucleation rate. The spatial dependence of k_n is shown above the resulting simulation. Waves of assembled tubulin are nucleated at the boundary and propagate towards the middle of the cell. The tubulin concentration is $40 \mu\text{M}$.

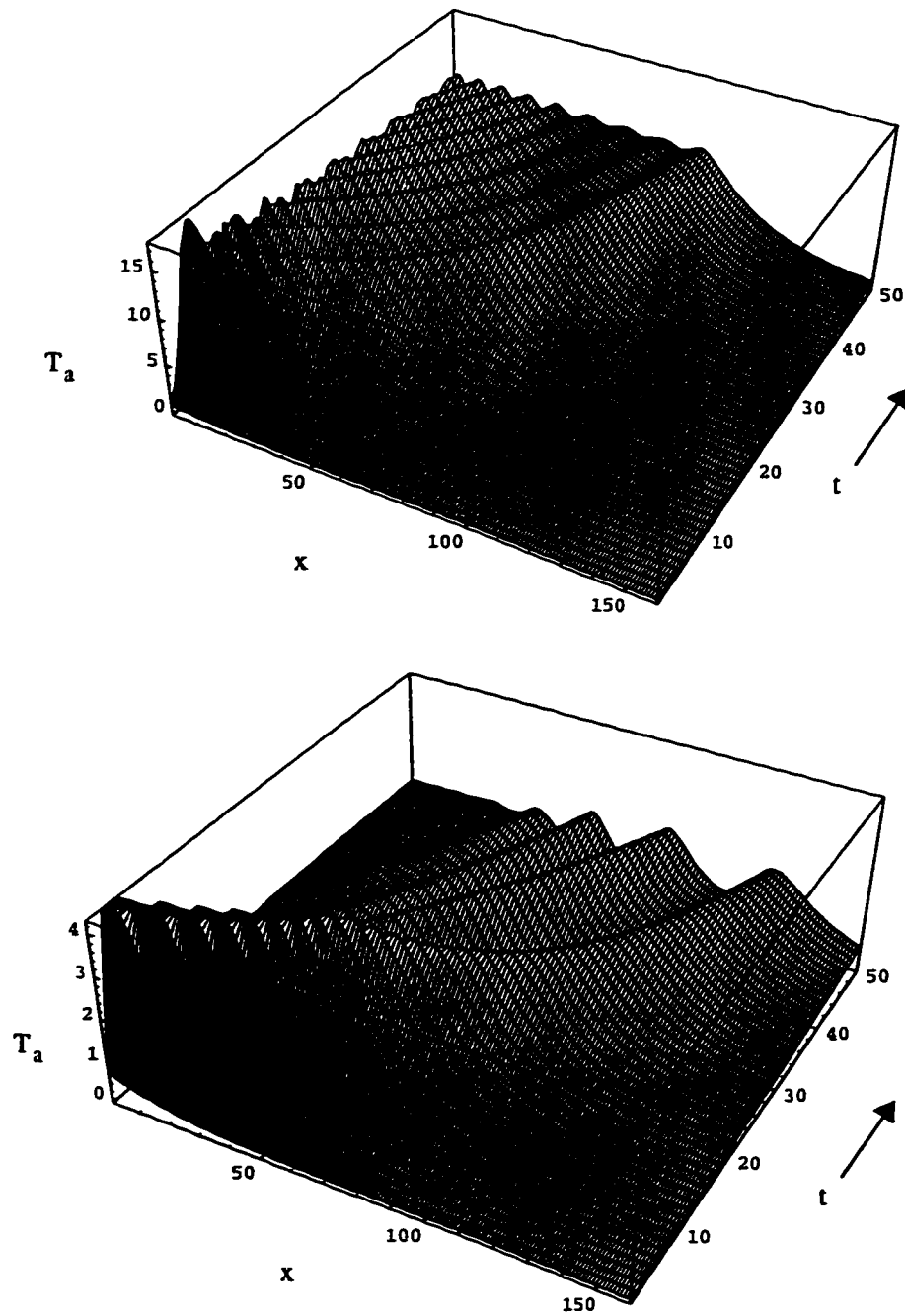


Figure 7.5: Simulation for an inhomogeneous nucleation rate for $100 \mu\text{M}$ tubulin. The spatial dependence of k_n is the same as in Figure 7.4 but $k_r = 2 \text{ s}^{-1}$ (top) and $k_r = 0.3 \text{ s}^{-1}$ bottom.

Having rate constants which are spatially inhomogeneous is a prime method of producing steady-state patterns within a system. Within the cell, the main Microtubule Organizing Center (MTOC) is the centrosome. Here, microtubules are nucleated and their '-' ends are embedded while the '+' end extend away from the centrosome. It is natural to assume that the rate of nucleation is higher at a MTOC than any other point within the cell. We can model this via the following. Suppose at the center of our cell we have an MTOC. Around this point the nucleation rate is highest in the center and drops off exponentially as shown in Figure 7.5. If this is the only inho-

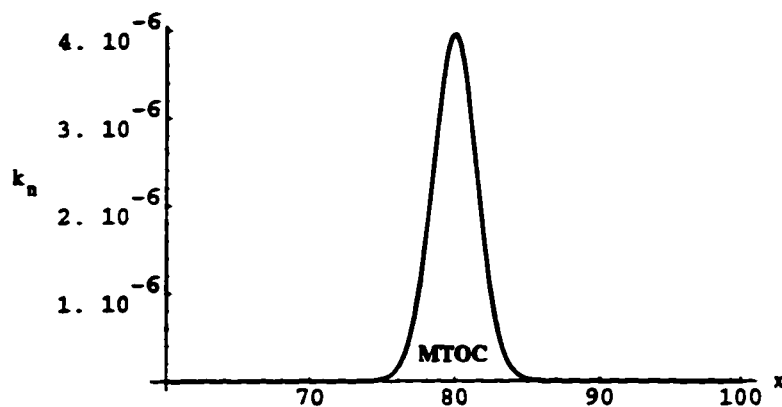


Figure 7.6: Spatial variation of the nucleation rate constant simulating the effect of a MTOC.

mogeneity and we begin the simulation with $40 \mu\text{M}$ tubulin, we get the results shown in Figure 7.6. Now we see that after the oscillations cease, we maintain a group of microtubules nucleated at the MTOC. From comparing the plots of N and T_a , we also see that the microtubules on the outer part of the MTOC are longer compared to the ones at the center.

This same type of effect can be realized by choosing any of our rate constants to have some spatial dependence. If more experimental data were available, it would be interesting to try to emulate observed patterns and formations. All in all, this chemical kinetics model, both with and without diffusion, has proven to be quite successful.

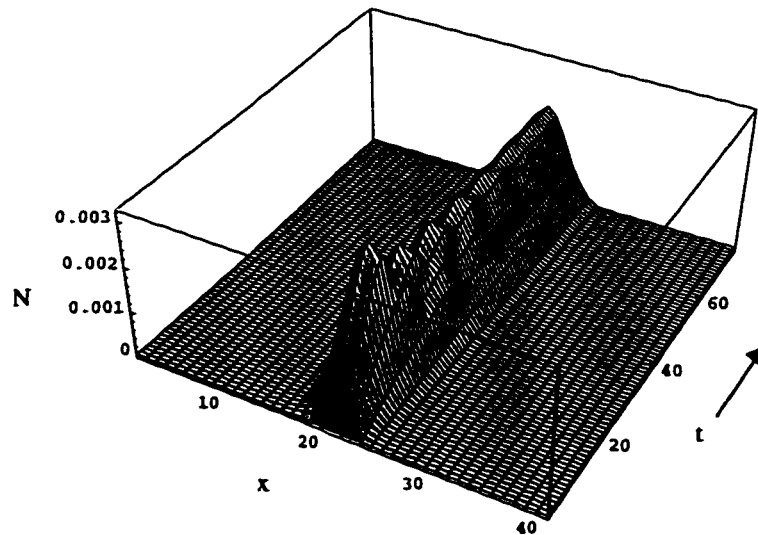
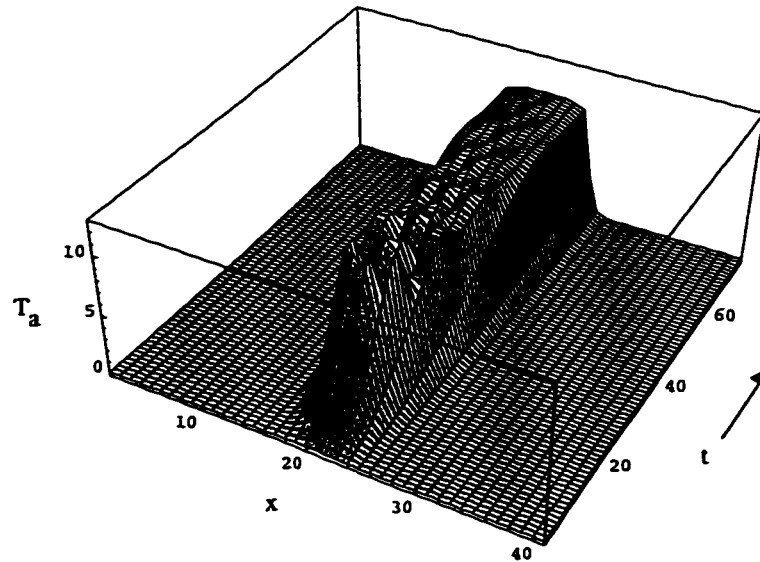


Figure 7.7: Simulation results for an inhomogeneous nucleation rate constant as shown in Figure 7.5 to simulate a MTOC. The profiles are the last time step for both N and T_a are steady-state profiles and indicated the the microtubules are longer on the edges of the MTOC.

It has a great deal of flexibility, but is also strongly based on experimental data and rate constants. The key underlying all of these simulations is the autocatalytic step where a collapse is induced by an excess of GTP rich tubulin. More research is needed into the effect of this to see whether or not this could be the mechanism responsible for producing these oscillations.

Chapter 8

Conclusions

As presented in this thesis, microtubules are intricate and dynamic structures which play a vital role within the cell. Aside from the many structural and organizational aspects of microtubules, their dynamical nature is why so much research is focused on these polymers. We have made an effort in this work to discover how the erratic growth of an individual microtubule evolves into the smooth oscillations of a group of microtubules.

Our first model was based on a stochastic map where at each time step the microtubule could grow or collapse based on certain probabilities. By changing the growth rate or the probability functions, we could alter the growth patterns to match any of the many variations observed in real cells. After selecting a successful model, we attempted to model a microtubule ensemble by coupling many of these maps together. The coupling in this case was due to the fact that all the microtubules were growing from a common pool of tubulin. By selecting different probability functions and including factors such as GTP regeneration, we found we could produce features such as growth to a steady-state including the possibility of an overshoot in assembled tubulin. Using this approach, we could not, however, produce oscillations. As had been determined in experiments, we found we required nucleation of new microtubules.

One new feature arising from this stochastic map formulation was the use of Hurst's rescaled range analysis in examining experimental data and models developed. Although the time series appeared very different in the three cases presented, the recursive maps and Hurst analysis demonstrated the common characteristics and was able to give us a measure for comparing the models developed here and by other authors.

To incorporate the nucleation of new microtubules we moved to a model which treated microtubule assembly as a first-order phase transition. We proceeded to perform a Landau free energy expansion in terms of an order parameter ϕ which corresponded to the density of our system. The control parameters we chose were the temperature and the tubulin concentration. In the 'liquid' state, ϕ was zero and no tubulin assembled. As either of the control parameters was increased, the 'solid' microtubule phase was introduced and ϕ became non-zero. The coefficients of the free energy expansion could be chosen such that this model produced a phase diagram for microtubule assembly which agreed with the experimental picture. We also arrived at an equation of motion by minimizing the free energy. With appropriate initial conditions, the solutions to this equation were damped oscillations in the order parameter. As the tubulin concentration was increased, the size and extent of oscillations grew in agreement with experiments. This simple model also made predictions as to the behaviour of the specific heat. If confirmed by experiment, this could verify our assumption of a first-order phase transition.

The next model was an improvement over the Landau-Ginzburg approach in that it directly modelled the interactions that take place in the assembly cycle. The basic reactions formed in the first models were growth, collapse and nucleation. Through mathematical analysis it was determined that a chemical kinetics model based on these three processes alone could not produce oscillations. We altered this set of reactions by first making the distinction between the two nucleotides GDP and GTP

and adding a mechanism for GTP regeneration. This expanded set of reactions still failed the mathematical criterion for oscillations. It had been suggested by several researchers that an excess of tubulin bound with GDP could effectively block microtubule ends from assembly competent dimers and in turn induce a collapse. We included such an autocatalytic reaction into our scheme. With this added reaction, the criterion for oscillations was met. Our system involved five reactions and hence five reaction rate constants. Most rates were determined from experimental data, some however were not readily available and were chosen to provide the best fit to the data. By finding the eigenvalues of the Jacobian, we could determine the temperatures and tubulin concentrations which gave rise to oscillations. This once again gave us a phase diagram which was in excellent agreement with experimental findings.

The growth patterns which this model produced were also very agreeable. The results could be matched to experimental results for different temperatures and tubulin concentrations. The oscillations in assembled tubulin and GTP-rich tubulin also matched experiment as did the simulations for the effect of temperature on nucleation. Other findings could also be modelled such as the addition of GTP after oscillations have ceased or the shearing of microtubules undergoing oscillations. The rate of GTP regeneration was found to be an extremely important factor in this model. The period of oscillations, as found in experiments, depended on this rate and oscillations would disappear if the rate was raised to a sufficient level. A further validation of this model would be to experimentally investigate the effect of GTP regeneration and of the GDP induced collapse.

Finally, we presented a reaction-diffusion model which expanded the chemical kinetics models to include inhomogeneous reactant concentrations and the effect of diffusion. This model displayed quite different dynamics when concentration or temperature gradients were applied. To simulate the assembly waves observed by experimentalists, we assumed a spatially dependent nucleation rate. This caused micro-

tubules to be nucleated at the boundary after which they would propagate to the interior of the cell. Such inhomogeneous rate constants could also replicate the effect of a MTOC such as the centrosome. In this case both the microtubule number and the assembled tubulin approached steady-state values which gave rise to longer microtubules on the edges of the MTOC.

The set of five reactions that we included can truly be regarded as the most basic set of processes we can consider. Apart from the induced collapse, all the other reactions are well known from experiments. Although this model can reproduce numerous experimental results, it does not include many other effects. Aside from the autocatalytic reaction, we assumed in our chemical reactions that the reactants did not catalyze their own production such that a process involving one reactant was first-order and one involving two reactants was second-order. These reactions may in fact be any order or even of fractional order which could change the dynamics considerably. To find the order of these reactions, we would need to find the rate constants as functions of the reactant concentrations for all five processes. This is possible to do, but certainly would not be a priority for many experimental groups and it may not improve on the results of the model. The effect of ions such as Mg^{2+} and Ca^{2+} could also be investigated. Within the cell, calcium waves are fairly well understood. Since calcium acts as a destabilizer, these waves could perhaps induce a wave of disassembly. Similarly with magnesium, since it promotes microtubule assembly, waves of magnesium ions may produce the opposite effect.

The success of the models presented here rests on the fact that they are based on experimental evidence, they are able to reproduce numerous experimental results and further, they can make predictions for future experiments. These models are also an improvement over previous modelling for several reasons. First, we have made a minimum number of assumptions about what happens at the molecular level. Concepts such as a GTP-cap of the conformational changes of tubulin have not been

assumed or precluded. Second, we have a small number of free parameters in our system since many rate constants have been determined from experimental data. We also fixed our constants so that we only had the freedom of adjusting the tubulin concentration and the temperature. Lastly, in both the case of the Landau-Ginzburg model and the reaction-kinetics models, we were able to reproduce both the correct dynamics and the proper phase diagram using exactly the same parameters. The ability of these systems to perform this feat leads us to the conclusion that our assumptions about the underlying dynamics must be correct. It is hoped that these ideas lead to future experimental and theoretical investigations.

Bibliography

- [1] H. Haken. *Synergetics*. Springer-Verlag, 1977.
- [2] B. Alberts et al. *Molecular biology of the cell*. Garland Publishing, 1994.
- [3] N.K. Wessels and J.L. Hopson. *Biology*. Random House, 1988.
- [4] D.M. Prescott. *Cells*. Jones and Bartlett Publishers, Boston, 1988.
- [5] J. Dayhoff, S. Hameroff, R. Lahoz-Beltra, and C.E. Swenberg. Cytoskeletal involvement in neuronal learning: A review. *Eur. Biophys. J.*, pages 79–93, 1994.
- [6] S.R. Hameroff. *Ultimate Computing: Biomolecular Consciousness and Nanotechnology*. North-Holland, Amsterdam, 1987.
- [7] S.R. Hameroff and R.C. Watt. Information processing in microtubules. *J. Theor. Biol.*, 98:549–562, 1982.
- [8] L.A. Amos and W.B. Amos. *Molecules of the cytoskeleton*. Macmillan Press, London, 1991.
- [9] R.B. Dye and Jr. R.C. Williams. Assembly of microtubules from tubulin bearing the nonhydrolyzable GTP analogue GMPPCP: Variability of growth rates and the hydrolysis of GTP. *Biochem.*, 35:14331–14339, 1996.

- [10] M.V. Semenov. New concept of microtubule dynamics and microtubule motor movement and new model of chromosome movement in mitosis. *J. Theor. Biol.*, 179:91–117, 1996.
- [11] D. Chrétien, S.D. Fuller, and E. Karsenti. Structure of growing microtubule ends: Two dimensional sheets close into tubes at variable rates. *J. Cell Biol.*, 129:1311–1328, 1995.
- [12] T. Mitchison and M. Kirschner. Microtubule assembly nucleated by isolated centrosomes. *Nature*, 312:232–237, 1984.
- [13] T. Mitchison and M. Kirschner. Dynamic instability of microtubule growth. *Nature*, 312:237–242, 1984.
- [14] F.D. Warner, P. Satir, and I.R. Gibbons, editors. *Cell Movement Vol. I: The dynein ATPases*. Wiley-Liss, 1989.
- [15] J.E. Dayhoff, S.R. Hameroff, C.E. Swenberg, R. Lahoz-Beltra, and A. Samsonovich. Biological learning with cytoskeletal signalling. *IEEE Intl. Joint Conf. on Neural Networks*, 2:II45–II50, 1992.
- [16] J. A. Tuszyński, S. Hameroff, M.V. Satarić, B. Trpišová, and M.L.A. Nip. Ferroelectric behavior in microtubule dipole lattices: Implications for information processing, signaling and assembly/disassembly. *J. Theor. Biol.*, 174:371–380, 1995.
- [17] J.A. Tuszynski, B. Trpisova, D. Sept, and J.A. Brown. Selected physical issues in the structure and function of microtubule. *J. Struct. Biol.*, 118:94–106, 1997.
- [18] S. Inoue. Polarization optical studies of the mitotic spindle I. The demonstration of spindle fibers in living cells. *Chromosoma*, 5:500, 1953.

- [19] T. Horio and H. Hotani. Visualization of the dynamic instability of individual microtubules by dark field microscopy. *Nature*, 321:605–607, 1986.
- [20] M. Kirschner and T. Mitchison. Beyond self-assembly: From microtubules to morphogenesis. *Cell*, 45:329–342, 1986.
- [21] R.A. Walker, N.K. Pryer, and E.D. Salmon. Dilution of individual microtubules observed in real time in vitro: evidence that cap size is small and independent of elongation rate. *J. Cell Biol.*, 114:114, 1991.
- [22] L. Cassimeris, N. K. Pryer, and E.D. Salmon. Real-time observations of microtubule dynamic instability in living cells. *J. Cell Biol.*, 107:2223, 1988.
- [23] M.A. Billger, G. Bhattacharjee, and Jr. R.C. Williams. Dynamic instability of microtubules assembled from MAP-free tubulin: Neither variability of growth and shortening rates nor 'rescue' requires MAPs. *Biochem.*, 35:13656–13663, 1996.
- [24] L. Cassimeris. Regulation of microtubule dynamic instability. *Cell. Motil. Cyto.*, 26:275–281, 1993.
- [25] H.P. Erickson and E.T. O'Brien. Microtubule dynamic instability and GTP hydrolysis. *Annu. Rev. Biophys. Struct.*, 21:145–166, 1992.
- [26] M.F. Carrier, D. Didry, and D. Pantaloni. Stabilization of microtubules by inorganic phosphate and its structural analogues, the fluoride complexes of aluminum and beryllium. *Biochem.*, 27:3555–3559, 1988.
- [27] M. Caplow, R. Ruhlen, J. Shanks, R.A. Walker, and E.D. Salmon. Stabilization of microtubules by tubulin-GDP-Pi subunits. *Biochem.*, 28:8136–8141, 1989.
- [28] R. Melki, M.-F. Carrier, and D. Pantaloni. Direct evidence for GTP and GDP- p_i intermediates in microtubule assembly. *Biochem.*, 29:8921–8932, 1990.

- [29] R.J. Stewart, K.W. Farrell, and L. Wilson. Role of GTP hydrolysis in microtubule polymerization: Evidence for a coupled hydrolysis mechanism. *Biochem.*, 29:6489–6498, 1990.
- [30] F. Pirollet, D. Job, R.L. Margolis, and J. Garel. An oscillatory mode for microtubule assembly. *EMBO J.*, 1987.
- [31] R. Melki, M.-F. Carlier, and D. Pantaloni. Oscillations in microtubule polymerization: the rate of GTP regeneration on tubulin controls the period. *EMBO J.*, 7:2653–2659, 1988.
- [32] M.F. Carlier, R. Melki, D. Pantaloni, T.L. Hill, and Y. Chen. Synchronous oscillations in microtubule polymerization. *Proc. Natl. Acad. Sci. USA*, 84:5257–5261, August 1987.
- [33] R.H. Wade, F. Pirollet, R.L. Margolis, J. Garel, and D. Jobb. Monotonic versus oscillating microtubule assembly: a cryo-electron microscope study. *Biol. Cell*, 65:37–44, 1989.
- [34] M. Caplow and J. Shanks. Mechanism for oscillatory assembly of microtubules. *J. Biol. Chem.*, 265(3):1414–1418, 1990.
- [35] Y. Engelborghs. *Microtubule Proteins*, chapter Dynamic aspects of microtubule assembly. CRC Press, 1990.
- [36] Oosawa and Asakura. *Thermodynamics of the polymerization of protein*. Academic Press, 1975.
- [37] H. Obermann, E.-M. Mandelkow, G. Lange, and E. Mandelkow. Microtubule oscillations. *J. Biol. Chem.*, 265:4382–4388, 1990.
- [38] E.-M. Mandelkow and E. Mandelkow. Microtubule oscillations. *Cell Motil. and Cytoskel.*, 22:235–244, 1992.

- [39] E. Mandelkow, E.M. Mandelkow, H. Hotani, B. Hess, and S. Müller. Spatial patterns from oscillating microtubules. *Science*, 246:1291–1293, 1989.
- [40] A.S. Bajer. Functional autonomy of monopolar spindle and evidence for oscillatory movement in mitosis. *J. Cell Biol.*, 93:33–48, 1982.
- [41] T.L. Hill and Y. Chen. Phase changes at the end of a microtubule with a gtp cap. *Proc. Natl. Acad. Sci. USA*, 81:5772–5776, 1984.
- [42] T.L. Hill. Introductory analysis of the gtp-cap phase-change kinetics at the end of a microtubule. *Proc. Natl. Acad. Sci. USA*, 81:6728–6732, 1984.
- [43] Y. Chen and T.L. Hill. Monte Carlo study of the GTP cap in a five-start helix model of a microtubule. *Proc. Natl. Acad. Sci. USA*, 82:1131–1135, 1985.
- [44] P.M. Bayley. What makes microtubules dynamic? *J. Cell Sci.*, 95:329–334, 1990.
- [45] S.R. Martin, M.J. Schilstra, and P.M. Bayley. Opposite-end behaviour of dynamics microtubules. *Biochim. et Biophys. Acta*, 1073:555–561, 1991.
- [46] S.R. Martin, M.J. Schilstra, and P.M. Bayley. Dynamics instability of microtubules: Monte Carlo simulation and application to different types of microtubule lattice. *Biophys. J.*, 65:578–596, 1993.
- [47] N.R. Glikzman, R.V. Skibbens, and E.D. Salmon. How the transition frequencies of microtubule dynamic instability (nucleation, catastrophe and rescue) regulate microtubule dynamics in interphase and mitosis: Analysis using a Monte Carlo computer simulation. *Mol. Biol. Cell*, 4:1035–1050, 1993.
- [48] H. Flyvbjerg, T.E. Holy, and S. Leibler. Stochastic dynamics of microtubules: A model for caps and catastrophes. *Phys. Rev. Lett.*, 73:2372, 1994.

- [49] Y. Chen and T.L. Hill. Theoretical studies on oscillations in microtubule polymerization. *Proc. Natl. Acad. Sci. USA*, 84:8419–8423, 1987.
- [50] A. Marx and E. Mandelkow. A model of microtubule oscillations. *Eur. Biophys. J.*, 22:405–421, 1994.
- [51] B. Houchmandzadeh and M. Vallade. Collective oscillations in microtubule growth. *Phys. Rev. E*, 53(6):6320–6324, 1996.
- [52] D.J. Odde, L. Cassimeris, and H.M. Buettner. Kinetics of microtubule catastrophe assessed by probabilistic analysis. *Biophys. J.*, 69:796–802, 1995.
- [53] D.J. Odde, H.M. Buettner, and L. Cassimeris. Spectral analysis of microtubule assembly dynamics. *AIChE J.*, 42:1434–1442, 1996.
- [54] J. Feder. *Fractals*. Plenum Press, 1988.
- [55] D.K. Fygenson, E. Braun, and A. Libchaber. Phase diagram of microtubules. *Phys. Rev. D*, 50:1579–1588, 1994.
- [56] P.W. Atkins. *Physical chemistry*. W.H. Freeman and Company, 1990.
- [57] P. Gray. Instabilities and oscillations in chemical reactions in closed and open systems. *Proc. R. Soc. Lond.*, 415:1–34, 1988.
- [58] B.P. Belousov. . *Sb. Ref. Radiats. Med.*, page 145, 1959.
- [59] F.A. Brown, J.W. Hastings, and J.D. Palmer. *The biological clock*. Academic Press, 1970.
- [60] A. Ghosh and B. Chance. Oscillations of glycolytic intermediates in yeast cells. *Biochem. Biophys. Res. Commun.*, 16:174, 1964.

- [61] W.A. Knorre. Oscillations of the rate of synthesis of beta-galactosidase in *Escherichia coli* ml 30 and ml 308. *Biochem. Biophys. Res. Commun.*, 31:812, 1968.
- [62] G. Nicolis and J. Portnow. Chemical oscillations. *Chem. Rev.*, 73:365–384, 1973.
- [63] C. Connell McCluskey. Bendixson criteria for difference equations. Master's thesis, University of Alberta, 1996.
- [64] D. Kuchnir Fygenson, H. Flyvbjerg, K. Sneppen, A. Libchaber, and S. Leibler. Spontaneous nucleation of microtubules. *Phys. Rev. E*, 51:5058–5063, 1995.
- [65] R.G. Burns and M.F. Symmons. In vitro assembly of microtubule protein with GTP and 2'dGTP: Kinetic evidence for a preassembly conformational change. *Biochem.*, 34:2302–2308, 1995.
- [66] R.A. Walker, E.T. O'Brien, N.K. Pryer, M.F. Soboeiro, W.A. Voter, H.P. Erickson, and E.D. Salmon. Dynamic instability of individual microtubules analyzed by video light microscopy: Rate constants and transition frequencies. *J. Cell Biol.*, 107:1437–1448, 1988.
- [67] P.M. Bayley, F.M.M. Butler, D.C. Clark, E.J. Manser, and S.R. Martin. The assembly of microtubule protein *in vitro*. *Biochem. J.*, 227:439–455, 1985.
- [68] Y. Engelborghs and L.C.M. de Maeyer. A kinetic analysis of the assembly of microtubules *in vitro*. *FEBS Lett.*, 80:81–85, 1977.
- [69] K.A. Johnson and G.G. Borisy. Kinetic analysis of microtubule self-assembly *in vitro*. *J. Mol. Biol.*, 117:1, 1977.
- [70] J. Bryan. A quantitative analysis of microtubule elongation. *J. Cell Biol.*, 71:749–767, 1976.

- [71] M.B. Jackson and S.A. Berkowitz. Nucleation and the kinetics of microtubule assembly. *Proc. Natl. Acad. Sci. USA*, 77(12):7302–7305, 1980.
- [72] S. Wolfram. *Mathematica*. Addison-Wesley, 1991.
- [73] Q. Lu and R.F. Ludueña. In vitro analysis of microtubule assembly of isotypically pure tubulin dimers. *J. Biol. Chem.*, 269:2041–2047, 1994.
- [74] G. Lange, E.M. Mandelkow, A. Jagla, and E. Mandelkow. Tubulin oligomers and microtubule oscillations. *Eur. J. Biochem.*, 178:61–69, 1988.
- [75] R.A.B. Keates and F.R. Hallett. Dynamic instability of sheared microtubules observed by quasi-elastic light scattering. *Science*, 241:1642–1645, 1988.
- [76] Y. Kuramoto. *Chemical oscillations, waves and turbulence*. Springer-Verlag, 1984.
- [77] E.D. Salmon, W.M. Saxton, R.J. Leslie, M.L. Karow, and J.R. McIntosh. Diffusion coefficient of fluorescein labeled tubulin in the cytoplasm of embryonic cells of a sea urchin: Video image analysis of fluorescence redistribution after photobleaching. *J. Cell Biol.*, 99:2157–2164, 1984.
- [78] C. Canuto, M.Y. Hussanini, A. Quarteroni, and T.A. Zhang. *Spectral methods in fluid dynamics*. Springer-Verlag, 1988.
- [79] A.M. Turing. The chemical basis of morphogenesis. *Phil. Trans. R. Soc. Lond. B*, 237:37–72, 1952.
- [80] L. Wolpert. Positional information and spatial patterning. *Phil. Trans. R. Soc. Lond. B*, 259:441–450, 1981.